SPATIAL INTERACTIONS AND ECO-EVOLUTIONARY GAMES

A Dissertation
Presented to
The Academic Faculty

By

Yu-Hui Lin

In Partial Fulfillment
of the Requirements for the Degree
Doctor of Philosophy in the
School of Physics

Georgia Institute of Technology

August 2019

SPATIAL INTERACTIONS AND ECO-EVOLUTIONARY GAMES

Approved by:

Dr. Joshua S. Weitz, Advisor
School of Biological Sciences
School of Physics
Georgia Institute of Technology

Dr. Flavio H. Fenton
School of Physics
Georgia Institute of Technology

Dr. Kurt Wiesenfeld
School of Physics
Georgia Institute of Technology

Dr. Peter J. Yunker
School of Physics
Georgia Institute of Technology

Dr. Yao Yao
School of Mathematics
Georgia Institute of Technology

Date Approved: May 6, 2019

ACKNOWLEDGEMENTS

First of all, I would like to thank Prof. Joshua S. Weitz for his guidance and patience along the way of advising my thesis research. His expertise in science is of no doubt. His proficiency in managing, engagement in leading frontier scientific research, and courage in advocating for public issues have also been inspiring to me. During my time in the Weitz group, I have never ceased learning.

A productive and inclusive research group cannot exist without talented and supportive group members. I would like to thank every member in the Weitz group, Ceyhun Eskin, Joey Leung, Stephen Beckett, David Demory, Bradford Taylor, Chad Wigington, Keith Paarporn, Hend Alrasheed, Rong Jin, Shengyun Peng, Ashley Coenen, Daniel Muratore, Guanlin Li, Qi An, Rogelio Rodriguez, Marian Domínguez Mirazo, and Andreea Măgălie for teaching me how to play bowling and cheering for each point earned, like how you always do to help me and clap for me every time I take even just a tiny step forward.

Making progress in graduate school requires a solid foundation. I would like to thank Mr. Li-Shan Chuang, my high school physics teacher, for identifying my personality preference and igniting my passion in science, as well as advising my first scientific project as a mentor and a friend. I would like to thank Mr. Yi-An Chen, also my high school physics teacher, for many intriguing lectures that strengthened my background in physics after classes. My journey in science would not have started without these two dedicated teachers. I would also like to thank Dr. Chun-Yi David Lu and Dr. Yeng-Long Chen, my two former group principal investigators that guided me to explore the beauty and power of theory and simulations.

Outside the labs, I am lucky to have met many interesting people. I would like to thank all my friends, here and there, for the moments we shared. Those pieces in my life, all delicious foods and gorgeous scenes, the happy and goofy occasions, a lot

of blue sky conversations, many sentimental moments, a couple of struggling periods, etc., could not have been so vivid without them being (sometimes virtually) by my side 24/7, thanks to the time difference across the world.

It may sound clichéd, but I must thank my family for their unconditional love and support. The innate curiosity in Dad and generous kindness in Mom have influenced me to view the world around from a variety of angles, a core value as a scientist. Curiosity drives me to ask questions in more depth, and kindness reminds me to consider problems in others' shoes. I would also to thank my two brothers, though younger, for taking care of some of the 'adult' tasks, such as driving me around, when we spend time together. The maturity in my brothers is another reason that I am able to keep my somewhat childlike curiosity.

Most importantly, I would like to thank my husband, also soon-to-be Dr. Wen-Hao Tan, for hundreds of thousands of miles we have traveled together. I probably would not have embarked on the adventure of pursuing a Ph.D. without his encouragement, and I definitely would not be able to finish a Ph.D. without his company. Completing a Ph.D. may be worth celebrating, but finishing Ph.D.'s and crossing the obstacles in graduate school life together with a partner and the best friend is even better. The acknowledgment could not end without many thanks to the 'furmaly' members we adopted here, Mochi and Matcha, two most adorable cats, for further brightening my daily life.

TABLE OF CONTENTS

LIST OF TABLES

LIST OF FIGURES

SUMMARY

Organisms compete for limited resources to reproduce. Reproduction depends on behaviors that are modified by abiotic and biotic factors, including the behavior of other organisms. This thesis adopts and extends evolutionary game theory to understand the coupled dynamics of individual behavior and resources. In doing so, the work is motivated by the example of the Tragedy of the Commons introduced by Garret Hardin in which individuals, each acting in their own self-interest, overuse resources and lead to the collapse of the commons. Although Hardin claimed that the TOC is inevitable, there are many examples from ecology to economics that offer alternative outcomes. An explanation for this gap was recently proposed in a mean-field model of evolutionary games coupled to environmental feedback in which depletion of resources can change individual behavior, thus leading to the aversion of the tragedy. This thesis extends this continuous model of game-environment feedback to address three motivating questions: 1) How does demographic noise and spatial interactions shape the spatiotemporal dynamics of the system, 2) How does the relative speed of strategy and environment dynamics affect TOC, 3) What new insights can we learn regarding public good production in microbial systems when game and environment are reciprocally coupled. Our approach to answer these questions leverages a derivation of individual-based game rules that can recapitulate feedback given both demographic noise and spatially explicit interactions. These games rules recapitulate the mean-field model in the large system limit. Individual-based simulations of the game yield multiple findings. First, spatial and non-spatial simulations give different population dynamics with the same simulation parameter sets, suggesting that spatial interactions can shift regimes where TOCs occur. Second, the spatially explicit system shows coherent spatial-temporal patterns, including the expansion of clusters of resources and strategies. Additional findings highlight the role of diffusivity and

time-scales in modulating the coupled fates of behaviors and environment. Overall, the work helps identify consequences of the mutual feedback between behavior and environmental resources in finite-sized populations.

CHAPTER 1
INTRODUCTION AND BACKGROUND

Living together on the same planet, interactions among organisms and between organisms and their environments are inevitable. The simplest forms of interactions are those involving only two organisms. Pairwise interactions between organisms can be roughly categorized into several types based on the consequence on two sides [1]. The interacting organisms can both suffer from the interaction, e.g. as during competition. Sometimes benefit for one side comes from the harm of the other side. Predation and parasitism are two instances [2, 3, 4]. Commensalism, in which there is a net benefit for one side without loss from the other side is also possible [5, 6]. Moreover, mutualism denotes the case when the two sides can both benefit from the interactions in some [7, 8].

Among the types of interactions mentioned, the mutually beneficial interactions, such cooperative interactions, are of particular interest because the interactions are susceptible to invasion by cheaters. In game theory, cheaters are defined as individuals who do not cooperate but take advantage of the benefit coming from cooperating individuals [9, 10, 11]. The risk of cheating and its possible negative outcomes can be further illustrated by an example Garrett Hardin described in his paper in 1968 [12]. Hardin postulated a situation where there is a common grassland (the "commons") every shepherd can access. The shepherds are able to maintain a herd of cows of reasonable size if they all cooperate and use the grassland in moderation. However, a shepherd will benefit more by grazing more cows on the grassland. A rational but selfish shepherd would choose to put as many cows as possible to utilize the grassland most. Given a group of selfish shepherds (cheaters, or defectors hereafter), the grassland would soon be depleted due to their collective defective behavior. Hardin termed

this situation as "the tragedy of the commons" (TOC) and argued it was inevitable.

Yet, cooperation still seems to be ubiquitous despite the existence of defectors. Theoretical analysis and field studies have shown that a sustainable system of managing the commons without regulations from a central authority are possible. By deliberately arranging the timing of utilizing the commons with regulations from authorities at the intermediate levels, individuals can continue to derive benefits from a common resource [13, 14, 15, 16, 17].

In this thesis, we aim to examine an additional class of mechanisms by which cooperation persists in spite of the risk of being defeated by defectors. The core idea is to consider a class of game theory problems in which the game affects the environmental state which, in turn, affects the game. This feedback lies outside the scope of most approaches to game theory analysis focusing on static games. The core innovation is to examine such games in a spatial context. To do so, we take the following approach.

In Chapter 2, we introduce game theory, a mathematical framework to study how rationale individuals choose a strategy, e.g., to cooperate or to defect, based on their strategy-dependent payoffs. We also introduce replicator dynamics, a mean-field ordinary differential equation (ODE) that captures the evolutionary dynamics of change in strategy frequency assuming each individual has an equal chance to play games with another in the system. Further, we derive a set of individual-based game rules and prove that it can recapitulate the replicator dynamics at the mean-field limit with the master equation approach. Examining the convergence from the macroscopic individual-based game rules developed to the population-level replicator dynamics helps disentangle the effects of demographic noises and spatial coupling on the system dynamics from the impact of other possible individual-based updating rules. The game rules developed here serve as a foundation for the following chapters, where we use individual-based model (IBM) to explore the strategy dynamics in the

spatial and non-spatial context under the influence of variations in the environment.

In Chapter 3, we briefly review a recent ODE model on coevolutionary dynamics between the environment and the strategy [18]. In this model, the payoffs of the games are functions of the environment. Namely, individuals are able to adjust their strategies given an accurate perception of the environment. The individuals are assumed to favor defect when the environment is abundant but could play different games when the environment is depleted. By exploring possible payoffs when the environment is depleted, Weitz *et. al.* proved aversion of TOC is possible. The analysis of the ODE model also reveals the existence of an oscillating TOC (o-TOC), a dynamical behavior that the environment oscillates with increasing amplitudes until approaching the extremum. We construct a hybrid *in silico* model that leverages the game rules derived in Chapter 2 and updates the environment with numerical integration to simulate the coevolutionary dynamics including demographic noise. The non-spatial individual-based simulations recapitulate the ODE solution, further confirming the game rules are capable of representing 2-by-2 symmetric games of different types, even when the payoff matrix is dependent on another variable. The individual-based game rules can be quickly adapted to spatial simulations by limiting game players to be in the vicinity of each other. By realizing the game rules on a two-dimensional (2D) lattice, we find the spatial coupling can shift the domain where a TOC can be averted. We also identify that spatial coevolutionary games can at least display three kinds of spatiotemporal dynamics with different environment diffusivity D_n. The spatial pair correlation analysis on the spatial-temporal dynamics indicates how the value of D_n alters the spatial-temporal dynamics.

In Chapter 4, we further investigate the effect of relative speed of strategy dynamics and environment dynamics. Adopting the same simulation model as described in Chapter 3, we find that the dynamical behavior of the IBM recapitulates the ODE solution with only one exception. An o-TOC occurs given an IBM in a situation

that generally leads to a TOC. In the case of slow strategy dynamics, the chance of winning for cooperators and defectors becomes comparable, and the stochastic nature of the individual-based game rules make it possible for cooperators to invade even when the environment is not ideal for them. We also run spatial simulations with several different combinations of D_n and different speed parameter, which controls the relative speed of strategy and environment. We again find system dynamics diverge from ODE prediction and non-spatial simulations due to spatial coupling. By performing spatial simulations with different speed parameters, we find the simulations with $D_n = 1$ are most vulnerable to a TOC and provide an possible explanation for it. The spatial temporal structure and spatial pair-correlation function reveals slow environment dynamics leads to delay between cooperator invasion and local environment enhancement. Hence, a slow responding environment can sometimes result in spatial anti-correlation between strategy and environment dynamics as found in simulations with a low D_n. In contrast, a fast responding environment leads to highly localized environment distributions, contributing to the decrease of cooperators and environment clusters in size.

Up until Chapter 4, we have only considered scenarios in which the environment responds to change in strategies. In Chapter 5, we also take intrinsic dynamics of the environment into account, that is, the dynamics without the impact of individual strategies. We mainly focus on the case of an exponentially decaying resource, i.e., without autonomous regenerative capacity. Following the process in the paper by Tilman *et. al.* [19], we use the coupled ODEs for coevolutionary dynamics with a decaying environment as the basis of updating rules for the environment. In doing so, we confirm that our non-spatial hybrid simulation model still captures the features of the ODE model given intrinsic environment dynamics. In contrast, spatial simulations reveal that spatial coupling shifts the system dynamics in a way we have not found in the previous chapters. While we attribute the increasing amplitudes in

oscillating dynamics to strong spatial coupling in Chapter 3, we find this is not the case for systems with an intrinsically decaying environment. Rather, a large value of environmental diffusivity seems to dampen the oscillations in the spatial simulations of the model considered in this chapter.

In summary, evolutionary game theory and replicator has been used to study how the frequency of strategists change over time. Building upon prior work, this thesis explores how feedback between game and environment in a spatially explicit context can lead to new patterns and mechanisms that avert an 'inevitable' tragedy of the commons.

CHAPTER 2

THEORETICAL BASIS OF INDIVIDUAL-BASED GAMES

Adapted from Y.-H. Lin, and J. S. Weitz. (2019). Spatial Interactions and Oscillatory Tragedies of the Commons. Physical review letters 122(14), 148102.

2.1 Introduction

Game theory is a mathematical framework to understand the actions of rationale individuals and of populations of individuals with distinct strategies [20]. Essentially, a game can be described by a payoff matrix, of which elements are the payoffs to each player involved in a game with a set of strategies. One of the simplest forms is a symmetric, 2-by-2 game. The term "symmetric" means the payoffs only depend on the strategies the players chose. By 2-by-2, it means only two strategies are available, and only two players are involved in a game. The payoff matrix of a 2-by-2 symmetric game can be written as

$$A = \begin{bmatrix} a_{11} & a_{12} \\ a_{21} & a_{22} \end{bmatrix}. \tag{2.1}$$

The elements a_{ij} denotes the payoff awarded to the focal player when it plays strategy i and its opponent plays strategy j. In this thesis, strategy 1 is to cooperate and strategy 2 is to defect. A rational individual always chooses the strategy with a better payoff.

A symmetric 2-by-2 game can have a different outcome determined by the payoffs, and we can classify the games based on the relative values of a_{ij}. Some of the classical types of games are 1.) When $a_{11} > a_{12} \geq a_{21} > a_{22}$, the players would choose to cooperate regardless of the opponent's strategy and the overall payoff is better for both parties if they cooperate. This kind of game is called a harmony

game. 2.) When $a_{11} > a_{12} \geq a_{22} > a_{21}$, the focal player prefers to play the same strategy as its opponent, but the cooperation of both parties lead to better overall payoff than defection. This kind of game is called a stag hunt game. 3.) When $a_{21} > a_{22} \geq a_{12} > a_{11}$, the focal player prefers to play the opposite strategy as its opponent, but the cooperative player gets a better payoff. This kind of game is called a hawk-dove game or a snow-drift game [21, 22]. 4.) When $a_{21} > a_{11} \geq a_{22} > a_{21}$, both player would choose to defect regardless of the opponent's strategy, *but* the overall payoff is actually better if they both choose to cooperate. This kind of game is called a prisoner's dilemma (PD) game [22, 23].

The PD game is of particular interest because it is the situation that leads to a social dilemma termed as 'Tragedy of the Commons' (TOC) by Garrett Hardin [12]. The social dilemma arises when two individuals choose amongst distinct strategies to utilize a limited public good. Both individuals receive the maximal combined benefit if they utilize the public good with restraint, *i.e.*, if they 'cooperate'. However, each receives the maximal personal benefit if they utilize the public good without restraint, *i.e.*, if they 'defect', while their opponent cooperates. As a consequence, individuals acting rationally will cheat leaving all worse off. Hardin argued that such a TOC is inevitable [12].

Evolutionary dynamics arising from a TOC dilemma can be modeled in terms of changes in the frequencies of individuals from two populations. Individuals interact and receive payoffs that depend on their strategy and the strategy of their opponent [21]. In replicator dynamics [24], the payoff represents a relative fitness which determines the growth of cooperators, with frequency x, and of defectors, with frequency $1 - x$, i.e.,

$$\dot{x} = x(1 - x)(r_C(x, A) - r_D(x, A)). \tag{2.2}$$

The values r_C and r_D denote the context-dependent fitness payoff to cooperators and defectors respectively, given the payoff matrix $A = \left[\begin{smallmatrix} R & S \\ T & P \end{smallmatrix}\right]$, where $r_C = Rx + S(1-x)$, $r_D = Tx + P(1-x)$, such that R denotes the reward to cooperation, T denotes the temptation to cheat, S denotes the sucker's payoff, and P denotes the punishment given mutual defection. Plugging $r_C(x)$ and $r_D(x)$ into Eq. 2.2, it becomes

$$\dot{x} = x(1-x)\left((R-T)x + (S-P)(1-x)\right), \tag{2.3}$$

and a TOC occurs when $T > R$, $P > S$, and $P < R$, namely, a prisoners' dilemma.

This 2-by-2, symmetric game model forms the basis for our development and analysis of an individual-based framework to assess the influence of noise and spatially explicit interactions on the emergent dynamics. In this chapter, we derive the expected mean field dynamics for the frequency of cooperators $x \equiv \lim_{N,n_c\to\infty}\left(\frac{n_C}{N}\right)$ from the master equation:

$$\dot{x} = x(1-x)\left[(k_1 - k_3)x + (k_2 - k_4)(1-x)\right]. \tag{2.4}$$

We recover the replicator dynamics of the coevolutionary model when $k_1 = R(n)$, $k_2 = S(n)$, $k_3 = T(n)$, and $k_4 = P(n)$. Hence, transition rates are a function of resource- and social-context dependent payoffs. We also show that, in contrast, mean field dynamics derived via a two-player individual-based model formulation (IBM2) result in a logistic dependency on x distinct from the cubic nonlinearity in Eq. 2.3.

2.2 Derivation of individual-based game rules recovering replicator dynamics

Here we derive the individual based game rules that are able to recover replicator dynamics

$$x' = x\,(1-x)\,(r_C(x,n) - r_D(x,n)), \tag{2.5}$$

in the continuous limit. The time is scaled by parameter ϵ for more compact expression. The normalized time $\frac{t}{\epsilon}$ will be denoted as τ hereafter. We express the time derivation with respect to normalized time with the prime symbol. We postulate that individuals undergo a birth-death process: a focal player that wins against its opponent in a game can reproduce a new individual with the same strategy and replace (A) another random player in the system or (B) the opponent. Here we show the derivation process of the scenario where a game involves three players (A), which recapitulates the form of replicator dynamics first. The game rules involving three player in a game is termed 'IBM3' in the following chapters. We then show the derivation of a similar process involving two individuals in which reproduction, when it occurs, always replaces the opponent. The game rules involving only two players is termed 'IBM2' in the following chapters.

2.2.1 Individual-based rules involving 3 players in a game

We write the events in a chemical reaction form with reaction rates k_i. The total number of players in the system is constant as a result of the birth-death process, $N = n_C + n_D$, where n_C and n_D denote the number of cooperators and defectors respectively. With C denoting a cooperator and D denoting a defector, the possible combinations of players involved in a game in which there is a change in the frequency of cooperators are

$$\begin{aligned}
&\overbrace{C}^{\text{focal}} + \overbrace{C}^{\text{opponent}} + \overbrace{D}^{\substack{\text{random}\\\text{player}}} \xrightarrow{k_1} \overbrace{C}^{\text{focal}} + \overbrace{C}^{\text{opponent}} + \overbrace{C}^{\text{replaced}} \\
&C + D + D \xrightarrow{k_2} C + D + C \\
&D + C + C \xrightarrow{k_3} D + C + D \\
&D + D + C \xrightarrow{k_4} D + D + D
\end{aligned} \tag{2.6}$$

The transition rates of Eq. 2.6 are

$$\mathbb{T}(n_C+1|n_C) = k_1 \cdot n_C \cdot \overbrace{\frac{n_C-1}{N-1}}^{\substack{\text{randomly choosing}\\ \text{an opponent C}}} \cdot \overbrace{\frac{n_D}{N-1}}^{\substack{\text{a random D to}\\ \text{be replaced}}} + k_2 \cdot n_C \cdot \overbrace{\frac{n_D}{N-1}}^{\substack{\text{randomly choosing}\\ \text{an opponent D}}} \cdot \overbrace{\frac{n_D}{N-1}}^{\substack{\text{a random D to}\\ \text{be replaced}}}$$

$$\mathbb{T}(n_C-1|n_C) = k_3 \cdot n_D \cdot \overbrace{\frac{n_C}{N-1}}^{\substack{\text{randomly choosing}\\ \text{an opponent C}}} \cdot \overbrace{\frac{n_C}{N-1}}^{\substack{\text{a random C to}\\ \text{be replaced}}} + k_4 \cdot n_D \cdot \overbrace{\frac{n_D-1}{N-1}}^{\substack{\text{randomly choosing}\\ \text{an opponent D}}} \cdot \overbrace{\frac{n_C}{N-1}}^{\substack{\text{a random C to}\\ \text{be replaced}}} . \tag{2.7}$$

The terms in the above equations describe the change in number of two types of players in a probabilistic perspective: there are n_C (n_D) cooperators (defectors) in the system, each of which has probability to pick another player, either a cooperator ($\frac{n_C-1}{N-1}$) or a defector ($\frac{n_D-1}{N-1}$), as an opponent. At each time increment, the focal player can produce a new individual with reaction rate $k_i\Delta\tau$. All players other than the focal player in the system has an equal chance to be replaced by the newborn individual. The individual to be replaced is a cooperator (defector) with probability $\frac{N_c-1}{N-1}$ ($\frac{N_D-1}{N-1}$). Combining the transition probability of all the possible events listed above, the master equation that governs the change in n_C is

$$\begin{aligned}\mathbb{P}\left(n_C, \tau+\Delta\tau\right) = \mathbb{P}\left(n_C,\tau\right) &+ \mathbb{T}(n_C|n_C-1)\mathbb{P}(n_C-1,\tau)\Delta\tau + \mathbb{T}(n_C|n_C+1)\mathbb{P}(n_C+1,\tau)\Delta\tau \\ &- \mathbb{T}(n_C+1|n_C)\mathbb{P}(n_C,\tau)\Delta\tau - \mathbb{T}(n_C-1|n_C)\mathbb{P}(n_C,\tau)\Delta\tau + \mathcal{O}(\Delta\tau^2).\end{aligned} \tag{2.8}$$

Rearranging the master equation Eq. 2.8, dividing both sides by $\Delta\tau$ and taking $\Delta\tau$ to be infinitesimal yields

$$\begin{aligned}\mathbb{P}'\left(n_C,\tau\right) = \mathbb{T}(n_C|n_C-1)\mathbb{P}(n_C-1,\tau) &+ \mathbb{T}(n_C|n_C+1)\mathbb{P}(n_C+1,\tau) \\ -\mathbb{T}(n_C+1|n_C)\mathbb{P}(n_C,\tau) &- \mathbb{T}(n_C-1|n_C)\mathbb{P}(n_C,\tau).\end{aligned} \tag{2.9}$$

To examine if the master equation derived from the individual-based events recovers replicator dynamics in the continuous limit, we need to derive the time differential equation of the expected value of n_C from the master equation Eq. 2.9. To proceed, we denote the expected value of a variable with angular brackets. The definition of the expected value of a random variable X is

$$\langle X(\tau)\rangle = \sum_X X\mathbb{P}(X,\tau). \tag{2.10}$$

Next, we multiply each term in the master equation Eq. 2.9 with n_C and sum over all possible values of n_C to obtain the time differential equation describing the dynamics of $\langle n_C\rangle$.

$$\begin{aligned}
\sum_{n_C=0}^{N} n_C\mathbb{P}'(n_C) &= \sum_{n_C=1}^{N} n_C\mathbb{T}(n_C|n_C-1)\mathbb{P}(n_C-1) + \sum_{n_C=0}^{N-1} n_C\mathbb{T}(n_C|n_C+1)\mathbb{P}(n_C+1) \\
&\quad - \sum_{n_C=0}^{N} n_C\mathbb{T}(n_C+1|n_C)\mathbb{P}(n_C) - \sum_{n_C=0}^{N} n_C\mathbb{T}(n_C-1|n_C)\mathbb{P}(n_C) \\
&= \sum_{n_C=0}^{N} (n_C+1)\mathbb{T}(n_C+1|n_C)\mathbb{P}(n_C) + \sum_{n_C=0}^{N} (n_C-1)\mathbb{T}(n_C-1|n_C)\mathbb{P}(n_C) \\
&\quad - \sum_{n_C=0}^{N} n_C\mathbb{T}(n_C+1|n_C)\mathbb{P}(n_C) - \sum_{n_C=0}^{N} n_C\mathbb{T}(n_C-1|n_C)\mathbb{P}(n_C) \\
&= \sum_{n_C=0}^{N} \mathbb{T}(n_C+1|n_C)\mathbb{P}(n_C) - \sum_{n_C=0}^{N} n_C\mathbb{T}(n_C-1|n_C)\mathbb{P}(n_C).
\end{aligned} \tag{2.11}$$

Plugging the expressions of transition rates in Eq. 2.7 into the last equation Eq. 2.11 leads to

$$\begin{aligned}
\langle n_C\rangle' &= \langle \mathbb{T}(n_C+1|n_C)\rangle - \langle \mathbb{T}(n_C-1|n_C)\rangle \\
&\approx k_1\cdot\langle n_C\cdot\frac{n_C}{N}\cdot\frac{n_D}{N}\rangle + k_2\cdot\langle n_C\cdot\frac{n_D}{N}\cdot\frac{n_D}{N}\rangle - k_3\cdot\langle n_D\cdot\frac{n_C}{N}\cdot\frac{n_C}{N}\rangle - k_4\cdot\langle n_D\cdot\frac{n_C}{N}\cdot\frac{n_D}{N}\rangle.
\end{aligned} \tag{2.12}$$

when $N, n_C, n_D >> 1$. As stated earlier, $N = n_C + n_D$ is a constant in the system.

We then define $x \equiv \frac{n_C}{N}$, and thus $\frac{n_D}{N} = 1 - x$. Dividing both sides of Eq. 2.12 by N, we find

$$\langle x \rangle' = k_1 \cdot \langle x^2(1-x) \rangle + k_2 \cdot \langle x(1-x)^2 \rangle - k_3 \cdot \langle x^2(1-x) \rangle - k_4 \cdot \langle x(1-x)^2 \rangle. \quad (2.13)$$

For sufficiently large populations, fluctuations around the average value are expected to be sufficiently small, and by ignoring correlations, we approximate the expected values with actual values and omit the angular brackets. Rearranging Eq. 2.14 and omitting angular brackets, we get

$$x' = x(1-x)\left[(k_1 x + k_2(1-x)) - (k_3 x + k_4(1-x))\right], \quad (2.14)$$

which recovers replicator dynamics with growth rates

$$\begin{bmatrix} r_C \\ r_D \end{bmatrix} = \begin{bmatrix} k_1 & k_2 \\ k_3 & k_4 \end{bmatrix} \begin{bmatrix} x \\ 1-x \end{bmatrix} = \begin{bmatrix} k_1 x + k_2(1-x) \\ k_3 x + k_4(1-x) \end{bmatrix}.$$

Compared with Eq. 2.3 , it is apparent that the values of k_i's should be

$$\begin{cases} k_1 &= R \\ k_2 &= S \\ k_3 &= T \\ k_4 &= P \end{cases}.$$

which correspond to the payoffs of focal players.

2.2.2 Individual-based rules involving 2 players in a game

Interactions between individuals in a chemical equation form with reaction rates k_i are

$$\begin{aligned} \overbrace{C}^{\text{focal}} + \overbrace{D}^{\text{opponent}} &\xrightarrow{k_1'} \overbrace{C}^{\text{focal}} + \overbrace{C}^{\substack{\text{opponet}\\ \text{replaced}}} \\ D \quad + \quad C \quad &\xrightarrow{k_2'} \quad D \; + \quad D \end{aligned} \tag{2.15}$$

Transition rates of Eq. 2.15 are

$$\begin{aligned} \mathbb{T}(n_C + 1 | n_C) &= k_1' \cdot n_C \cdot \overbrace{\frac{n_D}{N-1}}^{\substack{\text{randomly choosing}\\ \text{an opponent C}}} \\ \mathbb{T}(n_C - 1 | n_C) &= k_2' \cdot n_D \cdot \overbrace{\frac{n_C}{N-1}}^{\substack{\text{randomly choosing}\\ \text{an opponent C}}} \quad . \end{aligned} \tag{2.16}$$

Following the same derivation from Eq. 2.9 to Eq. 2.11 and plugging the expressions of transition rates in Eq. 2.16,

$$\begin{aligned} \langle n_C \rangle' &= \langle \mathbb{T}\left(n_C + 1 | n_C\right) \rangle - \langle \mathbb{T}\left(n_C - 1 | n_C\right) \rangle \\ &\approx k_1' \cdot \langle n_C \cdot \frac{n_D}{N} \rangle - k_2' \cdot \langle n_D \cdot \frac{n_C}{N} \rangle, \end{aligned} \tag{2.17}$$

when $N, n_C, c_D >> 1$. As before, $N = n_C + n_D$ is a constant in the system. We define $x \equiv \frac{n_C}{N}$ and thus $\frac{n_D}{N} = 1 - x$. Dividing both sides of Eq. 2.17 gives

$$\langle x \rangle' = k_1' \cdot \langle x(1-x) \rangle - k_2' \cdot \langle x(1-x) \rangle. \tag{2.18}$$

For large populations, the fluctuations around expected values are negligible, and by assuming the absence of higher-order correlation, we find

$$x' = (k_1' - k_2') x(1-x). \tag{2.19}$$

This mean field dynamics in the IBM2 model is quadratic in x assuming k_i's do not depend on information other than payoffs, rather than being cubic in x as expected in the replicator dynamics for the IBM3 model.

2.3 Conclusions

We have shown that the individual-based game rules based on the payoff matrix can recapitulate the mean-field replicator dynamics of the same payoff matrix with the master equation approach. The individual-based game rules are general yet flexible form two aspects. For one, we did not assign particular conditions on the value of the elements of the payoff matrix, so the approach is general enough to simulate various kinds of symmetric games, and possibly be able to capture the features of environment-dependent games. For the other, the rules can be easily adapted to both non-spatial and spatial simulations. In the following chapters, we will use the game rules developed in this chapter to address three questions: 1) How demographic noise and spatial extension alter the mean field dynamics predicted by the ordinary differential equations (ODE) model proposed in [18]. 2.) How the relative speed of environment and strategy in the ODE model proposed in [18] interacts with demographic noise and spatial extension. 3) How demographic noise and spatial extension alter the mean field dynamics while the environment intrinsically decays while also responds to the individual strategy [19].

CHAPTER 3
EFFECT OF DEMOGRAPHIC NOISE AND SPATIAL EXTENSION ON COEVOLUTIONARY GAMES

Adapted from Y.-H. Lin, and J. S. Weitz. (2019). Spatial Interactions and Oscillatory Tragedies of the Commons. Physical review letters 122(14), 148102.

3.1 Introduction

In the previous chapter, we discussed how a tragedy of the commons (TOC) can arise when individuals in the population play prisoner-dilemma (PD) games. However, in contrast to standard game theory assumptions, payoffs are unlikely to remain fixed after repeated decisions that degraded commonly-held resources. To address this issue, a recent model [18] considered dynamics arising given resource-dependent payoff matrices $A(n) = A_0(1-n) + A_1(n)$, which interpolate between A_0 and A_1, the payoff matrices given deplete and replete resource states, respectively, *i.e.*, $A(n) = \left[\begin{smallmatrix} R_0 & S_0 \\ T_0 & P_0 \end{smallmatrix}\right](1-n) + \left[\begin{smallmatrix} R_1 & S_1 \\ T_1 & P_1 \end{smallmatrix}\right]n$. This model of coevolutionary game dynamics included feedback with the environmental state denoted by $0 \leq n \leq 1$, such that

$$\epsilon \dot{x} = x(1-x)\left[r_C(x, A(n)) - r_D(x, A(n))\right], \tag{3.1}$$

$$\dot{n} = n(1-n)\left(\theta x - (1-x)\right). \tag{3.2}$$

where ϵ is a speed parameter and θ denotes the strength of cooperators in restoring the environment. In this coevolutionary model, the payoff matrices A_0 and A_1 can have markedly different Nash equilibria [20]. For example, when defection is uniformly favored when $n = 1$ and cooperation is favored when $n = 0$, then the system can exhibit a novel phenomenon termed an 'oscillatory tragedy of the commons' (o-TOC).

An o-TOC denotes a trajectory in the phase plan that approaches a heteroclinic cycle. Given a replete environment, the population rapidly switches from cooperation to defection, which then degrades the environment. In the depleted environment, cooperators re-establish, improving the environment, then defectors invade and the cycle repeats. Other outcomes, including a TOC and the aversion of a TOC can emerge given other payoff matrices [18].

We aim to simulate this coevolutionary game model with game rules derived in Ch. 2 and assess the influence of noise and spatially explicit interactions on the emergent dynamics of social context and resources.

3.2 Simulation details

In order to further evaluate stochastic dynamics of the IBM formulation, we simulated the joint dynamics of resources n and social context x using $N = 10^4$ individuals. A single time step over an interval Δt includes N game steps followed by changes in resource levels, $n(t)$ according to Eq. 3.2. Hence, in this formulation stochasticity is introduced only at the level of the individuals. Given the master equation analysis, we define reproduction rates k_i based on the current environmental state $n(t)$ (See section 3.2.1).

To study the combined effects of spatial structure and demographic noise (see [25]) we extended the IBM3 framework to a 2-dimensional fully occupied lattice with L sites per dimension given periodic boundary conditions, where the $N = L^2$ individuals are either cooperators or defectors. The focal player is selected at random, and the opponent is chosen randomly from the von Neumann neighborhood of the focal player. We denote the position of the focal player (opponent) as $\vec{r}_F$ ($\vec{r}_O$). The focal player reproduces with probability rate $k_m(s_F, s_O, \bar{n})$ given the strategy set of focal player and opponent, s_F and s_O, and the average local environment, $\bar{n} = (n(\vec{r}_F) + n(\vec{r}_O))/2$.

Environmental state dynamics $n(\vec{r}, t)$ are augmented by diffusion, i.e.,:

$$\frac{\partial n}{\partial t} = n(1-n)\left(\theta x - (1-x)\right) + D_n \nabla^2 n. \tag{3.3}$$

The diffusivity D_n controls the redistribution of resources relative to population dynamics. In the case of finite diffusion, the corresponding partial differential equation is replaced by its spatially discretized version (See section 3.2.2).

3.2.1 Non-spatial individual-based model

To simulate the coevolutionary dynamics in an individual-based, game-theoretic perspective, we adopt the individual-based game rules derived in section 2.2.1. We simulate N games sequentially to allow an equal chance of each individual to be involved in a game within a time step Δt. At the beginning of each time step, each player is labeled by an integer ranging from 1 to N. In practice, three randomly permuted series of individuals ranging from 1 to N are generated. The $i-$th elements in the three random number series represent the index of the focal player, the opponent, the individual to be replaced in the $i-$th game respectively. A random number $r \in [0, 1)$ is generated for each of N games, and the birth-death process happens if $r > k_i \Delta\tau = k_i \frac{\Delta t}{\epsilon}$. k_i is the reaction rate and depends on the strategies of the focal player and the opponent. We complete a time step by updating environment n with the second order Runge-Kutta method (RK2),

$$\begin{aligned} n(t+\Delta t) &= n(t) + \frac{\Delta t}{2}\left[\dot{n}(x_{old}(t), n(t)) + \dot{n}(x_{new}(t), n(t))\right] \\ &= n(t) + \frac{\Delta t}{2}\big[n(t)(1-n(t))\left(\theta x_{old}(t) - (1-x_{old}(t))\right) \\ &\qquad + n(t)(1-n(t))\left(\theta x_{new}(t) - (1-x_{new}(t))\right)\big], \end{aligned} \tag{3.4}$$

after N games. The subscript *old* denotes that the value of x in $\dot{n}$ is taken to be the one before N games, while the subscript *new* denotes that the value of x in $\dot{n}$ is

taken to be the one after N games. A simulation proceeds to the next time step after both x and n are updated and stops when the total number of time steps reaches an assigned simulation horizon. A brief description of RK2 is documented in 3.2.3.

3.2.2 Spatially-explicit individual-based model

We perform spatially-explicit simulations on a 2D $L \times L$ lattice. Each lattice site can only be occupied by a single player, either a cooperator or a defector. The rules for updating individual strategy in spatially-explicit simulations are similar to those in non-spatial simulations. Instead of generating three random number series, only a randomly permuted number series is generated to represent the index of the focal player in each game. The opponent player and the individual to be replaced are then chosen in the von Neumann neighborhood of the focal player.

After N sequential games, the spatial profile of the environment is updated in two steps.

$$\begin{aligned} n_{i,j,s}(t) &= n_{i,j}(t) + \frac{\Delta t}{2}\left[\dot{n}(x_{i,j,old}(t), n_{i,j}(t)) + \dot{n}(x_{i,j,new}(t), n_{i,j}(t))\right] \\ &= n_{i,j}(t) + \frac{\Delta t}{2}\big[n_{i,j}(t)(1-n_{i,j}(t))\left(\theta x_{i,j,old}(t) - (1 - x_{i,j,old}(t))\right) \\ &\quad n_{i,j}(t)(1-n_{i,j}(t))\left(\theta x_{i,j,new}(t) - (1 - x_{i,j,new}(t))\right)\big] \end{aligned} \tag{3.5a}$$

$$n_{i,j,f}(t+\Delta t) = \begin{cases} n_{i,j,s}(t) + D_n \frac{\Delta t}{\Delta x^2}(n_{i-1,j,s}(t) - 2n_{i,j,s}(t) + n_{i+1,j,s}(t) \\ \qquad +n_{i,j-1,s}(t) - 2n_{i,j,s}(t) + n_{i,j+1,new}(t)) & \text{for } D_n = 0 \text{ or } 1 \\ \frac{\Sigma_{i,j} n_{i,j,s}(t)}{L \cdot L}, & \text{for } D_n = \infty \end{cases} . \tag{3.5b}$$

The first step (Eq. 3.5a) accounts for change in n due to individual strategies adopted in previous games in the same time step with RK2. The second step accounts for diffusion was calculated with standard explicit forward-time centered-space method

(Eq. 3.5b). The subscripts i, j denote the value at coordinate (i, j). The subscript *old* in x_{old} again denotes the quantity before N games and the subcript *new* in x_{new} again denotes the updated quantity after N games. The subscript s in $n_{i,j,s}$ means the value of n is only affected by the individual strategies but has not yet accounted for the effect of diffusion. The subscript f in $n_{i,j,f}$ indicates this is the final value for n after a time step Δt. As before, a spatial simulation proceeds to the next simulation step after both x and n are updated.

3.2.3 Second order Runge-Kutta (RK-2) for numerical integration

Consider the ODE system $\dot{\vec{u}}(t) = f(t, \vec{u}(t))$, the 2-nd order Runge-Kutta (RK2) numerically finds the solution by computing two vectors

$$\begin{cases} \vec{K}_1 &= f(t, \vec{u})\Delta t \\ \vec{K}_2 &= f(t + \Delta t, \vec{u} + \vec{K}_1)\Delta t \end{cases} \tag{3.6}$$

and obtain the value of the next step $\vec{u}(t + \Delta t)$ with

$$\vec{u}(t + \Delta t) = \vec{u}_t + \frac{1}{2}(\vec{K}_1 + \vec{K}_2). \tag{3.7}$$

Essentially, RK2 estimates the change over a small time step Δt by multiplying the step size Δt with the averaged value of slope at the beginning, $\vec{K}_1/\Delta t = f(t, \vec{u}(t))$, and at the end of the step, $\vec{K}_2/\Delta t = f(t + \Delta t, \hat{\vec{u}}(t + \Delta t))$. The unknown value $\hat{\vec{u}}(t + \Delta t)$ is estimated to the first order, $\hat{\vec{u}}(t + \Delta t) = \vec{u}(t) + f(t, \vec{u}(t))\Delta t = \vec{u}(t) + \vec{K}_1$. Plugging in the estimation $\hat{\vec{u}}(t + \Delta t) = \vec{u} + \vec{K}_1$ back to $\vec{K}_2/\Delta t = f(t + \Delta t, \hat{\vec{u}}(t + \Delta t))$ recovers the form of $\vec{K}_2$ listed above.

In our system, $\vec{u}(t) = \begin{pmatrix} x(t) \\ n(t) \end{pmatrix}$. In the simulations $x(t + \Delta t)$ is determined by individual-based game rules, so we only need to calculate $n(t + \Delta t)$, the second

element in vector $\vec{u}(t+\Delta t)$

$$\begin{aligned} n(t+\Delta t) &= n(t) + \frac{1}{2}\left(K_{1,n} + K_{2,n}\right) \\ &= n(t) + \frac{\Delta t}{2}\left[\dot{n}(x(t), n(t)) + \dot{n}(\hat{x}(t+\Delta t), \hat{n}(t+\Delta t))\right] \end{aligned} \tag{3.8}$$

The subscript n denotes the second element in $\vec{K}_i$ vectors estimating the change in n. Being a continuous function, the change in n over a time step Δt is approximately $\dot{n}\Delta t$ to the first order of Δt. The second variable in $K_{2,n}$ is then $\hat{n}(t+\Delta t) = n(t)+\dot{n}(t)\Delta t = n(t) + K_{1,n}$. However, x is a discretized value given it is obtained by individual-based rules. Estimating the change in x over a time step h by $\dot{x}(x(t), n(t))\Delta t$ does not reflect the intrinsic demographic noise in x that we wanted to emphasize with the individual-based model. To incorporate the demographic noise in the calculation of $n(t)$ with RK2, we estimate the value of x before playing games, $x_{old}(t)$, to be $x(t)$, and x after playing games in the same time step, $x_{new}(t)$, to be $x(t+\Delta t)$. With all these factors considered, the modified RK2 for calculation of $n(t)$ in our hybrid simulation model is

$$\begin{aligned} n(t+\Delta t) &= n(t) + \frac{1}{2}\left(K_{1,n} + K_{2,n}\right) \\ &= n(t) + \frac{\Delta t}{2}\left[\dot{n}(x_{old}(t), n(t)) + \dot{n}\left(x_{new}, n(t) + \dot{n}(x_{old}(t), n(t))\Delta t\right)\right] \end{aligned} \tag{3.9}$$

3.3 Results and discussion

3.3.1 Non-spatial simulations

Consistent with our finding from the master equation, the simulation results of the individual-based model involving three players (IBM3) recapitulate predictions of the mean-field replicator dynamics model (see Fig. 3.1-bottom). Specifically, we identify seven distinct phases corresponding to the relative the magnitude of payoffs given the resource deplete state. The phases and their asymptotic behavior agree qualitatively

with mean-field predictions. In contrast, if the focal player reproduces and replaces the opponent (which we term IBM2, as is often assumed in two-player variants of spatial games), then the individual-based simulations diverge from predictions (see Fig. 3.1-top) as anticipated from expected mean field dynamics (see Chap. 2). There are two notable quantitative differences in the IBM3 simulations with respect to predictions from replicator dynamics. First, whereas mean-field dynamics predict convergence to a heteroclinic cycle (see 'o-TOC' region in Fig. 3.1-top), the IBM simulations stochastically reach an absorbing state on the boundary. Such a result is anticipated in any finite size simulation, given that heteroclinic cycles asymptotically approach the boundary. Second, the mean field model predicts closed periodic orbits given certain symmetric properties of A_0 and A_1 (corresponding to the line with slope $(T_1 - R_1)/(P_1 - S_1)$ in Fig. 3.1-bottom.) In contrast, the IBM simulations have demographic noise, which can lead to repeated oscillations with modulated amplitudes (see Fig. 3.2).

In addition to demographic noise, the method of numerical integration also has a minor effect on dynamics. With some numerical experiments, we found updating the environment with the Euler method, which only updates $n(t)$ to the first order of Δt,

$$n(t + \Delta t) = n(t) + \dot{n}(t)\Delta t, \tag{3.10}$$

could lead the system in the vicinity one of the absorbing states to be fixed in the absorbing state (see Fig. 3.3) - such variability is another hallmark of using finite populations for individuals and a continuous state space for resources. Although qualitative results agree,, we will report the simulation dynamics with RK2 in all the chapters except for Fig. 3.3

3.3.2 Spatial simulations

Simulations of coevolutionary game-environmental dynamics reveal dramatic changes in outcomes given spatially explicit interactions. Fig. 3.4 compares dynamics of non-spatial and spatial IBM models with three different diffusivities, $D_n = 0, 1, \infty$, classifying outcomes based on whether there is a TOC or not (the latter we term averted, see section for criteria).

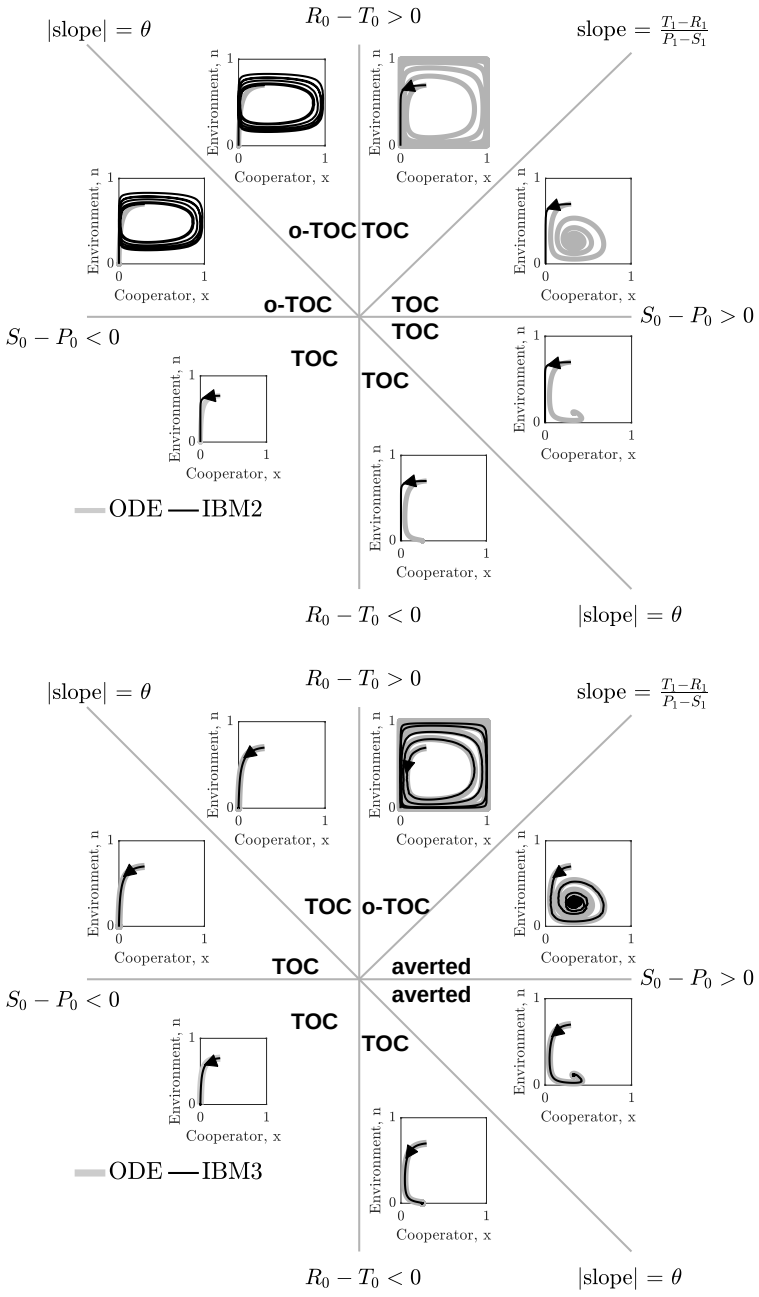

Figure 3.1: Coevolutionary dynamics of strategies and resources in replicator and IBM dynamics. (top) The dynamics with 'IBM2', in which offspring of the focal player replace the opponent. (bottom) The dynamics with 'IBM3', in which offspring of the focal player replaces a random individual. In both panels, parameter space is divided according to the sign of $R_0 - T_0$, $S_0 - P_0$. In each section in the parameter space, a phase diagram with different A_0 is shown, where the x-axis represents x and the y-axis denotes n. Light gray trajectories are mean field solutions and black trajectories denote IBM dynamics where arrows denote the flow of time. Visualized IBM trajectories are the average of 100 replicates with the same parameter set, except for oscillatory dynamics, given phase differences that can arise due to demographic noise. Common parameters for all replicates: $\theta = 2$, $\epsilon = 0.5$, $\Delta x = 1$, and $\Delta t = 0.05$, $A_1 = [3, 0; 5, 1]$; A_0 varies by region. Full parameter list for A_0 in Fig. 3.7.

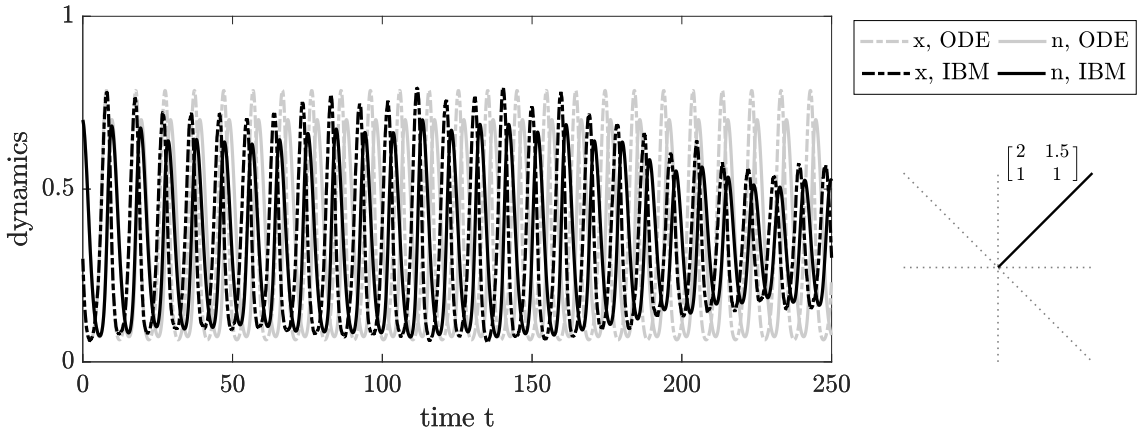

Figure 3.2: Demographic noise can alter the dynamical behaviors of the coevolutionary system. Persistent oscillations with varying amplitudes with IBM (black lines). The values of A_0 in this figure are $\left[2, 1.5; 1, 1\right]$.

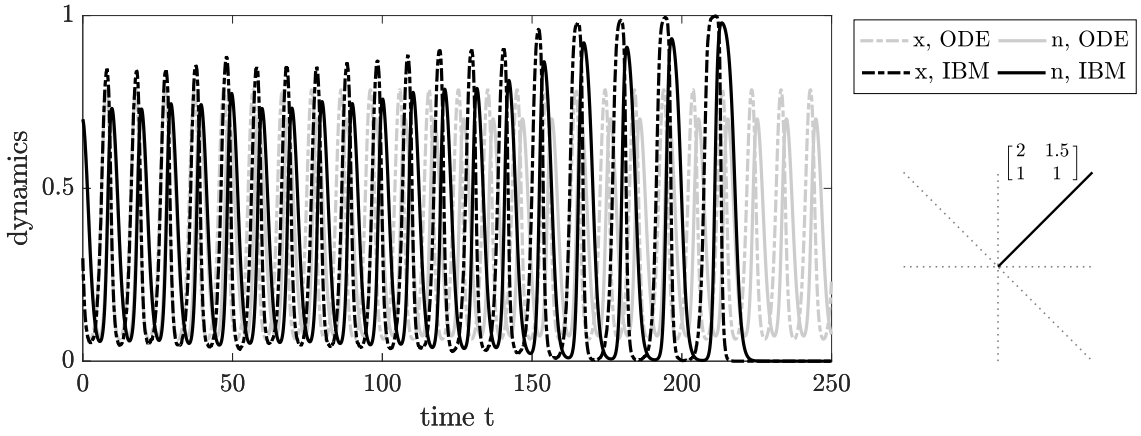

Figure 3.3: Numerical integration of lower order can be another factor altering the dynamical behaviors of the coevolutionary system and leads to an o-TOC. The values of A_0 in this figure are $\left[2, 1.5; 1, 1\right]$.

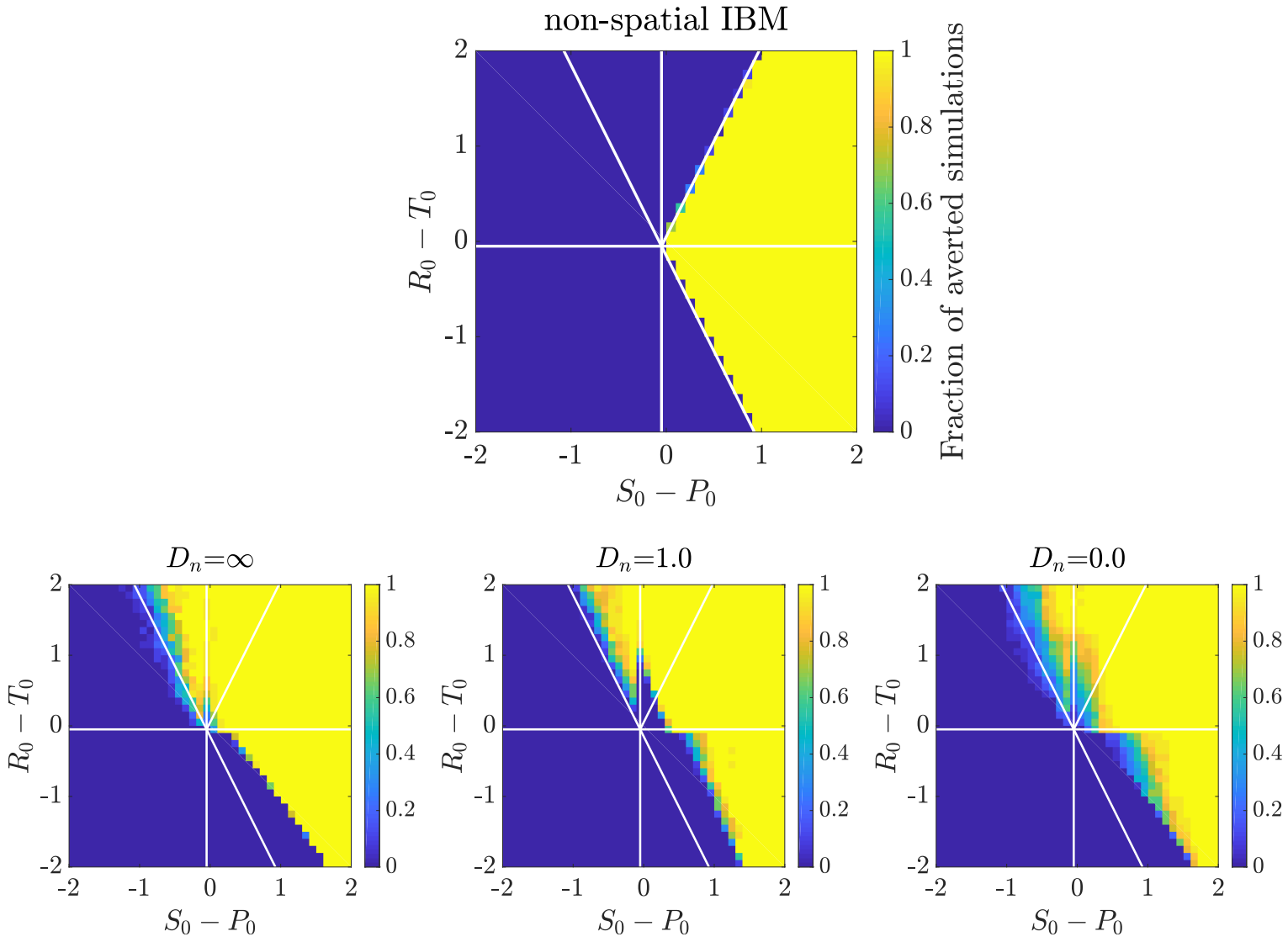

Figure 3.4: Strategy-resource dynamics given spatial interactions. Colors in each heat-map denote the fraction of averted dynamics out of 20 replicates with different A_0's. The horizontal axis of the heat maps are $S_0 - P_0$ and the vertical ones are $R_0 - T_0$. Each grid on the heat maps has increment 0.1. The diffusivity D_n is showed in the title of each panel. Other parameters for all replicates are $L = 100$, $\theta = 2$, $\epsilon = 0.5$, $\Delta x = 1$, and $\Delta t = 0.05$, $A_1 = [3, 0; 5, 1]$. The white lines mark out the boundary of different dynamics predicted by the mean field model. Full parameter list for A_0 in Fig. 3.8.

The heat maps show the proportion of averted cases among all replicates. Spatial interactions enable TOC aversion when cooperation is favored given a coordination game context ($R_0 > T_0$ and $S_0 < P_0$, could be a stag-hunt game as $n \approx 0$. See Fig. 3.4 upper left). However, spatial interactions also restrict the parameter regimes where a TOC can be averted given an anti-coordination game context ($R_0 < T_0$ and $S_0 > P_0$, could be a hawk-dove game as $n \approx 0$. See Fig. 3.4 bottom right). This observation is consistent with the previous findings that spatial extension can promote cooperation in stag hunt games and suppress cooperation in hawk-dove games [26]. For long-term dynamics, we find that oscillating dynamics are typical in $D_n = \infty$ cases. Such oscillatory dynamics can spiral inwards when TOC-s are averted or outwards to the boundary. Of note, amongst IBM models we only observe a persistent o-TOC when $D_n = \infty$; indicating the role of strong spatial coupling to induce oscillations. As shown in Fig. 3.5, oscillations are present across a large range of the $(S_0 - P_0) - (R_0 - T_0)$ parameter space. Some of the oscillations may lead to a TOC (Fig. 3.5(a)), while others may have various amplitudes but the population persists over multiple runs, in these cases until the end of the simulation (Fig. 3.5(b) - Fig. 3.5(d)). Given the absorbing conditions of the stochastic model, we cannot guarantee infinite-time persistence of oscillations in any finite simulation.

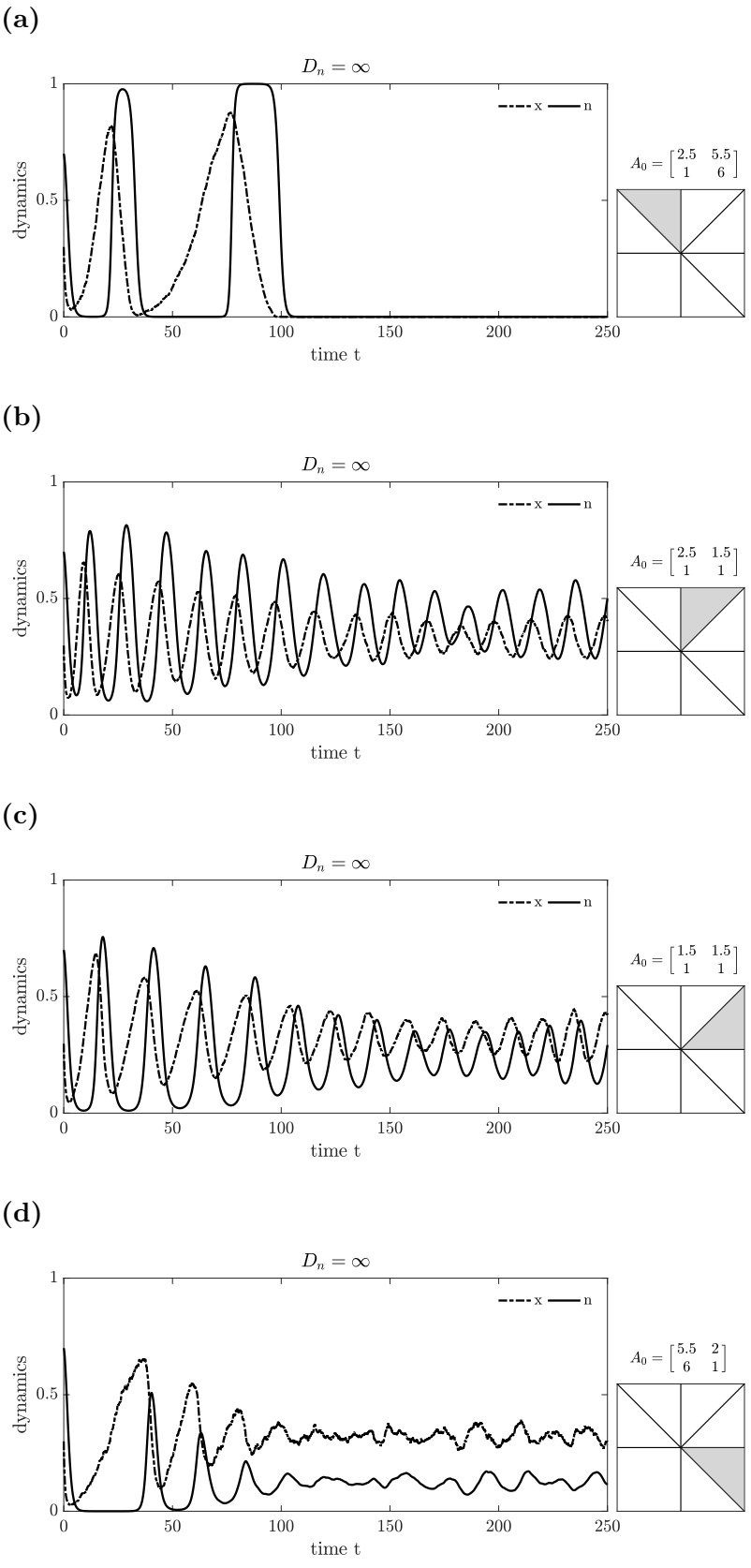

Figure 3.5: The oscillating dynamics are common with $D_n = \infty$ in a wide range of A_0. These four plots shows the temporal dynamics of a replicate with a specific A_0, and where it falls on the $(S_0 - P_0) - (R_0 - T_0)$ parameter space in the each inserted plot. The values of A_0's are (a) $\left[2.5, 5.5; 1, 6\right]$, (b) $\left[2.5, 1.5; 1, 1\right]$, (c) $\left[1.5, 1.5; 1, 1\right]$, and (d) $\left[5.5, 2; 6, 1\right]$, respectively.

We further investigated spatiotemporal dynamics focusing on variation in D_n given parameter regimes with both averted and TOC dynamics. These regimes correspond to the case where $S_0 < P_0$, $R_0 > T_0$ and where $R_0 > -\theta(S_0 - P_0) + T_0$ (see bottom panels of Fig. 3.4). The results of spatially explicit IBM3 model simulations are shown in Fig. 3.6 for $D_n = 0, 1$ and ∞. Notably, all cases appear to exhibit clustering amongst cooperators and the cases with heterogeneous environmental dynamics ($D_n = 0$ and $D_n = 1$) also appear to exhibit clustering between cooperators and environmental resource state. However, there are markedly different types of emergent spatial patterns give variation in the diffusivity of environmental resource state. In order to assess clustering quantitatively, we analyzed the joint structure of social context and resource levels by measuring the spatial cross-correlation function:

$$g_{CN}(r,t) = \frac{L^2}{\mathcal{A}(r)} \frac{\Sigma_{i,j}(\Sigma_{i',j'} x_{i,j}(t) \cdot n_{i',j'}(t))}{\Sigma_{i,j} x_{i,j}(t) \Sigma_{i,j} n_{i,j}(t)}, \tag{3.11}$$

and the spatial autocorrelation function of cooperator clustering:

$$g_{CC}(r,t) = \frac{L^2}{\mathcal{A}(r)} \frac{\Sigma_{i,j}(\Sigma_{i',j'} x_{i,j}(t) \cdot x_{i',j'}(t))}{(\Sigma_{i,j} x_{i,j}(t))^2}, \tag{3.12}$$

where $r < \sqrt{(i-i')^2 + (j-j')^2} \leq r + 1$, and $\mathcal{A}(r)$ denotes the number of lattice sites within this range in both cases. We then fit the short-range components of the observed correlation at a fixed time point to a decaying exponential, i.e., $g(r,t) \sim 1 + \alpha(t) e^{-r/\xi(t)}$ given pre-factor α and correlation length ξ.

The spatial autocorrelation analysis confirms the emergence of clustering amongst cooperators when the TOC is averted, i.e., $g_{CC}(r) > 1$ for $r \to 1$ (see black lines in the sub-panels of Fig. 3.6). Yet there are marked differences in the dynamics of the cross-correlation between cooperators and the environmental state.

For $D_n = 0$, the environment and cooperative population propagate outward as a wave. The cooperative population spreads leaving patches of resource replete

environments. The $g_{CN}(r)$ plots show that x and n can be positively correlated as a wave initiates but negatively correlated once defectors invade and replace resource replete environments, leading to (often disjoint) patchy distributions of both resources and cooperators. In contrast, for $D_n = 1$, small clusters of cooperators and localized resources form after initial transient dynamics. This feature is captured by the $g_{CN}(r)$ analysis, revealing strongly elevated cross-correlation (see the middle row of Fig. 3.6) as well as similar pattern in the dynamics of $g_{CC}(r)$ and $g_{CN}(r)$. We note that these 'gangs' of cooperators and their environmental 'tail' are chased by a dominant group of defectors (see [27] for related findings in evolutionary PD models without environmental feedback). Finally, given $D_n = \infty$, the resources are uniform across space. Cooperative clusters grow towards system sizes due to the strong spatial coupling mediated via fast resource diffusivity. The single large cooperator cluster expands and shrinks over time with increasing amplitude, as evidenced by the elevated autocorrelation of $g_{CC}(r)$ in the bottom row of Fig. 3.6, with rapid switches in resource state, leading to an eventual collapse of the cooperator population. We do not report $g_{CN}(r)$ given the uniform distribution of resources given $D_n = \infty$.

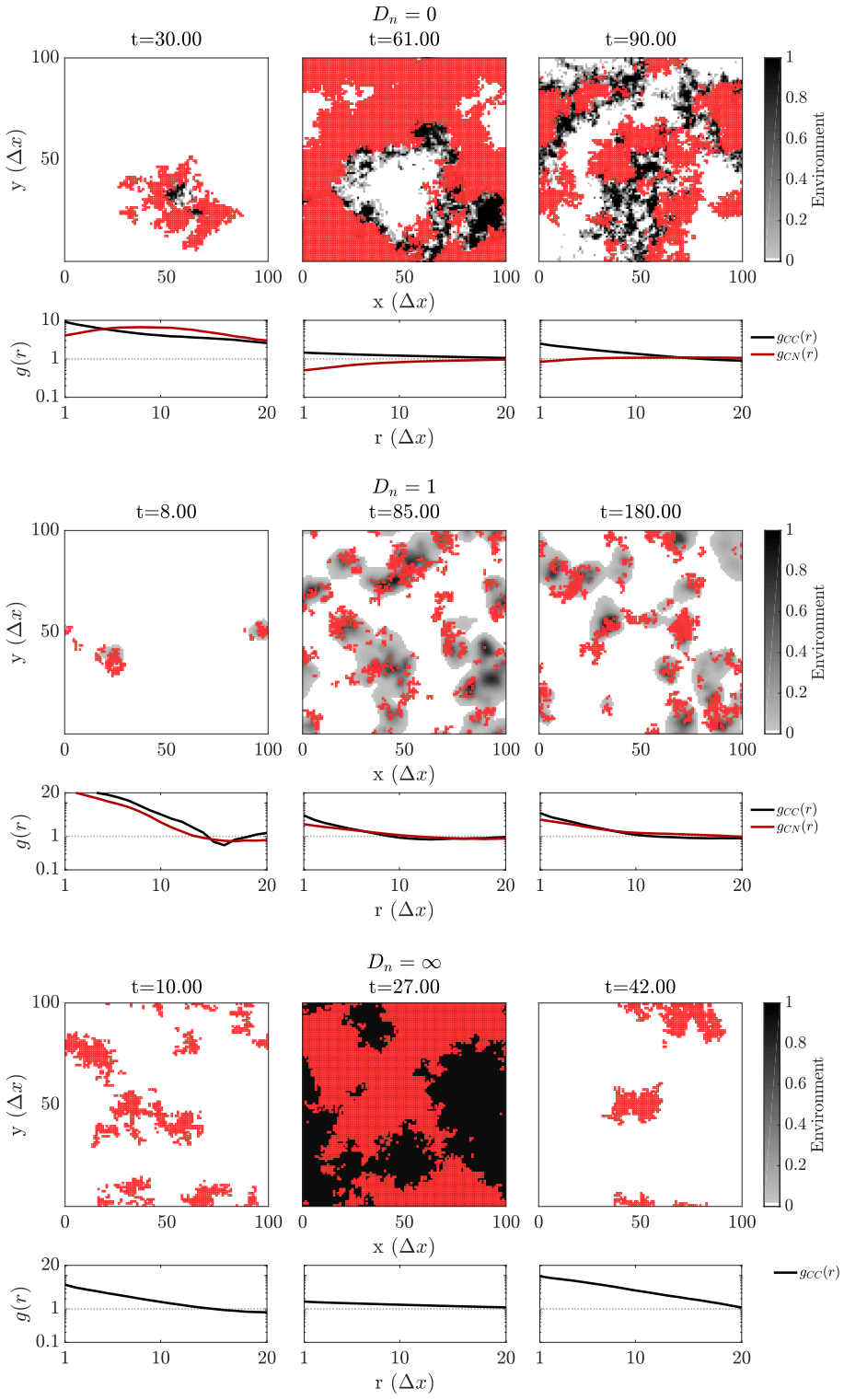

Figure 3.6: Spatiotemporal dynamics of resources and cooperation. The background color represents the environment, while a red square means a cooperator occupies the lattice site. The empty sites are occupied by defectors. (Top row) $D_n = 0$, a circular wave of cooperative population propagates outward. (Middle row) $D_n = 1$, a few small patches of cooperators move around and divide. (Bottom row) $D_n = \infty$, a large cooperator cluster expands and shrinks over time with increasing amplitude until extinction.

3.4 Conclusions

In summary, we have developed an individual-based framework to incorporate the effects of demographic noise and spatial interactions [25] in coevolutionary game dynamics that couple individual strategies and the environment. The IBM involving three players in a game recapitulates and generalizes earlier findings from a coevolutionary game model, including the emergence of an oscillatory tragedy of the commons [18]. Spatial interactions can shift the domains in which a tragedy of the commons may arise when compared to non-spatial models [28]. Spatially explicit dynamics also lead to novel, coherent spatiotemporal patterns [29, 30, 31, 32, 33], including diffusive clusters, flickering, and wave-like patterns. These joint dynamics of resources and social strategies suggest multiple avenues for future study, including formally deriving effective PDEs to characterize whether the system permits propagating waves in the large system limit. It will also be critical to evaluate the extent to which spatial interactions modify strategy-environment feedback in proposed generalizations [19] of the replicator framework underlying the present work [18] and in stochastic games with feedback between behavior and public good states [34]. Finally, the spatial framework developed here may also aid efforts to understand how microorganisms produce and utilize public goods, *e.g.,* siderophores – extracellular iron harvesting enzymes, as but one example of many [35, 36, 37, 38, 39, 40, 41, 42]. Given increasing pressures on limited resources, we intend to leverage prior work on controlling mean-field strategy-environment dynamics [43] to identify ways in which local manipulation of resources, strategies, and/or perceptions can help stabilize and conserve the commons.

3.5 Appendix

3.5.1 Simulation parameters

We choose $\Delta x = 1$ and $\Delta t = 0.05$ to ensure the stability of 2D diffusion. Stability is ensured when $D_n \frac{\Delta t}{\Delta x^2} \leq \frac{1}{4}$ [44]. We use periodic boundary conditions for spatial simulations. The scaling value $\epsilon = 0.5$ was further chosen so that $\Delta\tau = \Delta t/\epsilon = 0.1$. This assures the largest transition probability of a birth-death process $k_i\Delta\tau$ will be smaller than 1 given payoff matrix values in the simulations. The model parameters are in arbitrary simulation units, and the values other than A_0 are shown in Table 3.1.

The parameters of simulations in Fig. 3.1 are shown in Table 3.1 and Fig. 3.7. In Fig. 3.1, each plot for stochastic individual-based model dynamics are averaged over 100 replicates except for oscillatory dynamics, given phase differences that can arise due to demographic noise. The parameters except for D_n of simulations in Fig. 3.4 are shown in Table 3.1 and Fig. 3.8. D_n is specified on each panel of Fig. 3.4 in the main text. The axes of heat maps ranging from -2 to 2, linearly increase with difference 0.1 on both the horizontal axis, $S_0 - P_0$ and the vertical axis, $R_0 - T_0$. There are thus $41 \cdot 41 = 1681$ grid points on each heat map. The value of each grid on the heat maps is the average over 20 replicates, representing a total of $41 \cdot 41 \cdot 20 \cdot 4 = 134480$ simulations in Fig. 3.4. The parameters except for D_n of simulations in Fig. 3.6 are shown in Table 3.1 and $A_0 = \left[\begin{smallmatrix} 2.5 & 5.5 \\ 1 & 6 \end{smallmatrix}\right]$. D_n is specified on each panel of Fig. 3.6 in the main text.

3.5.2 Classification criteria for TOC and averted dynamics

To separate quasi-periodic dynamics from an oscillating TOC, we categorize a simulation as by finding the difference between consecutive peaks and valleys in the environment $n(t)$, δn, and in the fraction of cooperators $x(t)$, δx. If the maximum δn or δx is larger than the threshold $1 - 2\delta$, it indicates the dynamics are an oscillating

Table 3.1: Model parameter values in simulation units.

Variable	Value
A_1	$\left[\begin{smallmatrix} 3 & 0 \\ 5 & 1 \end{smallmatrix}\right]$
A_0	see below for each figure
N	10000
ϵ	0.5
θ	2
D_n	$[0, 1, \infty]$
L	100
(x_0, n_0)	$(0.3, 0.7)$

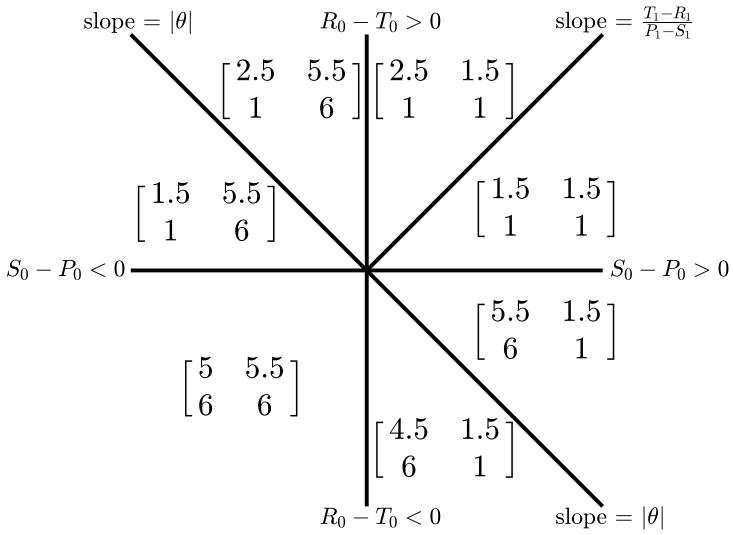

Figure 3.7: The values of matrix $A_0 = \left[R_0, S_0; T_0, P_0\right]$ in each section on the parameter space of Fig. 3.1 in the main text.

TOC because of the considerable variation in magnitude. δ is a smaller number set to be 0.01. Otherwise, we then take the mean of the final 20% time series of $x(t)$ and $n(t)$, i.e., $\bar{x}$ and $\bar{n}$ respectively. If $\bar{n} < \delta$, this simulation replication is classified as a TOC because the environment is depleted in the latter part of the simulation regardless of what the value of x is. Otherwise, a TOC is averted.

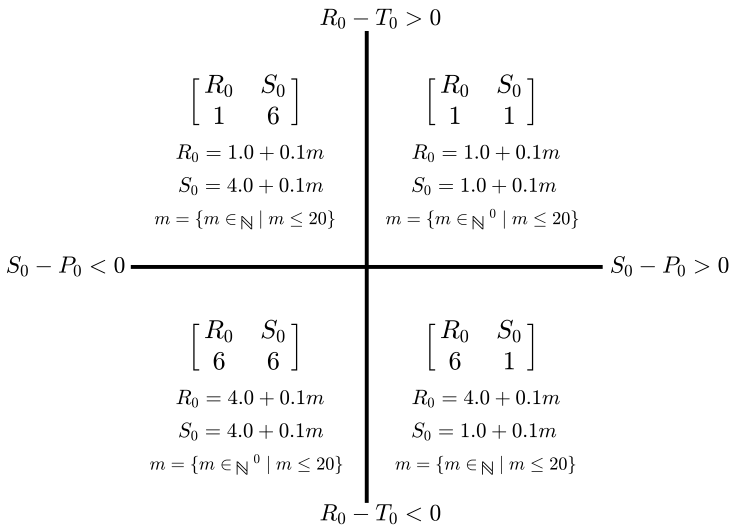

Figure 3.8: The values of matrix $A_0 = \left[R_0, S_0; T_0, P_0\right]$ in each section on the parameter space of Fig. 3.4 in the main text.

3.5.3 A brief analysis of Mean-field IBM2 System

Interactions between individuals in a chemical equation form with reaction rates k_i are

$$\begin{aligned} \overbrace{C}^{\text{focal}} + \overbrace{D}^{\text{opponent}} &\xrightarrow{k_1'} \overbrace{C}^{\text{focal}} + \overbrace{C}^{\substack{\text{opponet} \\ \text{replaced}}} \\ D + C &\xrightarrow{k_2'} D + D \end{aligned} \tag{3.13}$$

For large populations, the fluctuations around expected values are negligible, and by assuming the absence of higher-order correlation, we find

$$x' = (k_1' - k_2')x(1 - x). \tag{3.14}$$

The IBM2 model is quadratic in x assuming k_i's do not dependent on information other than payoffs. However, k_i's still depend on environment n. In the simulations, $k_1' = S(n) = S_0(1-n) + S_1 n$ and $k_2' = T(n) = T_0(1-n) + T_1 n$. The mean-field ODEs

now become

$$\begin{aligned} x' &= x(1-x)(\delta_0(1-n)+\delta_1 n) \\ n' &= n(1-n)(\theta x-(1-x)) \end{aligned} \tag{3.15}$$

with $\delta_0 \equiv S_0 - T_0$ and $\delta_1 \equiv S_1 - T_1$. The (possible) fixed points are $(x,n) = (0,0),(1,0),(0,1),(1,1)$ and (x^*,n^*) that lies within the unit square. To ensure $x'(x^*,n^*)=0$ and $n'(x^*,n^*)=0$,

$$\begin{aligned} \delta_0(1-n^*)+\delta_1 n^* &= 0 \\ \theta x^* - (1-x^*) &= 0 \end{aligned} \tag{3.16}$$

must be satisfied at the internal fixed point.

The diagonal elements of the Jacobian around the internal fixed point are

$$\begin{aligned} J_{11} &= \frac{\partial x'}{\partial x}|_{x^*,n^*} = [(1-x^*)-x^*](\delta_0(1-n^*)+\delta_1 n^*) = 0 \\ J_{22} &= \frac{\partial n'}{\partial n}|_{x^*,n^*} = [(1-n^*)-n^*](\theta x^* - (1-x^*)) = 0. \end{aligned} \tag{3.17}$$

The 0 elements on the diagonal indicate that neutral orbits are possible in mean-field IBM2. To further prove the existence of neutral orbits in the mean-field IBM2 system, we need to obtain the constant of motion. Dividing the equations in Eq. (6) gives

$$\frac{dx}{dn} = \frac{x(1-x)(\delta_0(1-n)+\delta_1 n)}{n(1-n)(\theta x-(1-x))}, \tag{3.18}$$

such that

$$\int \frac{\theta x-(1-x)}{x(1-x)}dx = \int \frac{\delta_0(1-n)+\delta_1 n}{n(1-n)}dn. \tag{3.19}$$

The integral on the left hand side of Eq. (10) is

$$\int \frac{\theta x-(1-x)}{x(1-x)}dx = -\theta \ln(1-x) - \ln x + Const. \tag{3.20}$$

The integral on the right hand side of Eq. (10) is

$$\int \frac{\delta_0(1-n)+\delta_1 n)}{n(1-n)}dn = \delta_0 \ln n - \delta_1 \ln(1-n). \tag{3.21}$$

Combing Eq. (11) and (12) leads to

$$H = \delta_0 \ln n - \delta_1 \ln(1-n) + \theta \ln(1-x) + \ln x = Const. \tag{3.22}$$

H is the constant of motion becasue

$$H' = \frac{\partial H}{\partial x}x' + \frac{\partial H}{\partial n}n' = 0. \tag{3.23}$$

CHAPTER 4
THE SPEED PARAMETER OF COEVOLUTIONARY GAMES

4.1 Introduction

In a more general form, we could write a coupled nonlinear ODE systems in this form,

$$\begin{aligned} \epsilon \dot{u} &= f(u, v) \\ \dot{v} &= g(u, v). \end{aligned} \tag{4.1}$$

The dynamics of coevolutionary games we have studied in the previous chapters is of the same form with $x \coloneqq u$ and $n \coloneqq v$. The parameter ϵ represents the relative speed of u compared to v. Because the magnitude of $\dot{u}$ is inversely proportional to ϵ, a small ϵ indicates u is much faster than v, and vice versa.

With a fundamental understanding of how demographic noise and spatial extension could affect environment-dependent coevolutionary games, we would like to further focus on the possible effects of the relative speed of the social context dynamics to the environmental dynamics. The interest arises due to the observations that relative speed could change the features of system dynamics in some ways illustrated below.

One of the well-known effects of parameter ϵ is to change the stability of the fixed points in addition to the relative speed of coupled dynamics. The FitzHugh-Nagumo model, a canonical set of equations often used to study excitable media, fully illustrates the effects of ϵ on stability [45, 46]. The FitzHugh-Nagumo model can be written as

$$\begin{aligned} \epsilon \dot{u} &= 3u - u^3 - v + I_{\text{ext}} \\ \dot{v} &= u - a - bv, \end{aligned} \tag{4.2}$$

and it is clear that the value of the fixed point (u^*, v^*) that satisfies $\epsilon\dot{u} = 0$ and $\dot{v} = 0$ is independent of ϵ. However, the stability of the fixed point changes even all other parameters except ϵ remain the same. Fig. 4.1 shows how the system dynamics vary with ϵ. For sufficiently large ϵ, the fixed point marked with an empty circle is unstable (Fig. 4.1, upper left). The phase trajectory starts from the initial point is thus attracted to the limited cycle, displaying persistent oscillations (Fig. 4.1, upper right). On the other hand, a smaller ϵ indicates a stable fixed point with the same value, (u^*, v^*) (the solid circle on Fig. 4.1, bottom left). The phase trajectory would be attracted to the stable fixed point with a smaller ϵ. The temporal dynamics without persistent oscillations are shown on the bottom right corner on Fig. 4.1.

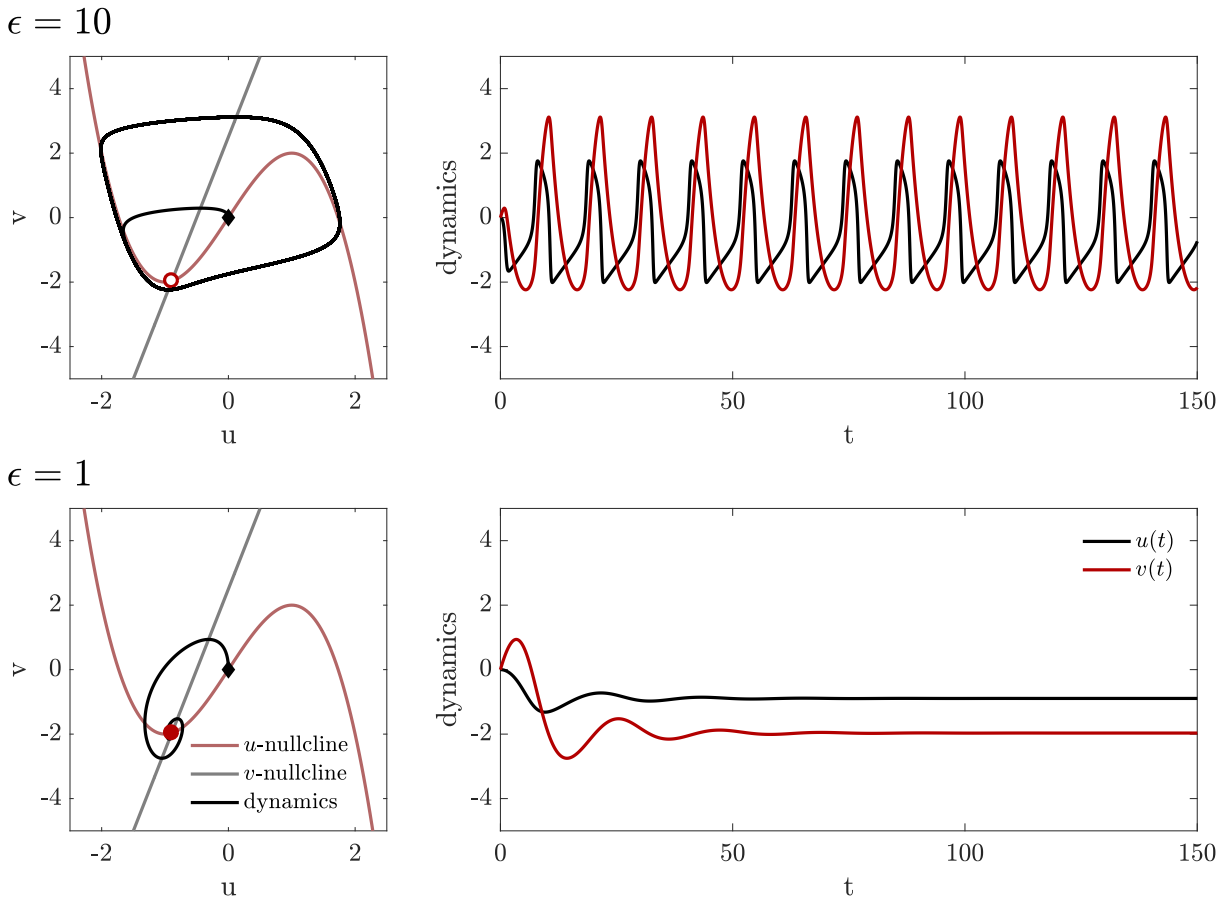

Figure 4.1: Solutions of the FitzHugh-Nagumo model with different ϵ. The system Eq. 4.2 displays persistent oscillations with $\epsilon = 10$ (top row) but approaches the fixed point with $\epsilon = 1$ (bottom row). On each row, the nullclines and the dynamical trajectory are plotted on the phase plane (left panel). The solid diamond marks the initial condition, and the empty (solid) circle stands for the unstable (stable) fixed point. The temporal dynamics of $u(t)$ and $v(t)$ are plotted on the right panel. The other parameters for the model are $I_{ext} = 0$, $a = -0.5$, $b = 0.2$, $u(0) = 0$, and $v(0) = 0$.

In addition to the present of persistent cycles, the relative speed of different biological process can also alter other features of ecological dynamics. A biologically relevant example of how the speed parameter matters is the time scale of the evolutionary process in prey-predator models. Classical ecological models of prey-predator systems, such as the Lotka-Volterra equations [47, 48], only consider the cases in which evolution is much slower than population dynamics, i.e., life history traits do not change much while the population size varies. However, this is not always the case. For some biological systems, individuals can reproduce and die at a rate much faster than that of change in total population sizes, so that the life history traits composition of a population differs when the population size remains about the same. Systems with rapid evolution have cycles of different features compared to the classical Lokta-Volterra model. For example, rapid evolution could result in peaks of predator leading peaks in prey while Lokta-Volterra predicts the reverse [49, 50, 51].

Although the previous paper by Weitz *et. al.* has shown the system dynamics of the coevolutionary games are qualitatively invariant for all ϵ [18], it is not clear whether this statement remains valid when demographic noise and spatial component is incorporated. To study the interactions between these three factors, we adopted the simulation model developed in previous chapters and report the results to identify possible mechanisms in altering the coevolutionary dynamics involving different ϵ.

4.2 Simulation details

The simulation model of non-spatial and spatial IBM is the same as described in chapter 3.2.1. For non-spatial simulations, a time step consists of N games in which the focal player, the opponent, and the individual replaced by the offspring of the focal player are randomly chosen, followed by environment updates based on the social context after the N games. For spatial simulations, the opponent and the individual replaced are chosen from the focal player's von Neumann neighborhood.

After N games, local environment not only reacts to local social context but also able to diffuse in spatial simulations. See chapter 3.2.1 for more details in implementation of simulations.

4.3 Results and discussion

4.3.1 Non-spatial simulations

Similar to results reported in chapter 3.3.1, the vast majority of IBM3 simulations recapitulates the dynamics predicted by the ODE system

$$\begin{aligned} \epsilon\dot{x} &= x(1-x)(r_C(x,n) - r_D(x,n)) \\ \dot{n} &= n(1-n)(\theta x - (1-x)). \end{aligned} \tag{4.3}$$

We again divide the parameter space according to the relative magnitude of elements of A_0 into seven sections (See Fig. 4.2) with distinct dynamics. For smaller relative speed, $\epsilon = 0.1$ and $\epsilon = 1$, all the simulations agree with ODE solutions.

However, an exception rises in non-spatial simulations with $\epsilon = 10$. The only exception happens at $\epsilon = 10$ and $A_0 = \left[\begin{smallmatrix} 2.5 & 5.5 \\ 1 & 6 \end{smallmatrix}\right]$ (See Fig. 4.3(a), upper-left section), where the ODE predicts a monotonic TOC. While most non-spatial IBM dynamics with $\epsilon = 10$ and $A_0 = \left[\begin{smallmatrix} 2.5 & 5.5 \\ 1 & 6 \end{smallmatrix}\right]$ resemble the ODE solution, 1 out of 20 simulations behaves like an o-TOC (see FIG. 4.3(b)). Although the exact mechanism for this exception is not identified, we might be able to explain it with an intuition of the probabilistic birth-death process in IBM3. While ϵ stands for the relative speed of environment dynamics to the social context dynamics in the ODE model, it may also be interpreted as the inverse of the reproduction rate under the IBM3 framework. The difference of reproduction rates between individuals of different strategies, $(r_C(x,n) - r_D(x,n))/\epsilon$, is smaller as ϵ becomes larger. With comparable reproduction probabilities of different strategies, the cooperators could have little but not infinitely

small chance to invade even when the the environment is not ideal for them [52], and thus leads to an o-TOC in a usually TOC regime.

(a) $\epsilon = 0.1$

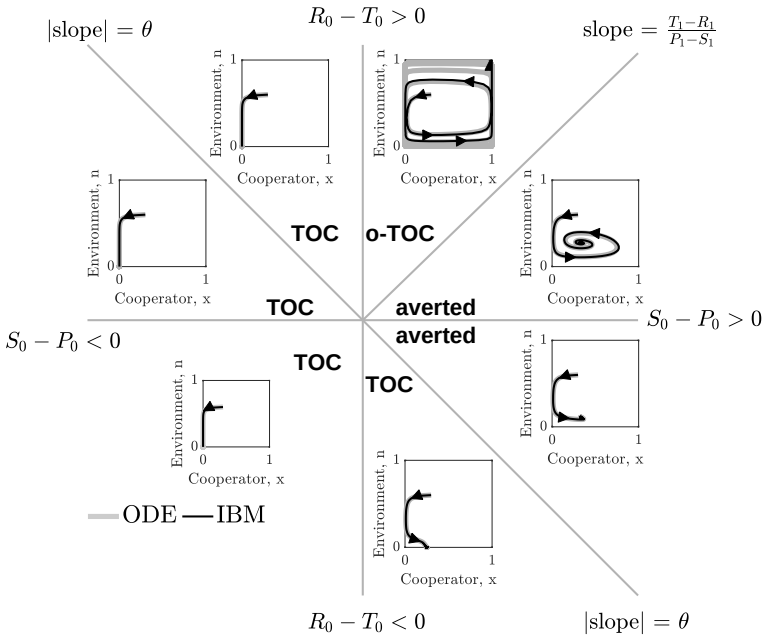

(b) $\epsilon = 1.0$

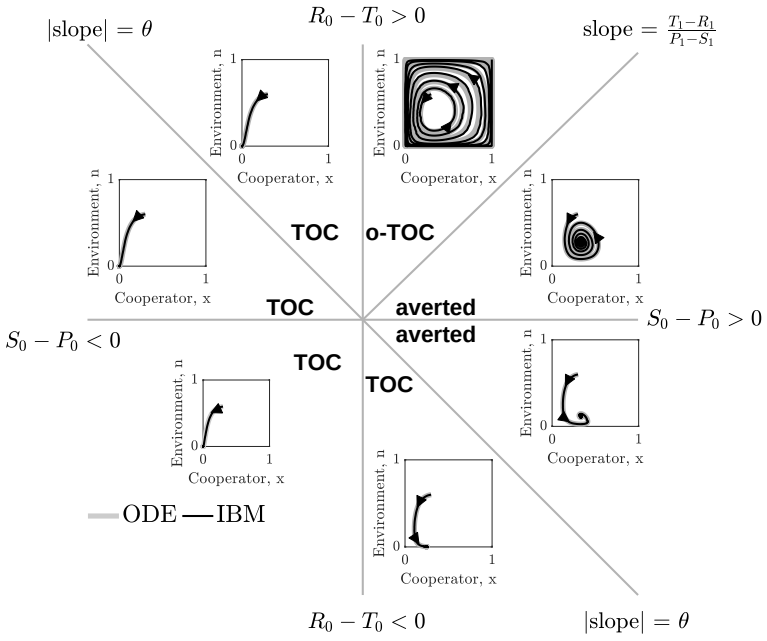

Figure 4.2: Coevolutionary dynamics of strategies and resources of non-spatial IBM dynamics. (top) The dynamics with $\epsilon = 0.1$, (bottom) the dynamics with $\epsilon = 1$. In all panels, parameter space is divided according to the sign of $R_0 - T_0$, $S_0 - P_0$. In each section in the parameter space, a phase diagram with different A_0 is shown, where the x-axis represents x and the y-axis denotes n. Light gray trajectories are mean field solutions and black trajectories denote IBM dynamics where arrows denote the flow of time. Visualized IBM trajectories are the average of 20 replicates with the same parameter set, except for oscillatory dynamics, given phase differences that can arise due to demographic noise. Common parameters for all replicates: $\theta = 2$, $\Delta x = 1$, and $\Delta t = 0.001$, $A_1 = [3, 0; 5, 1]$; A_0 varies by region. Full parameter list for A_0 in Fig. 4.11.

(a) $\epsilon = 10.0$

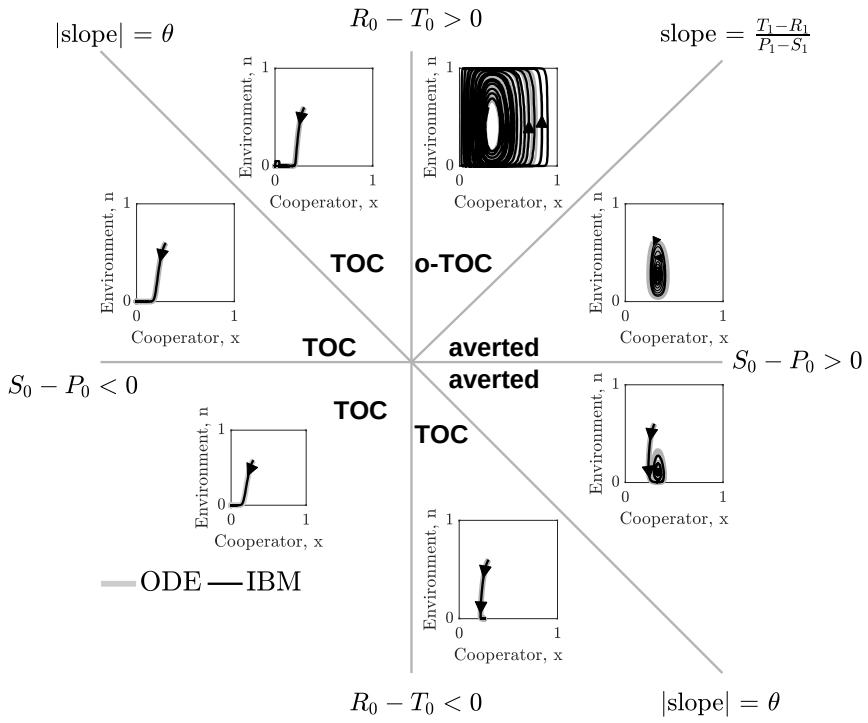

(b) an o-TOC in TOC region

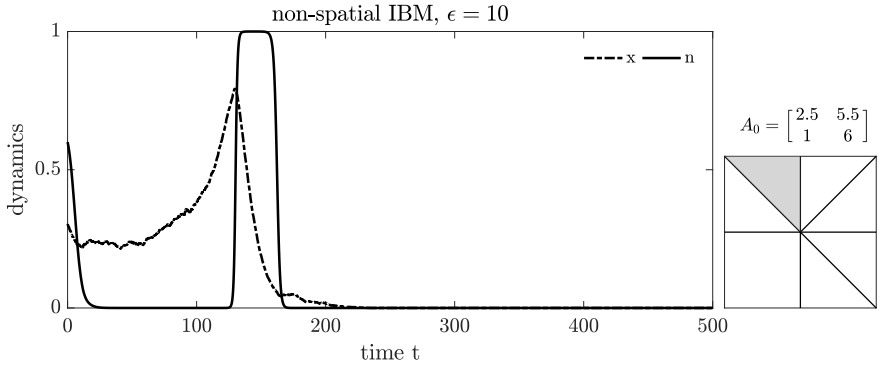

Figure 4.3: Coevolutionary dynamics of strategies and resources of non-spatial IBM dynamics. (top) The dynamics with $\epsilon = 10$, (bottom) temporal dynamics of the o-TOC arising in a TOC region. In the top panel, parameter space is divided according to the sign of $R_0 - T_0$, $S_0 - P_0$. In each section in the parameter space, a phase diagram with different A_0 in is shown, where the x-axis represents x and the y-axis denotes n. Light gray trajectories are mean field solutions and black trajectories denote IBM dynamics where arrows denote the flow of time. Visualized IBM trajectories are the average of 20 replicates with the same parameter set, except for oscillatory dynamics, given phase differences that can arise due to demographic noise. An o-TOC happens at the regime where the ODE system predicts a monotonic TOC. Common parameters for all replicates: $\theta = 2$, $\Delta x = 1$, and $\Delta t = 0.001$, $A_1 = [3, 0; 5, 1]$; A_0 varies by region. Full parameter list for A_0 in Fig. 4.11.

4.3.2 Spatial simulations

As shown in chapter 3.3.2, the dynamics of spatial simulations with different ϵ diverge from the those of non-spatial simulations and ODE solution. Among all ϵ we simulated, we can still observe the spatial coupling mediated by $D_n = \infty$ induced oscillations with a wide range of A_0 (FIG. 4.4).

(a) $\epsilon = 0.1$, $D_n = \infty$

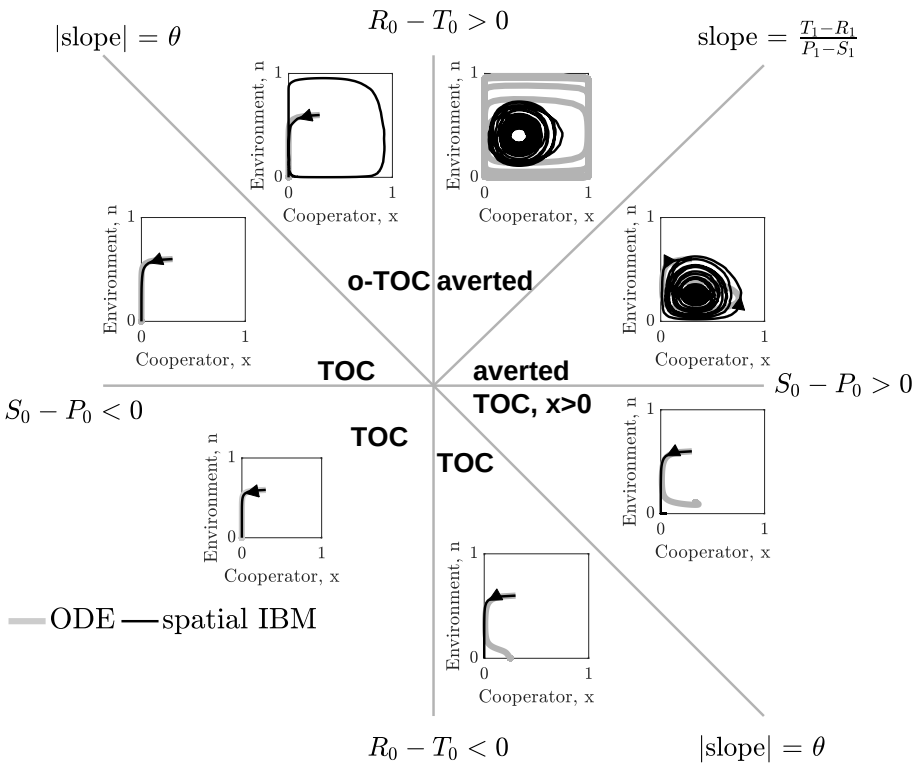

(b) $\epsilon = 1.0$, $D_n = \infty$

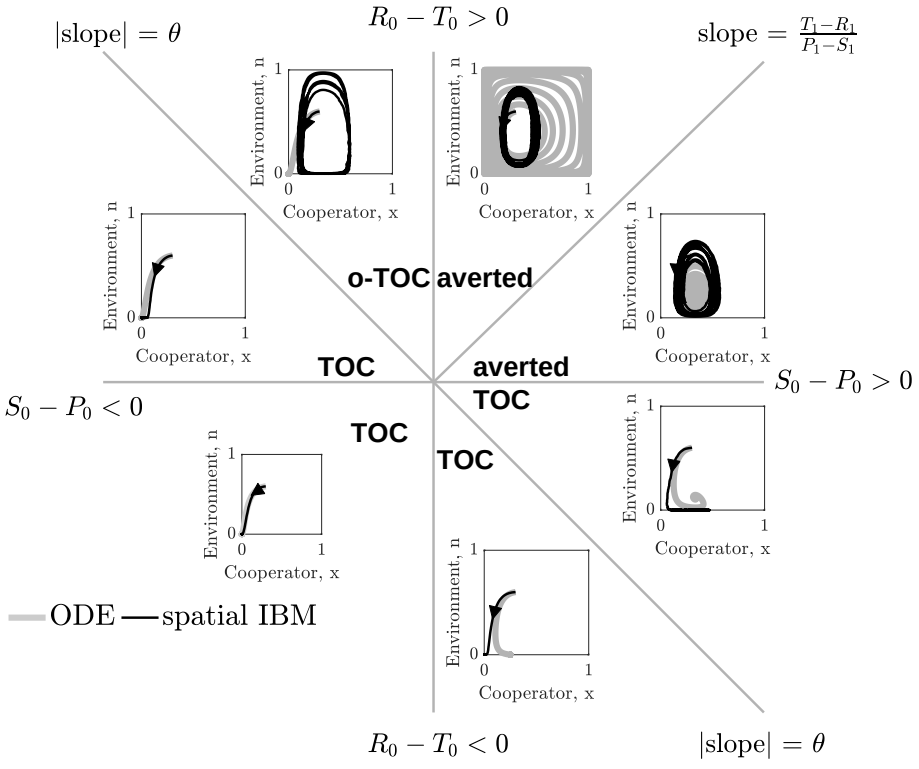

(c) $\epsilon = 10.0$, $D_n = \infty$

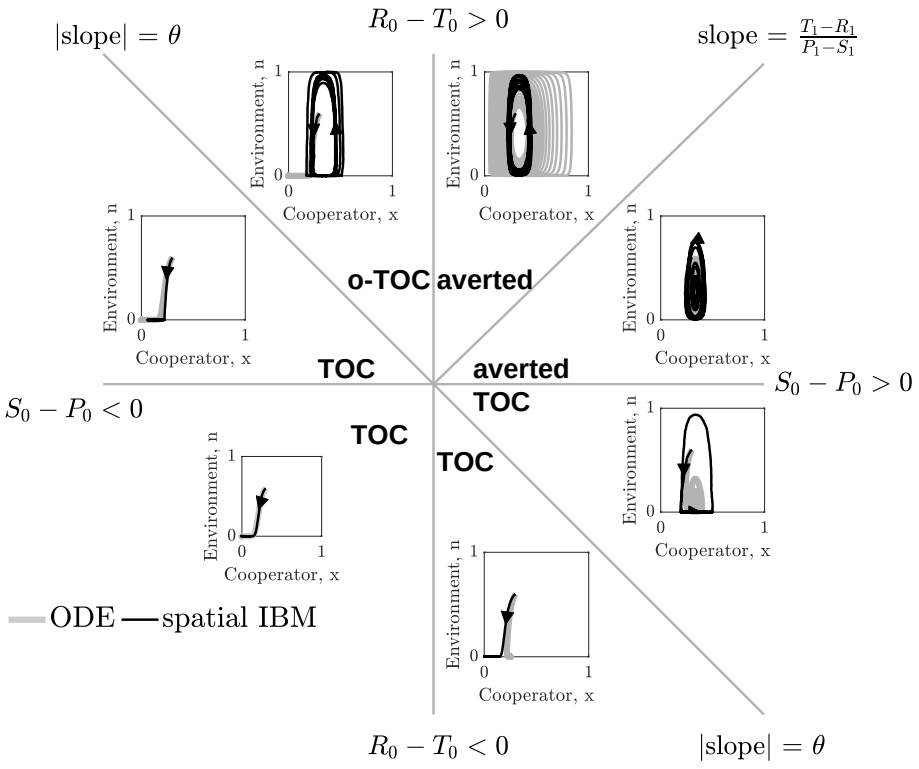

Figure 4.4: Oscillations are observed over a wide range of A_0 in spatial coevolutionary dynamics of strategies and resources with $D_n = \infty$. (a) The dynamics with $\epsilon = 0.1$, (b) the dynamics with $\epsilon = 1$, and (c) the dynamics with $\epsilon = 10$. In all panels, parameter space is divided according to the sign of $R_0 - T_0$, $S_0 - P_0$. In each section in the parameter space, a phase diagram with different A_0 in is shown, where the x-axis represents x and the y-axis denotes n. Light gray trajectories are mean field solutions and black trajectories denote IBM dynamics where arrows denote the flow of time. $\theta = 2$, $\Delta x = 1$, and $\Delta t = 0.001$, $A_1 = [3, 0; 5, 1]$; A_0 varies by region. Full parameter list for A_0 in Fig. 4.11.

Of all ϵ-s considered, simulations with $D_n = 1$ appear to be more vulnerable to TOCs for $\epsilon = 1$ and $\epsilon = 10$. On Fig. 4.5 and Fig. 4.6, we can see simulations with $D_n = 1$ can only be averted in the first quadrant on the A_0 parameter space. The finite diffusivity of the environment could provide the basis for resolving this discrepancy. Unlike the case with infinite diffusivity, where all individuals could benefit from a small amount of shared enhancement of environment due to cooperation, only a small group of defectors on the interface in contact with cooperators can utilize the enhanced environment from their cooperative neighbors when the diffusivity is finite. The enhanced environment shared among a small group of defectors significantly increases their fitness. A finite diffusivity is also better for the defectors than $D_n = 0$ because the defectors do not need to successfully reproduce and replace one of the cooperative neighbors with some chance to utilize the localized enhanced environment. Instead, the enhanced environment diffuses to the defectors on the interface deterministically and passively, so the defectors automatically gain higher payoff, thus more invasive, given the finite environmental diffusion.

However, for $\epsilon = 0.1$, the system dynamics of $D_n = 1$ and $D_n = 0$ are not markedly different (Fig. 4.7). This similarity could be due to that the environment dynamics is too slow to create a gradient in n among neighborhoods when $\epsilon = 0.1$. With small $\|\nabla n\|$ values, a finite diffusivity such as $D_n = 1$ cannot help much on re-distributing environment and thus could not make the system dynamics markedly different from those with $D_n = 0$.

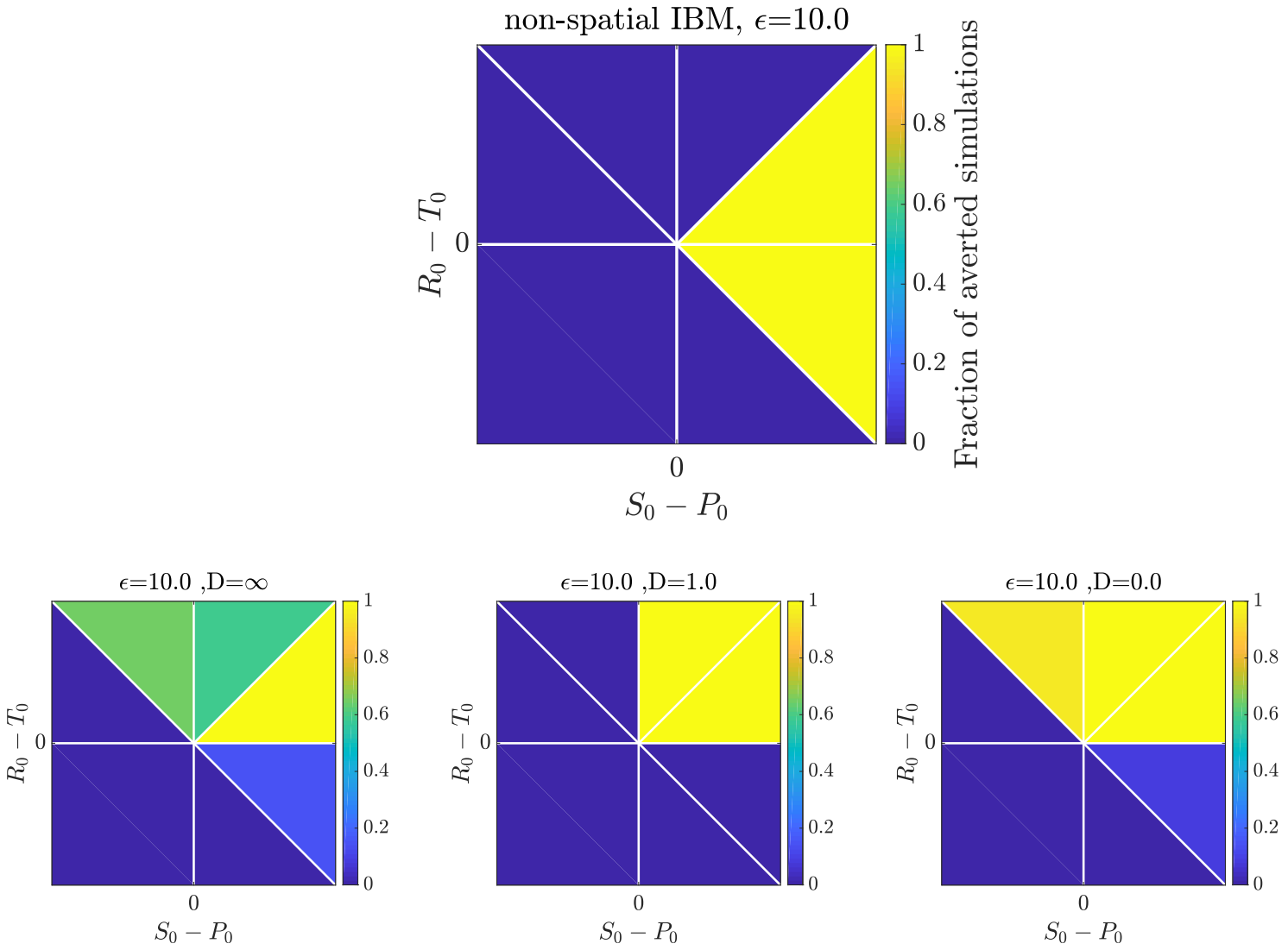

Figure 4.5: Strategy-resource dynamics given spatial interactions. Colors in each heat-map denote the fraction of averted dynamics out of 20 replicates with different A_0's. The horizontal axis of the heat maps are $S_0 - P_0$ and the vertical ones are $R_0 - T_0$. The diffusivity D_n is showed in the title of each panel. Other parameters for all replicates are $L = 100$, $\theta = 2$, $\epsilon = 10$, $\Delta x = 1$, and $\Delta t = 0.001$, $A_1 = [3, 0; 5, 1]$. The white lines mark out the boundary of different dynamics predicted by the mean field model. Full parameter list for A_0 in Fig. 4.11.

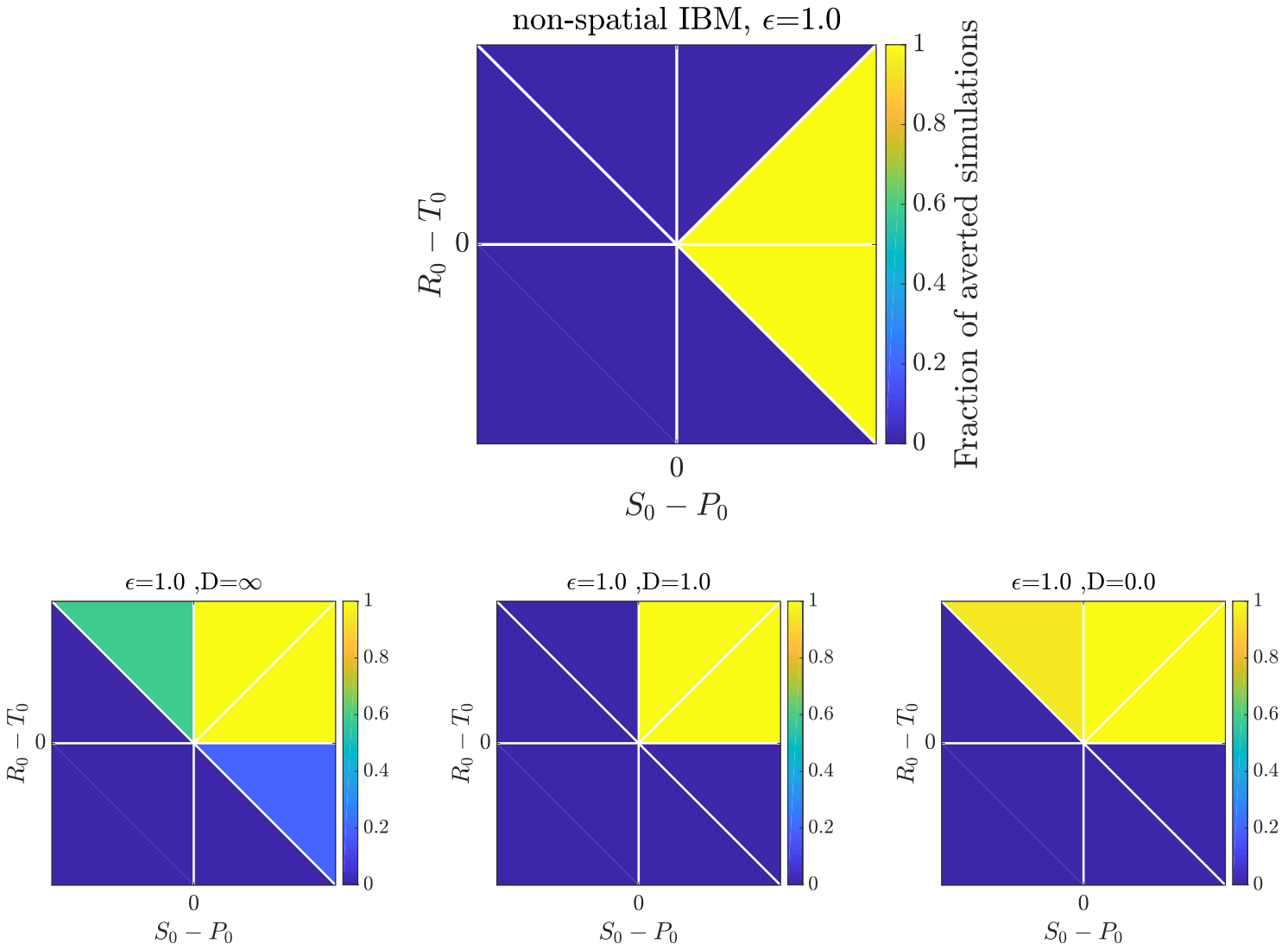

Figure 4.6: Strategy-resource dynamics given spatial interactions. Colors in each heat-map denote the fraction of averted dynamics out of 20 replicates with different A_0's. The horizontal axis of the heat maps are $S_0 - P_0$ and the vertical ones are $R_0 - T_0$. Each grid on the heat maps has increment 0.1. The diffusivity D_n is showed in the title of each panel. Other parameters for all replicates are $L = 100$, $\theta = 2$, $\epsilon = 1$, $\Delta x = 1$, and $\Delta t = 0.001$, $A_1 = [3, 0; 5, 1]$. The white lines mark out the boundary of different dynamics predicted by the mean field model. Full parameter list for A_0 in Fig. 4.11.

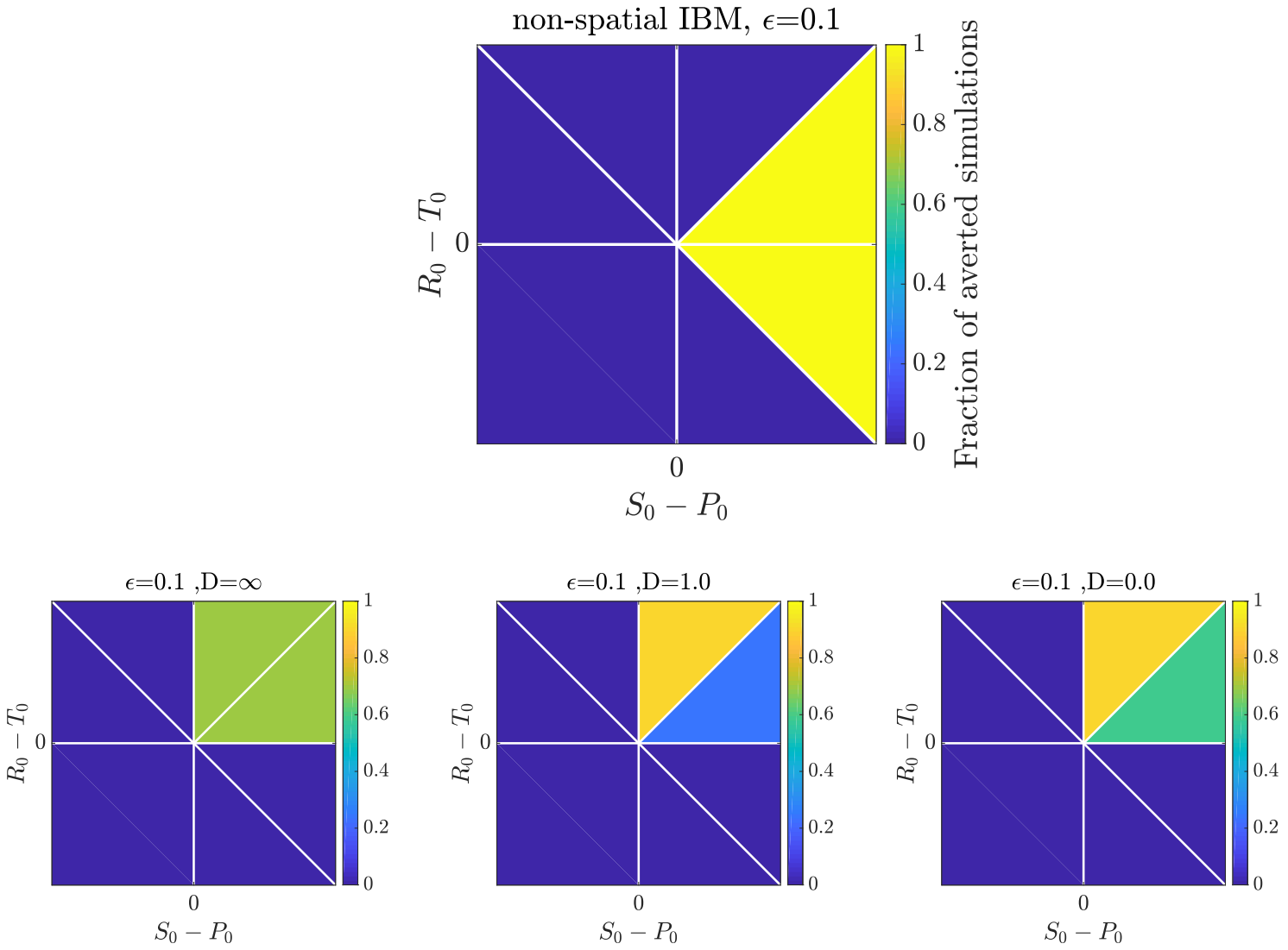

Figure 4.7: Strategy-resource dynamics given spatial interactions. Colors in each heat-map denote the fraction of averted dynamics out of 20 replicates with different A_0's. The horizontal axis of the heat maps are $S_0 - P_0$ and the vertical ones are $R_0 - T_0$. Each grid on the heat maps has increment 0.1. The diffusivity D_n is showed in the title of each panel. Other parameters for all replicates are $L = 100$, $\theta = 2$, $\epsilon = 0.1$, $\Delta x = 1$, and $\Delta t = 0.001$, $A_1 = [3, 0; 5, 1]$. The white lines mark out the boundary of different dynamics predicted by the mean field model. Full parameter list for A_0 in Fig. 4.11.

Moving a step forward to focus on the spatial structure, we calculated the pair correlation function $g(r)$ of a simulation with different combinations of ϵ and D_n. The simulations focused on are picked from the section of A_0 parameter space where averted and TOC samples are mixed or where the system has non-trivial transient dynamics (flickering clusters or several moving clusters). The simulations could lie in the section either with $A_0 = \left[\begin{smallmatrix} 2.5 & 5.5 \\ 1 & 6 \end{smallmatrix}\right]$ or $A_0 = \left[\begin{smallmatrix} 2.5 & 1.5 \\ 1 & 1 \end{smallmatrix}\right]$, the sections in the middle of the upper A_0 phase plane (See Fig. 4.5-Fig. 4.7). As described in Chapter 3.3.2, we can observe propagating waves, moving clusters, and flickering patches in the simulations. Nonetheless, there are several qualitative differences to be noted.

For $\epsilon = 0.1$, propagating waves are still observed with $D_n = 0$ (See Fig. 4.8, top row). However, the simulations with $D_n = 1$ also appears to exhibit propagating waves (See Fig. 4.8, middle row). Dynamics reveal a small patch of cooperators moving toward a specific direction followed by a high-environment patch during a short time before they collide and merge with another cluster, but overall the subtle difference can be assessed by analyzing $g_{CN}(r)$ for $D_n = 0$ and $D_n = 1$. For $D_n = 1$, where individuals and environment move with comparable speed, $g_{CN}(r,t) > 1$ for small r most of the time during the simulation. On the other hand, $g_{CN}(r,t)$ can sometimes be smaller than 1 for small r, indicating the time difference between the propagation of x and n (See the mid panel onFig. 4.8, top row). The observation of spatial-temporal dynamics with $\epsilon = 0.1$ further confirms the previous statement of the similarity between dynamics of $D_n = 0$ and $D_n = 1$ with $\epsilon = 0.1$. We may also infer that a small ϵ has a similar effect on the anti-correlation of distribution between social context and the environment as a very low D_n does. For the simulation of $D_n = \infty$ and $\epsilon = 0.1$, we can see a flickering cooperative cluster resembles what is reported in Chapter 3.3.2. (See Fig. 4.8, bottom row)

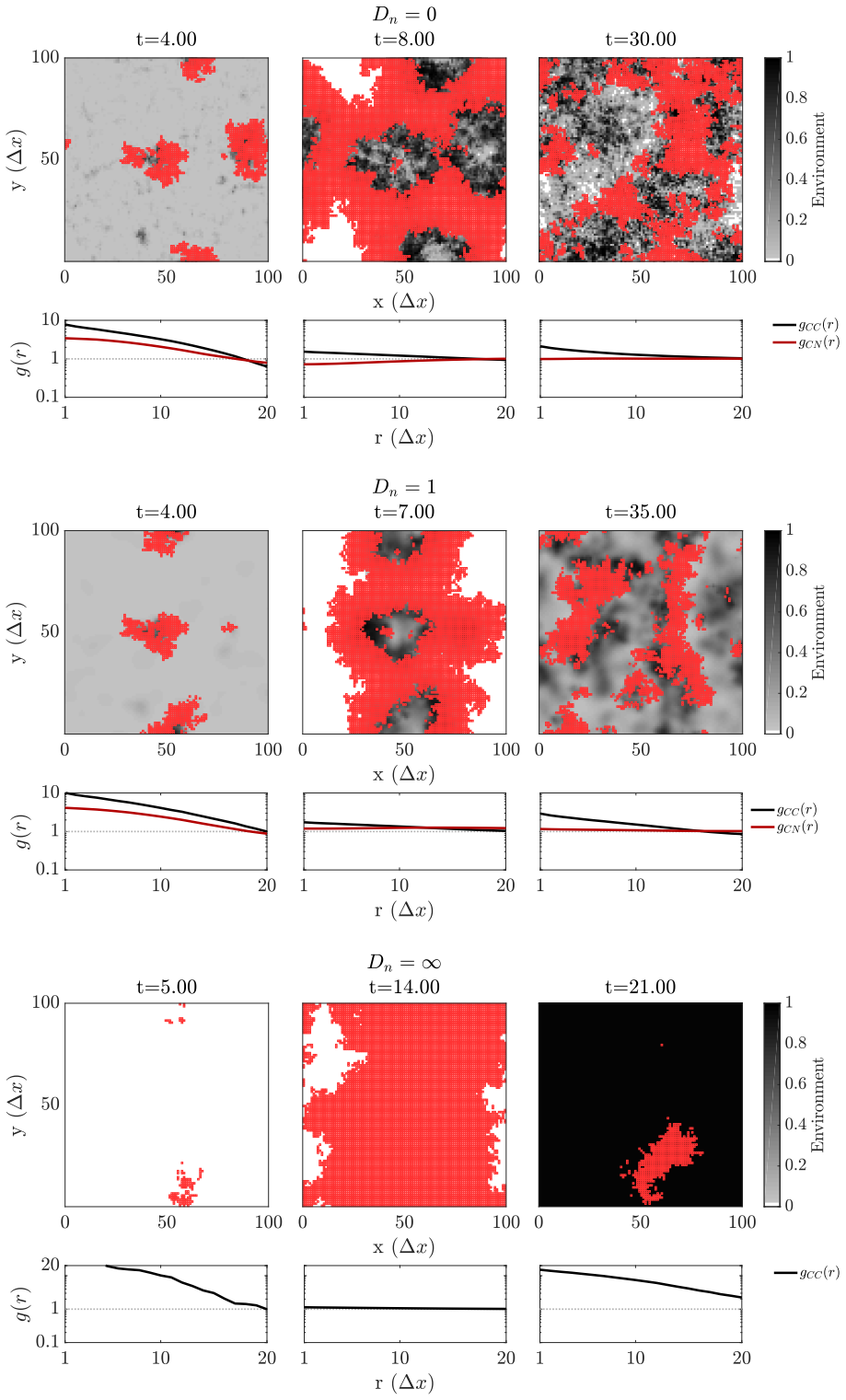

Figure 4.8: Spatiotemporal dynamics of resources and cooperation with $\epsilon = 0.1$. The background color represents the environment, while a red square means a cooperator occupies the lattice site. The empty sites are occupied by defectors. (Top row) $D_n = 0$, a circular wave of cooperative population propagates outward, $A_0 = \left[\begin{smallmatrix} 2.5 & 1.5 \\ 1 & 1 \end{smallmatrix}\right]$. (Middle row) $D_n = 1$, a small ϵ delays the correlation between social context and the environment, $A_0 = \left[\begin{smallmatrix} 2.5 & 1.5 \\ 1 & 1 \end{smallmatrix}\right]$. (Bottom row) $D_n = \infty$, a large cooperator cluster expands and shrinks over time with increasing amplitude, $A_0 = \left[\begin{smallmatrix} 2.5 & 5.5 \\ 1 & 6 \end{smallmatrix}\right]$.

The temporal dynamics of simulations with $\epsilon = 1$ and $\epsilon = 10$ are similar. In both cases, propagating waves happen in simulations with $D_n = 0$ (See the top rows in Fig. 4.9 and Fig. 4.10). For simulations with $D_n = 1$, cooperators and environment are positively correlated. Small clusters of cooperators emerge after initial transient dynamics. The several small clusters could move around or divide into even smaller clusters. While old cooperator clusters continue to move, a new cooperator cluster could emerge and grow larger, then move around and divide (See the middle rows in Fig. 4.9 and Fig. 4.10). For both simulations with $D_n = 1$, the cooperator clusters are all invaded by defectors at the end of the simulation. In the cases of $D_n = \infty$, the cooperator clusters shrink and expand over time. However, the amplitudes of shrinking and expanding of cooperator clusters are less than that in the case of $\epsilon = 0.1$ and $D_n = \infty$ despite the large oscillations in the environment n. Considering the faster environment dynamics with larger ϵ, the trend of decaying amplitudes in cooperators with increasing ϵ is intuitive. Regardless of similar spatial-temporal dynamics of different D_n, there are two differences between simulations with $\epsilon = 1$ and $\epsilon = 10$ to note. First, the dynamics with $\epsilon = 10$ takes a longer time to evolve because the time scale of social context dynamics is inverse to ϵ. Second, the clusters of cooperators and a good environment are generally more fragmented with $\epsilon = 10$. The fast response of the environment in accordance with social dynamics results in the highly localized environment, and hinders the growth of cooperator and defector clusters.

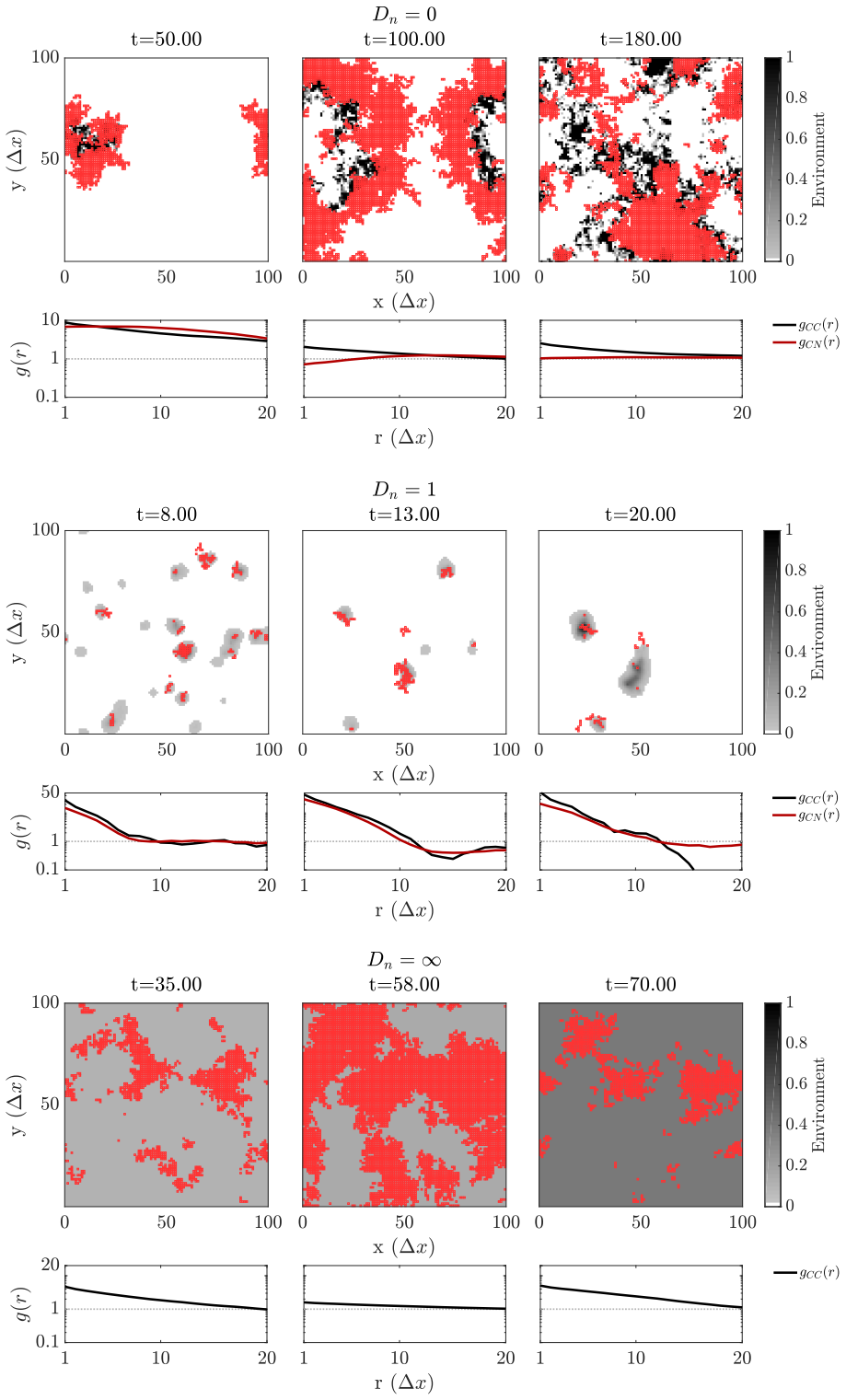

Figure 4.9: Spatiotemporal dynamics of resources and cooperation with $\epsilon = 1$. The background color represents the environment, while a red square means a cooperator occupies the lattice site. The empty sites are occupied by defectors. (Top row) $D_n = 0$, a circular wave of cooperative population propagates outward, $A_0 = \left[\begin{smallmatrix} 2.5 & 5.5 \\ 1 & 6 \end{smallmatrix}\right]$. (Middle row) $D_n = 1$, a few small patches of cooperators move around and divide, $A_0 = \left[\begin{smallmatrix} 2.5 & 5.5 \\ 1 & 6 \end{smallmatrix}\right]$. (Bottom row) $D_n = \infty$, a large cooperator cluster expands and shrinks over time with increasing amplitude, $A_0 = \left[\begin{smallmatrix} 2.5 & 5.5 \\ 1 & 6 \end{smallmatrix}\right]$.

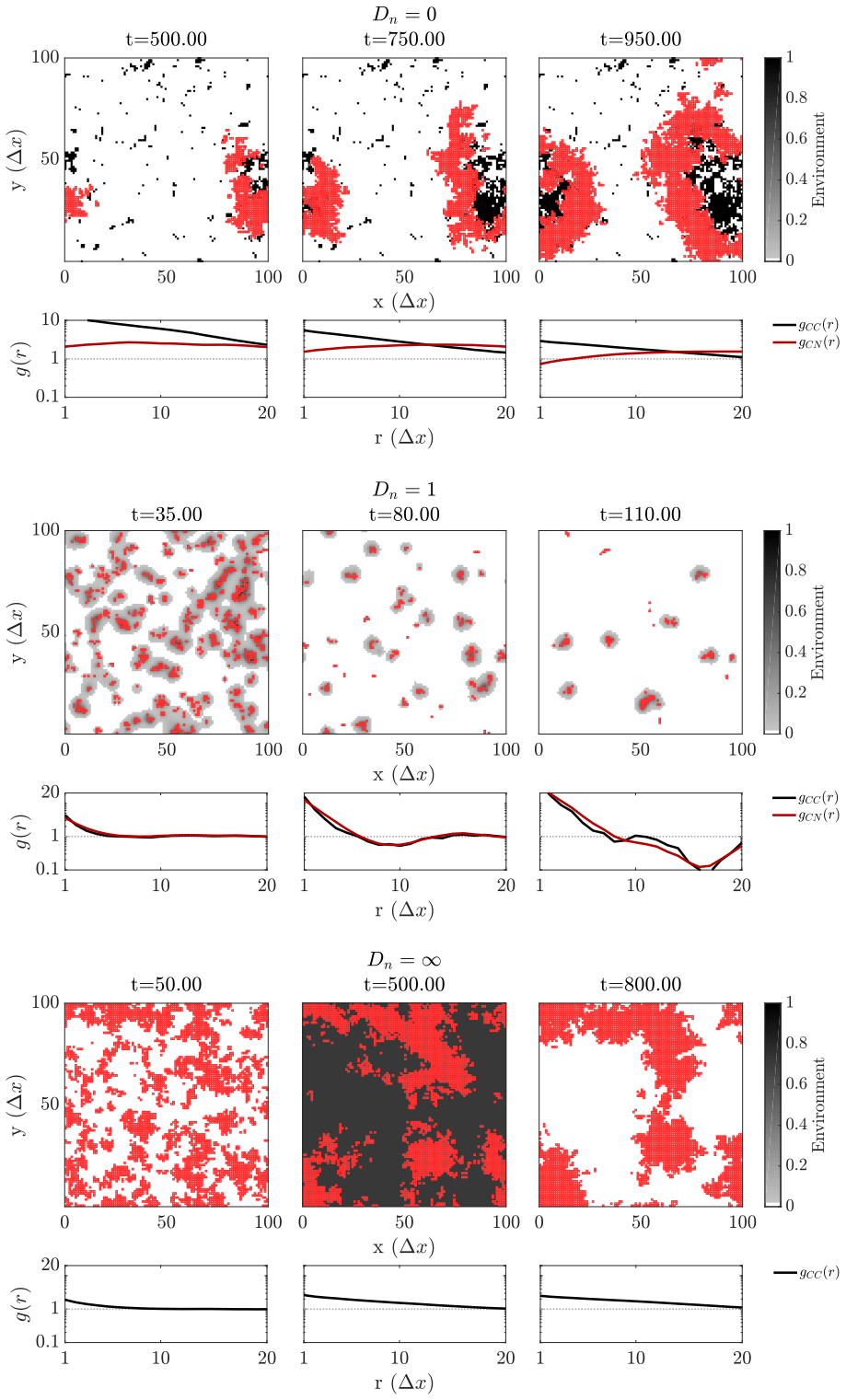

Figure 4.10: Spatiotemporal dynamics of resources and cooperation with $\epsilon = 10$. The background color represents the environment, while a red square means a cooperator occupies the lattice site. The empty sites are occupied by defectors. (Top row) $D_n = 0$, a circular wave of cooperative population propagates outward, $A_0 = \left[\begin{smallmatrix} 2.5 & 5.5 \\ 1 & 6 \end{smallmatrix}\right]$. (Middle row) $D_n = 1$, a few small patches of cooperators move around and divide, $A_0 = \left[\begin{smallmatrix} 2.5 & 5.5 \\ 1 & 6 \end{smallmatrix}\right]$. (Bottom row) $D_n = \infty$, a large cooperator cluster expands and shrinks over time, $A_0 = \left[\begin{smallmatrix} 2.5 & 5.5 \\ 1 & 6 \end{smallmatrix}\right]$.

4.4 Conclusion

In this chapter, we explored possible effects of the speed constant ϵ in both non-spatial and spatial individual-based models. As found in Chapter 3, the vast majority of non-spatial simulations recapitulates the ODE solution regardless of ϵ, while the spatial interactions can shift the domains where a TOC can be averted.

Comparing simulations with different ϵ-s, we found ϵ alters the system dynamics in several ways. In non-spatial simulations, a large ϵ makes the growth rates of individuals with two different strategies comparable and gives a chance for the apparently 'disadvantaged' strategies to invade. In spatial simulations, the magnitude of ϵ could further change the spatial patterns. A smaller ϵ indicates a slower response of the environment, leading to anti-correlation between the social context and the environment. A larger ϵ, on the other hand, implies a faster response of the environment to the social context and results in localization of the environment and more fragmented distribution of both social context and environment. We also found that the environment with $D_n = 1$ could give some advantage to defectors and the system could be more vulnerable to TOC.

In summary, we identify possible effects of ϵ in both spatial and non-spatial simulations. However, we only tested one A_0 in each section for each combination of ϵ and D_n. Simulations with more A_0 may be needed to further confirm our observations and hypothesis in this chapter, and to identify the possible interactions between the time scales of ϵ and D_n.

4.5 Appendix

4.5.1 Simulation parameters

We choose $\Delta x = 1$ and $\Delta t = 0.001$ to ensure the stability of 2D diffusion and for better precision in numerical integration. Stability is ensured when $D_n \frac{\Delta t}{\Delta x^2} \leq \frac{1}{4}$ [44].

We use periodic boundary conditions for spatial simulations. The speed parameter $\epsilon = 0.1, 1, 10$ was further chosen so that $\Delta\tau = \Delta t/\epsilon$ is smaller than $= 0.1$. This assures the largest transition probability of a birth-death process $k_i\Delta\tau$ will be smaller than 1 given payoff matrix values in the simulations. The model parameters are in arbitrary simulation units, and the values other than A_0 are shown in Table 4.1.

The common parameters of simulations are shown in Table 4.1, and A_0's for simulations in each section are shown on Fig. 4.11. The value of ϵ and D_n are noted in each figure panel.

Table 4.1: Model parameter values in simulation units.

Variable	**Value**
A_1	$\left[\begin{smallmatrix} 3 & 0 \\ 5 & 1 \end{smallmatrix}\right]$
A_0	see below for each figure
N	10000
ϵ	[0.1, 1, 10]
θ	2
D_n	[0, 1, ∞]
L	100
(x_0, n_0)	$(0.3, 0.6)$

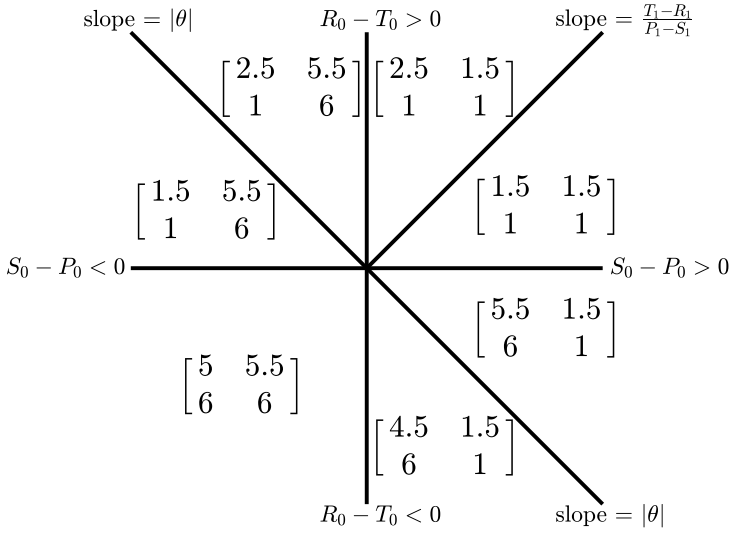

Figure 4.11: The values of matrix $A_0 = \left[R_0, S_0; T_0, P_0\right]$ in each section on the parameter space of figures in Chapter 4.

4.5.2 Classification criteria for TOC and averted dynamics

The detailed method to separate TOC and o-TOC from averted dynamics is as described in Chapter 3.5.2.

CHAPTER 5
COEVOLUTIONARY GAMES WITH INTRINSICALLY DECAYING ENVIRONMENT

5.1 Introduction and models

In the previous chapters, our model only considers the environment changes due to individual strategies. However, this is often not the case in the real world. Take the classical example Hardin considered to illustrate the tragedy of the commons as an instance, the grassland may have its own dynamics following the seasonal change that is independent of cow grazing. Another example is the siderophore-iron complexes as common goods for efficient uptake of scarce iron ions by microbes [36, 53, 54, 40]. While cooperators secrete siderophores to aid the uptake of iron ions, defectors use the siderophore-iron complexes without any effort. Other than individual strategies, binding to organic particles dilutes the concentration of the common good and limits the uptake of the complexes by individuals [54, 55]. Another example would be rainfall, exogenous to water resources as common good, which are spatially and temporally unevenly distributed [14, 15, 16] and largely independent of individual strategies.

Since the environment could affect which strategies the individuals adopt, an environment with its own dynamics may shift how the composition of strategies in a population evolves and alters the coevolutionary dynamics between environment and strategies as a whole. To examine the roles of demographic noise and spatial coupling in a system with intrinsic environment dynamics, we consider the model in a recent paper [19] and adopted our game rules based on it. Following the previous

literature [18, 19], the differential equation for strategy dynamics remains the same,

$$\epsilon \dot{x} = x(1-x)(r_C(x, A(n)) - r_D(x, A(n))). \tag{5.1}$$

The environment-dependent payoff matrix is again a linear combination of A_0, the payoff matrix when the environment is depleted, and A_1, the payoff matrix when the environment is at its best, i.e., $A(n) = A_1 n + A_0(1-n)$.

We consider only intrinsically decaying environment in this chapter. The equation for environmental dynamics considering both intrinsically decaying dynamics and the effect of individual strategies can be written as

$$\dot{m} = -\alpha m + \theta x + (1-x), \tag{5.2}$$

where α is the decaying rate of the environment and θ is the ratio of the rate of environment enhancement by cooperators at frequency x to that by defectors at frequency $1-x$.

To restrict the value of the environment to be between 0 and 1 , we further apply a linear transformation to variable m [19] by setting $n = \frac{m - m_{\min}}{m_{\max} - m_{\min}}$. The maximum possible value of m, m_{max}, occurs when all individuals choose to cooperate and thus can be derived by solving $\dot{m}|_{m_{max}, x=1} = 0$. Likewise, The minimum possible value of m, $m_{\min}$, happens when all individuals choose to defect and can be derived by solving $\dot{m}|_{m_{\min}, x=0} = 0$. The differential equation of the normalized environment n now becomes

$$\dot{n} = \alpha(x - n) \tag{5.3}$$

and is bounded between 0 and 1. The coupled ordinary differential equations now

become

$$\begin{aligned}\epsilon\dot{x} &= x(1-x)(r_C(x,A(n)) - r_D(x,A(n))) \\ \dot{n} &= \alpha(x-n)\end{aligned} \tag{5.4}$$

The full analysis of this ODE model shows that it has a possibly stable internal fixed point (x^*_-, n^*_-) and a saddle note fixed point (x^*_+, n^*_+) in addition to $(0,0)$ and $(1,1)$. The stability of (x^*_-, n^*_-) is determined by the product of the speed constant ϵ and the environmental decaying rate α. When $\epsilon\alpha < (\epsilon\alpha)_{crit}$, the internal fixed point becomes unstable and a limit cycle can emerge on the $x-n$ phase plane. Unlike the discussion in the previous chapters that only includes variations in A_0 given a fixed A_1, Tilman *et. al.* [19] allows variation in A_1 as well. As a result, the equilibrium they presented are combinations of elements of both payoff matrix, A_0 and A_1. The critical value under which limit cycles could exist is

$$\epsilon\alpha > (\epsilon\alpha)_{\text{crit}} = \frac{\begin{array}{c}\left(\sqrt{4\delta_{11}\delta_{00} + (\delta_{01}-\delta_{10})^2} - \delta_{01} - \delta_{10}\right) \\ \left(\sqrt{4\delta_{11}\delta_{00} + (\delta_{01}-\delta_{10})^2} - 2\delta_{11} + \delta_{01} - \delta_{10}\right) \\ \left(\sqrt{4\delta_{11}\delta_{00} + (\delta_{01}-\delta_{10})^2} - \delta_{01} + \delta_{10} - 2\delta_{00}\right)\end{array}}{8\left(\delta_{11} - \delta_{01} + \delta_{00}\right)^2}, \tag{5.5}$$

with $\delta_{11} \equiv T_1 - R_1$, $\delta_{10} \equiv T_1 - R_1$, $\delta_{01} \equiv P_1 - S_1$, $\delta_{10} \equiv R_0 - T_0$, and $\delta_{00} \equiv S_0 - P_0$. However, in this chapter, we will still focus on environment-dependent games that converges to a Prisoners' dilemma (PD) game when the environment is abundant. Namely, the Nash equilibrium of games with payoff matrix A_1 is defection. Because $A_1 = \left[\begin{smallmatrix}3 & 0\\ 5 & 1\end{smallmatrix}\right]$ is a constant matrix through all simulations, we will only discuss the system behavior in accordance to $\delta_{10} \equiv R_0 - T_0$ and $\delta_{00} \equiv S_0 - P_0$. Inserting $A_1 = \left[\begin{smallmatrix}3 & 0\\ 5 & 1\end{smallmatrix}\right]$ into the criteria, we obtain a heatmap of the value on the A_0 parameter space given chosen A_1 (See Fig. 5.1). Two conditions need to be met to ensure the possibility of the existence of a limit cycle within the unit square: a) one of the internal fixed

points exists and b) the internal point is unstable. The gray background of Fig. 5.1 indicates at least one of these two criteria is violated and thus there would be no limit cycles. The two conditions in terms of δ_{ij}'s defined, with $\delta_{11} = 5 - 3 = 2 > 0$ and $\delta_{10} = 1 - 0 = 1 > 0$ in our simulations, are

$$\begin{cases} \delta_{01} + \delta_{10} > 0 \text{ and } \delta_{01}\delta_{10} > \delta_{11}\delta_{00} & , \delta_{00} > 0 \\ \delta_{01} - \delta_{10} < -2\sqrt{-\delta_{11}\delta_{00}} & , \delta_{00} < 0 \end{cases} . \tag{5.6}$$

The condition on top governs the right plane of the A_0 parameter space and the bottom one governs the left plane of the A_0 parameter space given the definition that $\delta_{00} \equiv S_0 - P_0$. The region where a limit cycle could exist is almost perfectly corresponding to the region where o-TOC is found in the ODE model without intrinsic environment dynamics in the previous chapters.

Inspired by the previous finding that spatial coupling can lead the dynamical system to deviate from the mean-field prediction, we aim to focus on if and how the spatial coupling could determine the oscillatory dynamics of the coevolutionary games with the decaying environment in this chapter.

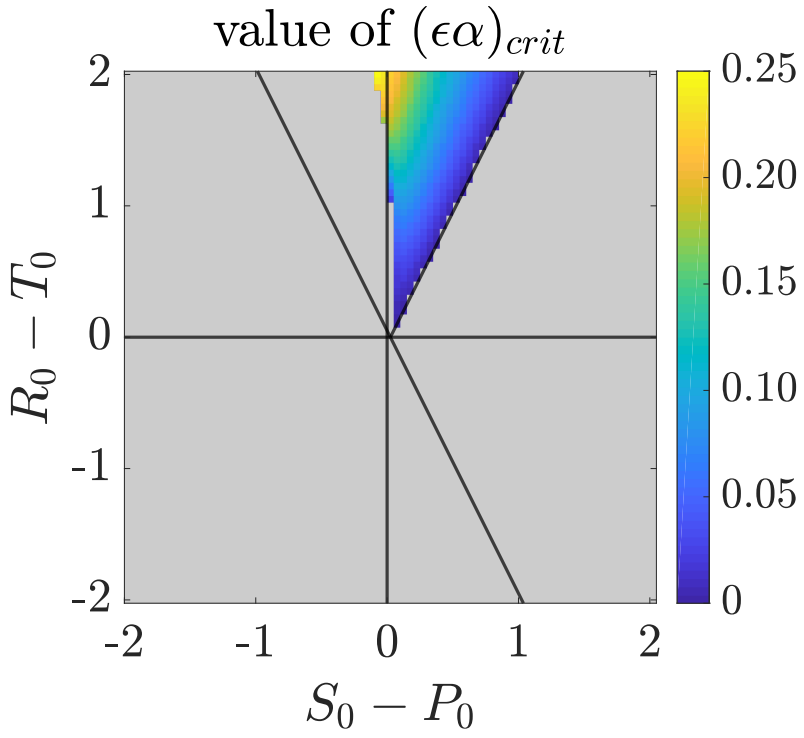

Figure 5.1: The heatmap of the critical values below which a limit cycle of the coevolutionary dynamics with a decaying environment could exist. The values are obtained by plugging $\delta_{00} \equiv S_0 - P_0 \in [-2, 2]$ and $\delta_{10} \equiv R_0 - T_0 \in [-2, 2]$ into Eq. 5.5. The gray background indicates that limit cycles cannot exist in the region based on Eq. 5.6. $A_1 = [3, 0; 5, 1]$.

5.2 Simulation details

The simulation model of non-spatial and spatial IBM are the same as described in chapter 3.2.1. For non-spatial simulations, a time step consists of N games in which the focal player, the opponent, and the individual replaced by the offspring of the focal player are randomly chosen, followed by environment updates based on the social context after N games. For spatial simulations, the opponent and the individual replaced are chosen from the focal player's von Neumann neighborhood. After N games, local environment not only reacts to local social context but also able to diffuse in spatial simulations. The only difference is to include the intrinsically decaying environmental dynamics, so the environment is updated by RK2 with $\dot{n}$ of a different form, $\dot{n} = \alpha(x - n)$. See chapter 3.2.1 for more details in implementation of simulations.

5.3 Results and discussion

5.3.1 Non-spatial dimulations

For the two payoff matrix chosen, $A_1 = [3, 0; 5, 1]$ and $A_0 = [2.5, 1.5; 1, 1]$ that falls into the region predicted to have limit cycles on the A_0 parameter space, $(\epsilon\alpha)_{crit} = 0.0522$. To capture the limit cycle and compare with the simulations without a limit cycle, we chose $\epsilon\alpha = 0.05$ and $\epsilon\alpha = 0.1$ and picked one A_0 in each of the three sections divided by the criteria where a limit cycle could exist and the line of $S_0 - P_0 = 0$. The vertical line $S_0 - P_0 = 0$ determines if an interior fixed point could exist in the no limit cycle region. For $\epsilon\alpha = 0.05$, we partition the value of ϵ and α in two different ways: $\epsilon = 0.1, \alpha = 0.5$ and $\epsilon = 1, \alpha = 0.05$ to probe whether one of them has more contribution of determining the existence of limit cycles when demographic noise is presented. For $\epsilon\alpha = 0.1$, the cases without limit cycles in ODE solution, we chose $\epsilon = 0.1, \alpha = 1$.

The non-spatial individual-based model again recapitulates the mean-field ODE solution for all combinations of ϵ and α. In Fig. 5.2, we show the non-spatial simulation dynamics where limit cycles are predicted with ODE. The top panel is for $\epsilon = 0.1, \alpha = 0.5$, and the bottom panel is for $\epsilon = 1, \alpha = 0.05$. We picked one simulation of each section to plot on the time axis on Fig. 5.3. From Fig. 5.3, we can see the dynamics are qualitatively similar. The different partitions of ϵ and α do not alter the existence of limit cycles when demographic noise is presented with all parameter sets studied. The only difference is due to the relative speed. The left column of Fig. 5.3 shows simulation dynamics of $\epsilon = 0.1$, where the environment n responds more quickly to social context x and leads to faster cycles. In contrast, the left column shows dynamics with a slower response and thus slower cycles. Fig. 5.3 also shows the effect of demographic noise on the dynamics. The amplitudes of limited cycles are modulated, and the dynamics fluctuate around the fixed point rather than staying on the same values.

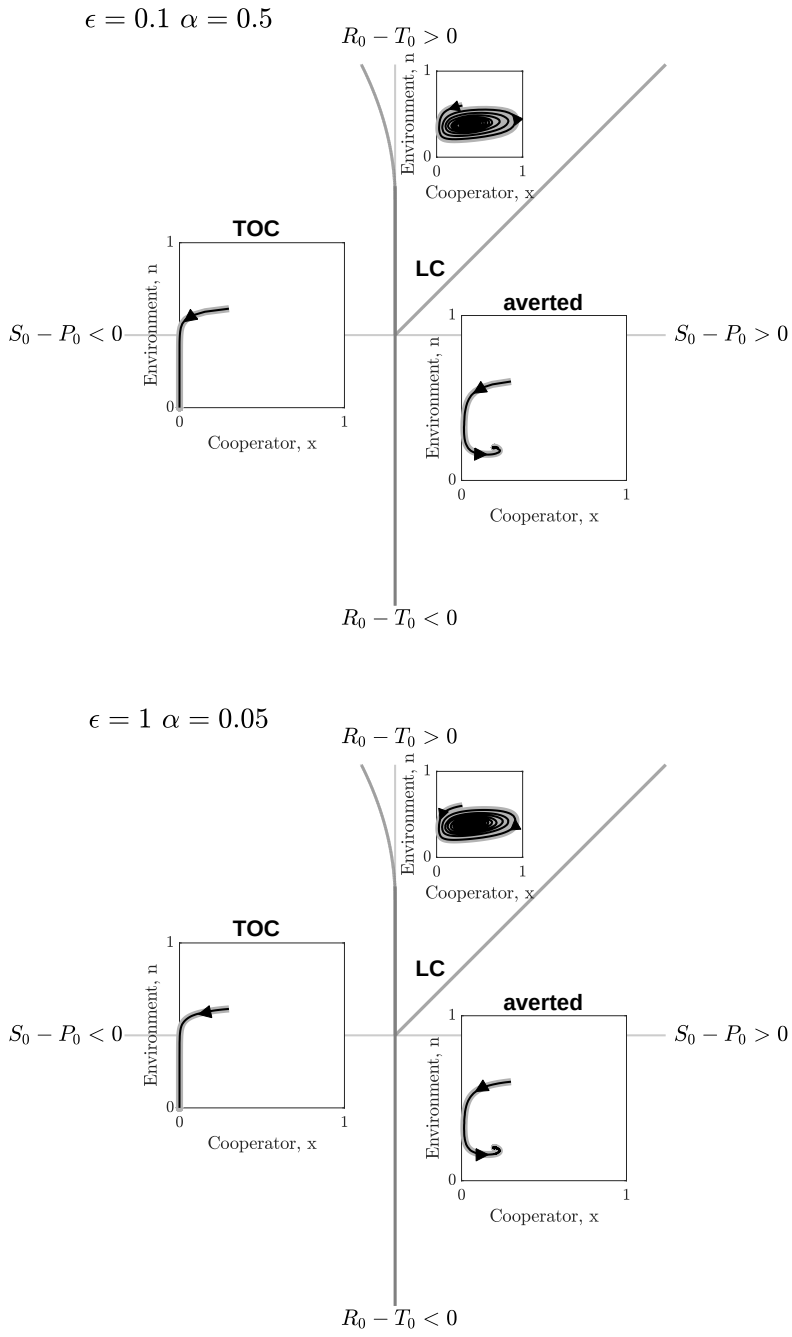

Figure 5.2: Coevolutionary dynamics of strategies and decaying resources of different partitions of $\epsilon\alpha = 0.05$ with non-spatial simulations. (top) The dynamics of non-spatial simulations with $\epsilon = 0.1, \alpha = 0.5$, (bottom) The dynamics of non-spatial simulations with $\epsilon = 1, \alpha = 0.05$. The dark gray lines marks the boundary of different dynamical behavior. The x-axis represents x and the y-axis denotes n. Light gray trajectories are mean field solutions and black trajectories denote IBM dynamics averaged over 20 simulations. 'LC' is an abbreviation for limit cycles. Common parameters for all replicates: $\Delta x = 1$, and $\Delta t = 0.001$, $A_1 = [3, 0; 5, 1]$, A_0 vary by region. Full parameter list for A_0 in Fig. 5.11.

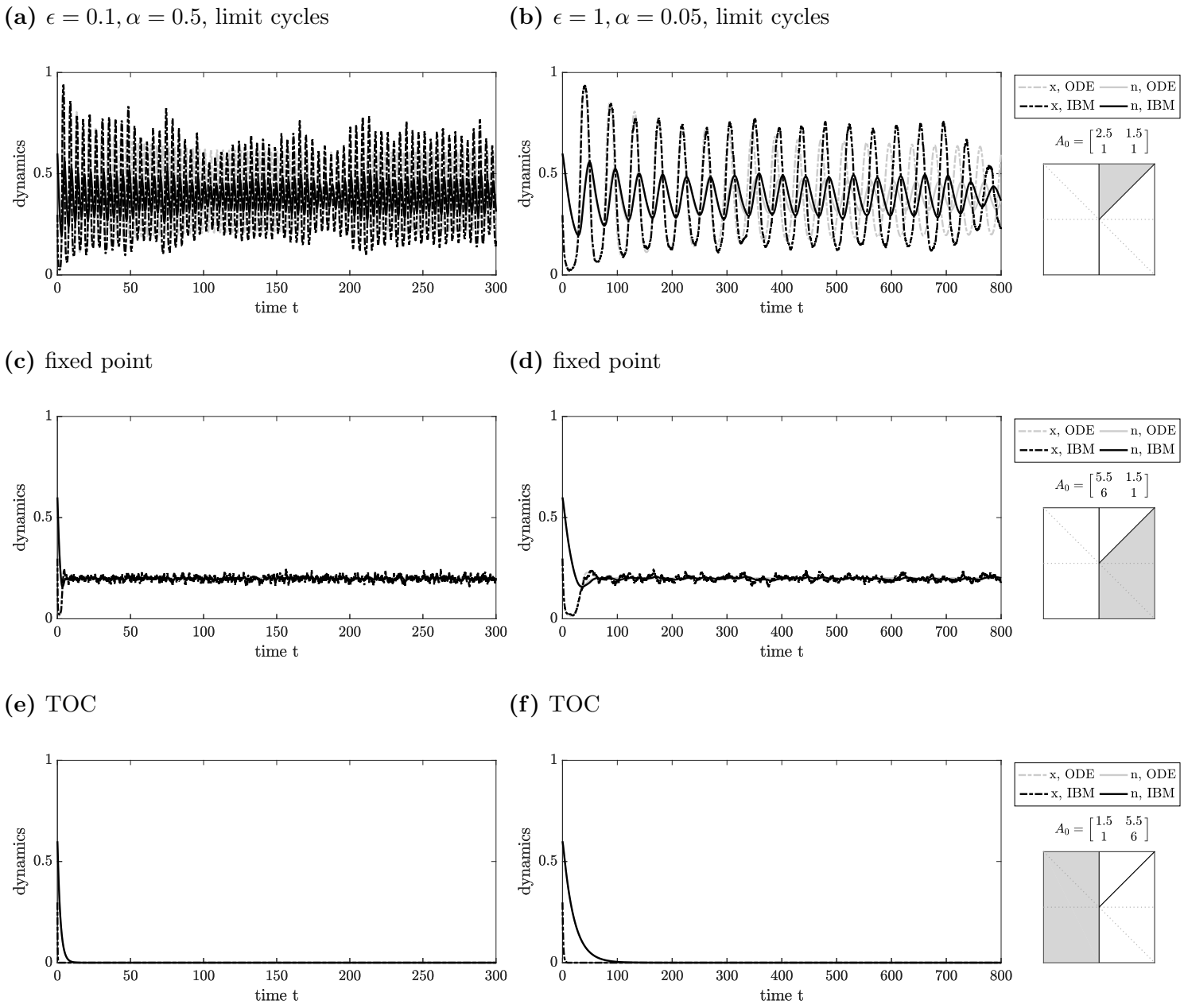

Figure 5.3: Temporal dynamics of strategies x and resources n of non-spatial IBM simulations. (left) The dynamics with $\epsilon = 0.1, \alpha = 0.5$, (right) the dynamics with $\epsilon = 1, \alpha = 0.05$. Light gray trajectories are mean field solutions and black trajectories denote IBM dynamics. Demographic noise shift the IBM dynamics slight compared to the ODE solution, but the IBM dynamics still resemble ODE solutions. Common parameters for all replicates: $\theta = 2$, $\Delta x = 1$, and $\Delta t = 0.001$, $A_1 = [3, 0; 5, 1]$; A_0 indicated on the right on each row.

For $\epsilon\alpha = 0.1$, the ODE model predicts no limit cycles. We plotted the non-spatial IBM dynamics by region in Fig. 5.4. Instead of limit cycles, the trajectory spirals towards the stable interior fixed point In the wedge-shaped region on the A_0 space. Fig. 5.5 shows the temporal dynamics of one replicate in each region on the A_0 space. For non-spatial individual simulations, the dynamics are subjected to the influence of demographic noise, so we can observe fluctuations around the internal fixed point. A point arose when comparing the first row and the second row of 5.5. We can see the amplitudes of fluctuations is larger on the first row, whose A_0 lies in the region that limit cycles could happen. Although ODE analysis shows that the existence of limit cycles changes suddenly when crossing a critical value of $\epsilon\alpha$, this observation indicates that the borderline might blur when demographic noise is included.

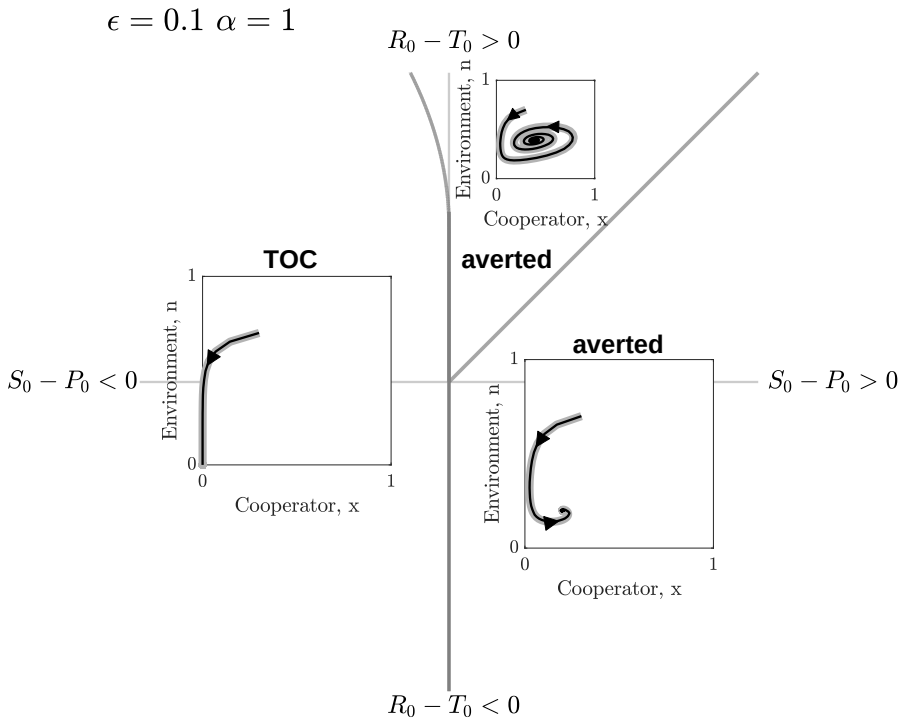

Figure 5.4: Coevolutionary dynamics of strategies and decaying resources of different values of $\epsilon\alpha = 0.1$ with non-spatial simulations with $\epsilon = 0.1, \alpha = 1$. The dark gray lines marks the boundary of different dynamical behavior. The x-axis represents x and the y-axis denotes n. Light gray trajectories are mean field solutions and black trajectories denote IBM dynamics averaged over 20 simulations. Common parameters for all replicates: $\Delta x = 1$, and $\Delta t = 0.001$, $A_1 = [3, 0; 5, 1]$, A_0 vary by region. Full parameter list for A_0 in Fig. 5.11.

(a) $\epsilon = 0.1, \alpha = 1$, fixed point, larger fluctuations

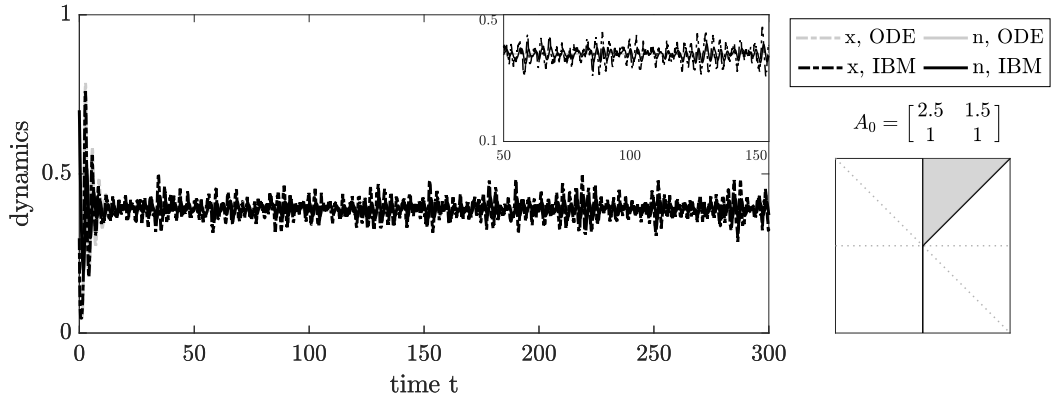

(b) fixed point, smaller fluctuations

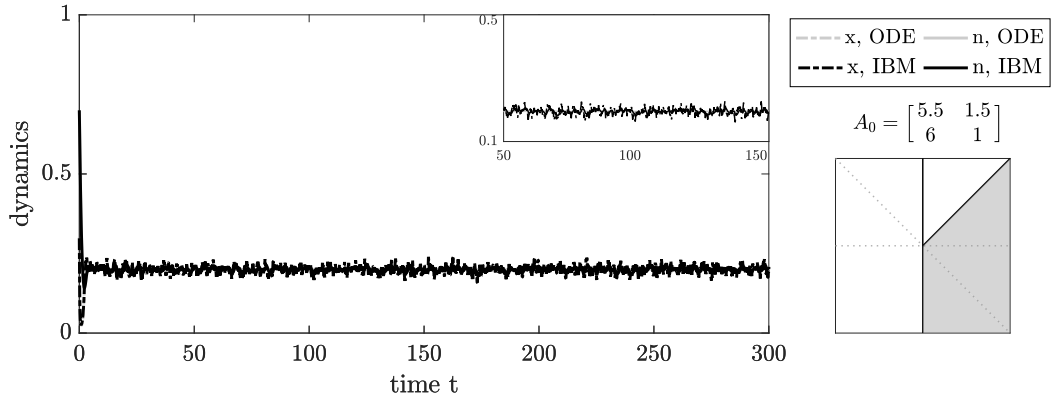

(c) TOC

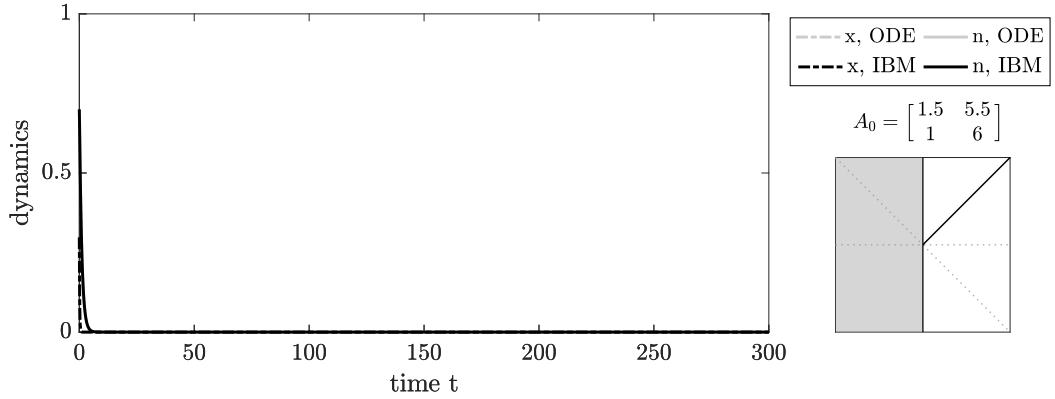

Figure 5.5: Temporal dynamics of strategies x and resources n of non-spatial IBM dynamics with $\epsilon = 0.1, \alpha = 1$. Light gray trajectories are mean field solutions and black trajectories denote IBM dynamics. Demographic noise shift the IBM dynamics slight compared to the ODE solution, but the IBM dynamics still resemble ODE solutions. Common parameters for all replicates: $\theta = 2$, $\Delta x = 1$, and $\Delta t = 0.001$, $A_1 = [3, 0; 5, 1]$; A_0 indicated on the right on each row. The inserted panels are zoom-in's of the dynamics to show the difference in amplitudes in two different sections. The horizontal and vertical axes of the inserted panels are the same as the main panels.

5.3.2 Spatial simulations

We selected $D_n = 0, 1$, or ∞ to combine with all the other parameters for non-spatial simulations to probe the effect of local spatial coupling and diffusivity of the environment. Again, we found spatial coupling alters the system dynamics. With spatial simulations, no matter what the value of D_n is, TOCs happen in all the no limit cycle region. Non-trivial dynamics only occur in the region where the mean field model predict limit cycles could exist. The differences from a stable internal fixed point in non-spatial simulations and a TOC in spatial simulations with the same parameter set can be explained by the same reason mentioned in Chapter 3. Because we happen to pick an A_0 of a stag-hunt game, the cooperation in a spatial game is suppressed, and the possibility of TOC increases. However, opposite to the observation that infinite diffusivity promotes cycles in the previous chapters, we found infinite diffusivity in spatial simulations seems to destabilize the limit cycle, if it exists ($\epsilon\alpha = 0.05 < 0.052$ for our parameters), and brings the trajectories to an internal point (Fig. 5.6). The effect of how infinitely large D_n dampens the limit cycles is more easy to see in simulations with $\epsilon = 1, \alpha = 0.05$ on the right column of Fig. 5.6. With slower variations over time, we can also observe the magnitude of damping effect decrease as D_n decreases more clearly. For $\epsilon\alpha = 0.1 > 0.052$, dynamics with $D_n = 0$ and $D_n = 1$ does not exhibit significantly larger fluctuations than the cases with $D_n = \infty$, but the values of the final fixed point somewhat deviates from the mean-field prediction (Fig. 5.7). The deviates in local equilibria could be explained by diffusive coupling. A new equilibrium value can be achieved by balancing the depletion (repletion) comes from the local gradient, and the concentration increase (decrease) comes from local reaction terms. This effect has been discussed in [28].

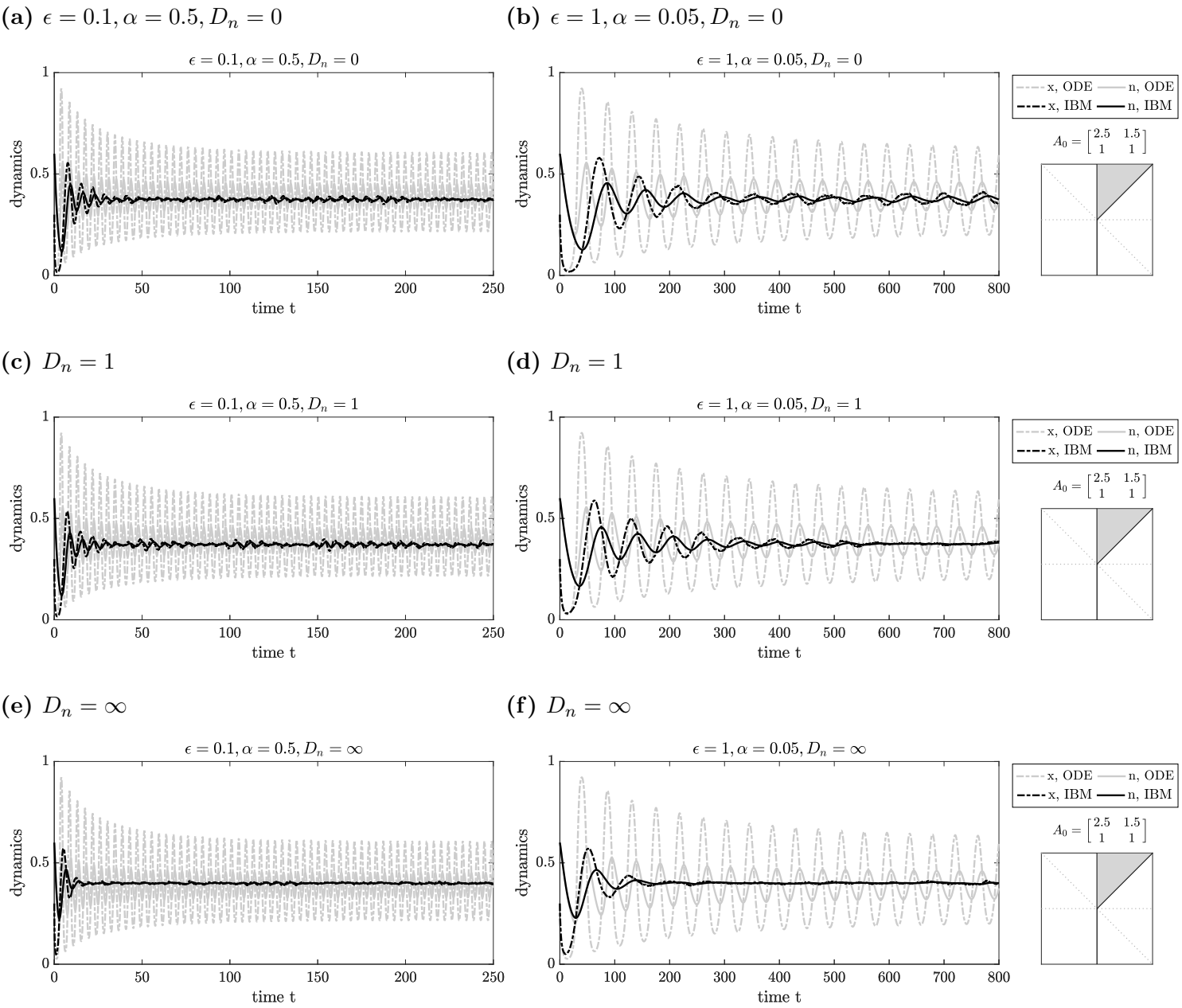

Figure 5.6: Temporal dynamics of strategies x and resources n of spatial IBM dynamics with $\epsilon\alpha = 0.05$, of which non-spatial simulations predict limit cycles. (left) The dynamics with $\epsilon = 0.1, \alpha = 0.5$, (right) the dynamics with $\epsilon = 1, \alpha = 0.05$. Light gray trajectories are mean field solutions and black trajectories denote IBM dynamics averaged over 20 simulations. Spatial coupling shift the IBM dynamics compared to the ODE solution and decrease the amplitudes of limit cycles. Common parameters for all replicates: $\theta = 2$, $\Delta x = 1$, and $\Delta t = 0.001$, $A_1 = [3, 0; 5, 1]$; $A_0 = [2.5, 1.5; 1, 1]$; D_n vary by panel, indicated in captions.

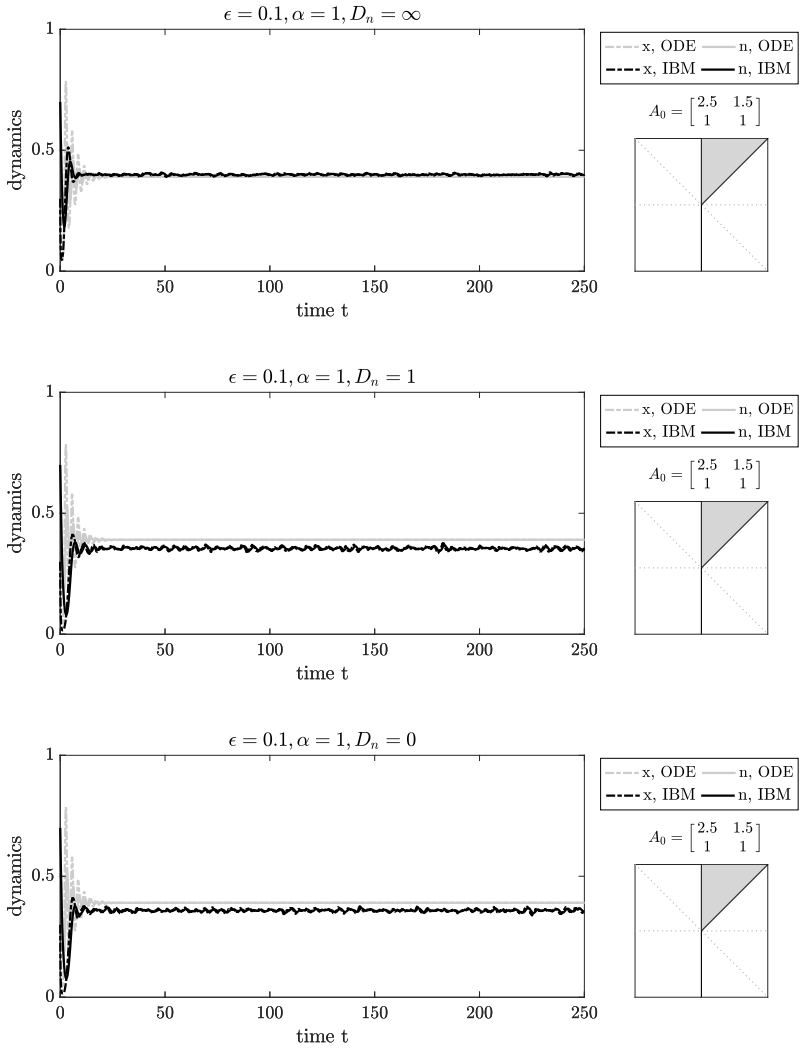

Figure 5.7: Coevolutionary dynamics of strategies and decaying resources of different values of D_n with spatial simulations with a parameter set of which non-spatial simulations predict a stable interior fixed point. (top) The dynamics of spatial simulations with $D_n = \infty$,(middle) The dynamics of spatial simulations with $D_n = 1$, (bottom) The dynamics of spatial simulations with $D_n = 0$. The dark gray lines mark the boundary of different dynamical behavior. The x-axis represents x and the y-axis denotes n. Light gray trajectories are mean field solutions, and black trajectories denote one of the IBM dynamics among 20 simulations. Common parameters for all replicates: $\Delta x = 1$, $\epsilon = 0.1$,$\alpha = 1$, and $\Delta t = 0.001$, $A_1 = [3, 0; 5, 1]$, $A_0 = [2.5, 1.5; 1, 1]$.

The spatial structure and pair correlation functions reveal a couple of differences between spatial-temporal dynamics of systems with and without intrinsically decaying environment (See Fig. 5.8, 5.9 and 5.10). First of all, cooperators and environment nearly always positively correlated in the simulations with $D_n = 0$. The value of $g_{CN}(r,t) > 1$ at small r most of the time. In addition, the size of cooperator and environment clusters do not change much over time compared to systems without intrinsically decaying environment over time for all D_n-s. This phenomena is more pronounced with $D_n = \infty$, in which only the interfaces between cooperators and defectors fluctuate. Possible explanations for both observation could lie behind the balance between the decrease in fitness of defectors and decay of the environment. In systems with $D_n = 0$, the decaying environment is unfavorable for defectors to arise and 'attack' the cooperator clusters at the tail, so the systems do not exhibit propagating waves. In systems with $D_n = \infty$, the global decay of the environment also limit the spatial invasion of the defectors on the interfaces and lead to relatively static clusters compared to systems without an intrinsically decaying environment.

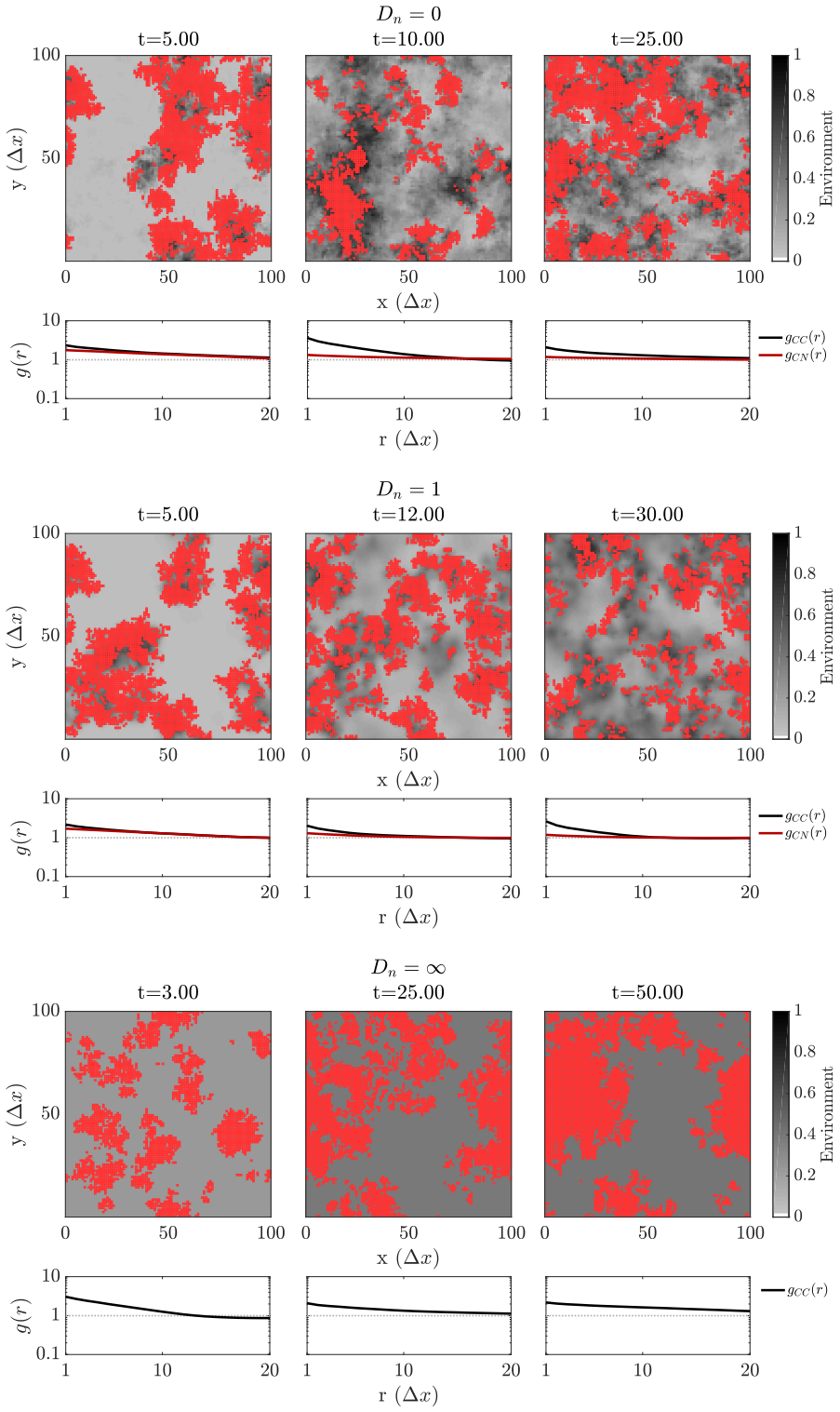

Figure 5.8: Spatiotemporal dynamics of resources and cooperation with $\epsilon = 0.1$ and $\alpha = 0.5$. The background color represents the environment, while a red square means a cooperator occupies the lattice site. The empty sites are occupied by defectors. (Top row) $D_n = 0$, (Middle row) $D_n = 1$, (Bottom row) $D_n = \infty$. $A_0 = \left[\begin{smallmatrix} 2.5 & 1.5 \\ 1 & 1 \end{smallmatrix}\right]$ for all panels.

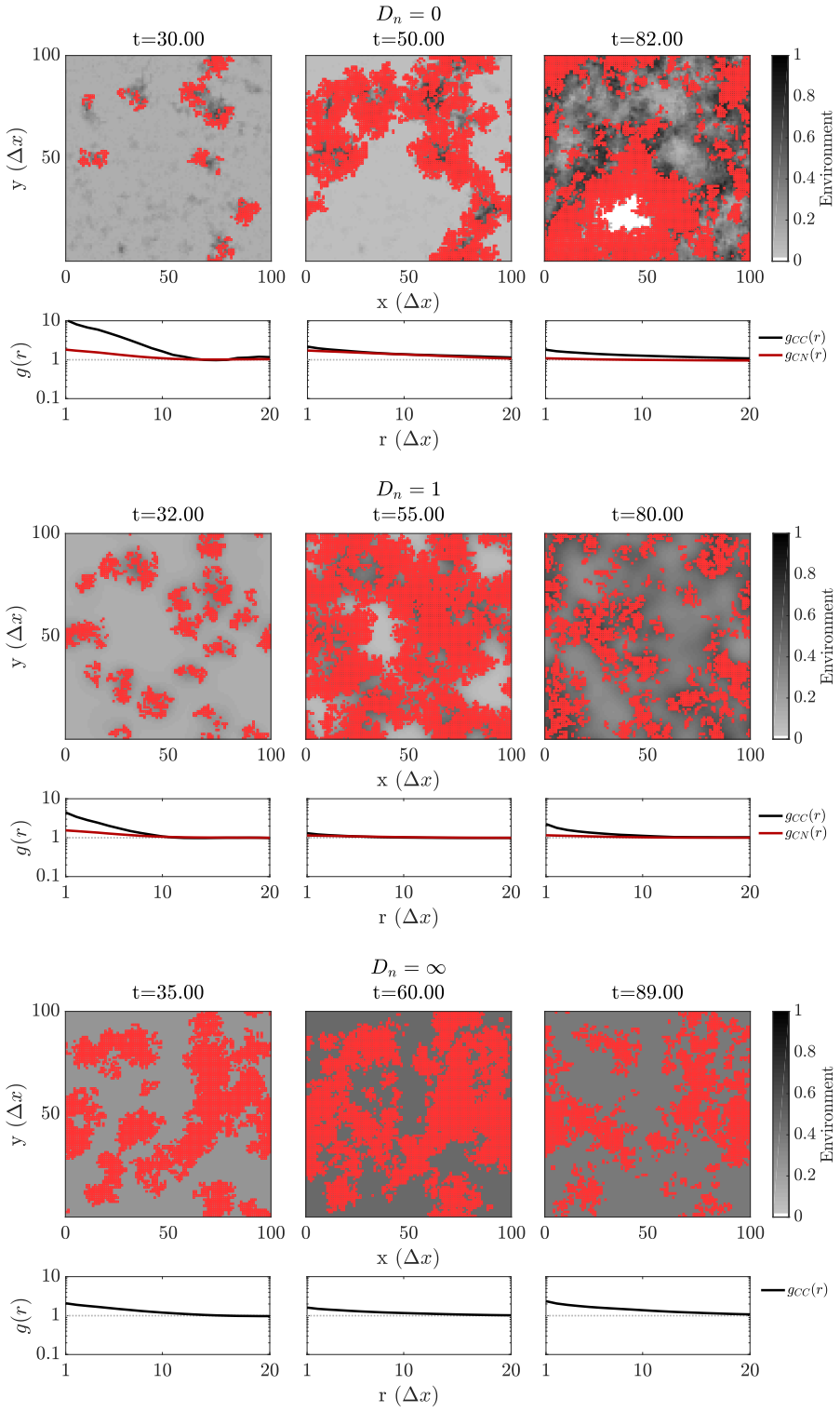

Figure 5.9: Spatiotemporal dynamics of resources and cooperation with $\epsilon = 1$ and $\alpha = 0.05$. The background color represents the environment, while a red square means a cooperator occupies the lattice site. The empty sites are occupied by defectors. (Top row) $D_n = 0$, (Middle row) $D_n = 1$, (Bottom row) $D_n = \infty$. $A_0 = \left[\begin{smallmatrix} 2.5 & 1.5 \\ 1 & 1 \end{smallmatrix}\right]$ for all panels.

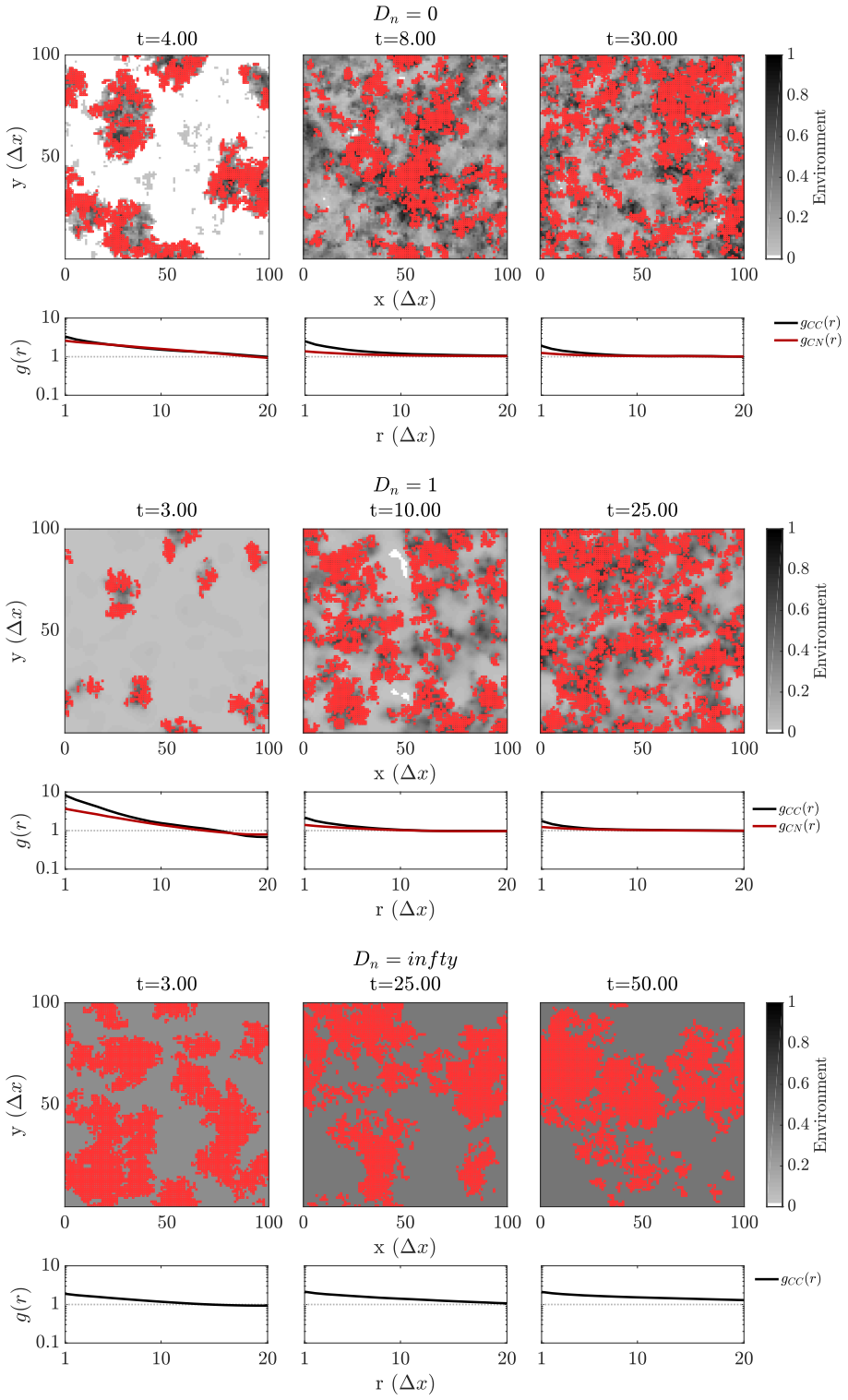

Figure 5.10: Spatiotemporal dynamics of resources and cooperation with $\epsilon = 0.1$ and $\alpha = 1$. The background color represents the environment, while a red square means a cooperator occupies the lattice site. The empty sites are occupied by defectors. (Top row) $D_n = 0$, (Middle row) $D_n = 1$, (Bottom row) $D_n = \infty$. $A_0 = \left[\begin{smallmatrix} 2.5 & 1.5 \\ 1 & 1 \end{smallmatrix}\right]$ for all panels.

5.4 Conclusion

The analysis shows that a TOC could still be averted in coevolutionary games considering intrinsically decaying environmental dynamics for a limited set of payoffs responding to the bad environment A_0. Oscillatory dynamics are also possible when the environment is naturally decaying, and the A_0 region leads to cyclic dynamics surprisingly resembles the region where an o-TOC is predicted in the models without intrinsic environmental dynamics. A possible reason for the similar but more stable limit cycles could be the antagonistic the effect between environment decay and the increase in fitness of defectors. When cooperators produce degradable public goods, they immediately degrade and thus hinders the reproduction of defectors, who have higher fitness when the environment is good. As a result, the system dynamics still oscillate but with smaller variations, preventing the event of an o-TOC.

Non-spatial simulations recapitulate the mean-field prediction for another model, further confirms the generality of the core individual-based framework. We also find differences generated by spatial coupling, some of which are in contrast to results from simulations without intrinsic environmental dynamics. For example, we find $D_n = \infty$ weaken the oscillations in system dynamics rather than increasing. We also find that the equilibrium state can be slightly different in spatial and non-spatial simulations.

Moving forward, more simulations with a larger variety of A_0's need to be evaluated to draw robust conclusions regarding how spatial coupling and/or demographic noise changes the boundary on the A_0 phase plane between regions of different dynamical behavior. Given that we observed the shift in equilibrium state could change in spatial simulations, it would also be interesting to see if there is any 'interactive' effect between A_0, D_n, and ϵ to the final equilibrium state. This kind of systematic investigation might help with developing policies to preserve scarce resource.

5.5 Appendix

5.5.1 Simulation parameters

We choose $\Delta x = 1$ and $\Delta t = 0.001$ to ensure the stability of 2D diffusion and for better precision in numerical integration. Stability is ensured when $D_n \frac{\Delta t}{\Delta x^2} \leq \frac{1}{4}$ [44]. We use periodic boundary conditions for spatial simulations. The speed parameter $\epsilon = 0.1, 1, 10$ was further chosen so that $\Delta\tau = \Delta t/\epsilon$ is smaller than $= 0.1$. This assures the largest transition probability of a birth-death process $k_i\Delta\tau$ will be smaller than 1 given payoff matrix values in the simulations. The model parameters are in arbitrary simulation units, and the values other than A_0 are shown in Table 5.1.

The common parameters of simulations are shown in Table 5.1, and A_0's for simulations in each section are shown on Fig. 5.11. The value of ϵ and D_n are noted in each figure panel.

Table 5.1: Model parameter values in simulation units.

Variable	**Value**
A_1	$\left[\begin{smallmatrix} 3 & 0 \\ 5 & 1 \end{smallmatrix}\right]$
A_0	see below for each figure
N	10000
ϵ	[0.1, 1]
α	[0.05,0.5,1]
D_n	[0, 1, ∞]
L	100
(x_0, n_0)	$(0.3, 0.6)$

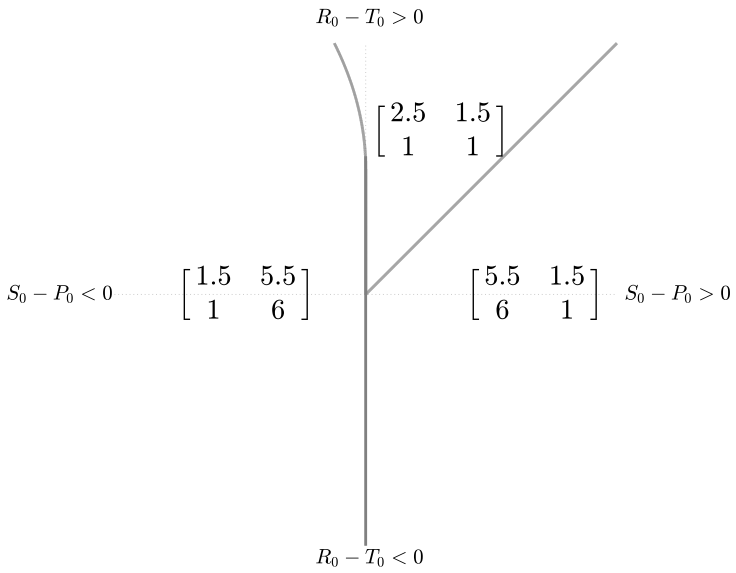

Figure 5.11: The values of matrix $A_0 = \left[R_0, S_0; T_0, P_0\right]$ in each section on the parameter space of Fig. 5.2 and Fig. 5.4.

CHAPTER 6
CONCLUSION

Why is cooperation ubiquitous despite theoretical claims that cooperators are likely outcompeted by defectors? This question remains a topic of intense interest amongst scientists and the public. Here, recognizing that interactions are core to shaping biological dynamics [56], we aimed to frame the interactions among individuals with the language of dynamical systems with the help of game theory and replicator dynamics.

Inspired by the theoretical tools of evolutionary game theory and replicator dynamics, we probed possible mechanisms of the long-standing dilemma - why is cooperation stable despite being exposed to the risk of a "tragedy of the commons". The game rules developed in Chapter 2 successfully link the temporal dynamics of strategy frequencies to the payoff matrix. The connection between games and evolutionary dynamics can be readily proved with a master equation approach.

Following a recent model that predicted the aversion of TOC with environment-dependent payoffs, we adapted our game rules developed in Chapter 2 to simulate the coevolutionary dynamics coupled between social context and the environment. The individual-based game rules naturally include demographic noise and are easily applied to simulations in both spatial and non-spatial cases. The non-spatial simulations confirm the game rules are general enough to include 2-by-2 symmetric games varying with environmental states. The spatial simulations not only show that the dynamical behavior could deviate from the non-spatial ones but also reveal rich spatial-temporal dynamics, suggesting the critical role of spatial coupling and diffusivity. The various spatial-temporal dynamics also open an avenue for physicists interested in pattern formation to explore possible governing mechanisms leading to the patterns.

Moving beyond our original framework, we then focus on how the relative speed

between social context and environment can change the system dynamics. Although the analysis on the coevolutionary ODE model shows the dynamics should be qualitatively similar across all range of relative speed, we found an exception with non-spatial simulations involving demographic noise. When the social context dynamics is slow, the comparable fitness between cooperators and defectors can give the cooperators some chance to survive under the invasion of defectors [52]. The spatial simulations, on the other hand, revealed the relative speed can also substantively change the spatial-temporal dynamics. When the environmental dynamics is slow, the delay between the environmental response to individual strategy can eliminate the spatial correlation between strategy and environmental dynamics. In contrast, fast environmental dynamics induces higher localization on both social context and environment.

Our model framework focused on cases where environmental states are driven largely by the actions of individuals, whether cooperation or defection. In contrast, many systems have resources that are also driven by their own intrinsic dynamics. Adapting a recent mean-field study of coevolutionary games, our game rules again recapitulate mean-field solutions with non-spatial simulations. We also found the strong spatial coupling mediated by infinitely large diffusivity has different effects on different models. While high diffusivity of environment induces oscillatory dynamics when the environment has no intrinsic dynamics, it helps stabilize the system from the oscillatory dynamics and lead the systems to an internal fixed point.

In summary, we find the game rules developed in this thesis can capture the dynamics of 2-by-2 symmetric games of various forms in the mean-field limit, including those varying with another independent variable such as environment abundance. Given the generality, this set of game rules can serve as a powerful tool to investigate ecological questions involving a wide range of pairwise interactions between individuals. From the physics perspective, the rich spatial-temporal dynamics emerging from

the spatial coevolutionary games opens another door for studies of pattern formation. Although the individual-based simulations converge to replicator dynamics in the non-spatial scenario, we have not yet derived a continuous spatial partial differential equation (PDE) model based on such game rules. Deriving a PDE model, for one, could be helpful to identify critical parameters in the emergence of spatial-temporal patterns observed given the various of techniques in the pattern formation literatures [45]. For another, a PDE model would help to pin down the effect of spatial coupling in the absence of demographic noise on the system of coevolutionary games. In addition, the phase transition of a specific universality class in spatial games has also been identified in spatial games [27]. We hope the game rules developed in this thesis could also help address whether the same or different universality classes can be identified in eco-evolutionary spatial games.

REFERENCES

[1] L. A. Urry, M. L. Cain, S. A. Wasserman, P. V. Minorsky, and J. B. Reece, *Campbell Biology (11th Edition)*. Pearson, 2016, ISBN: 0134093410.

[2] S. A. Frank, "Models of parasite virulence," *The Quarterly review of biology*, vol. 71, no. 1, pp. 37–78, 1996.

[3] P. A. Abrams, "The evolution of predator-prey interactions: Theory and evidence," *Annual Review of Ecology and Systematics*, vol. 31, no. 1, pp. 79–105, 2000.

[4] A. A. Berryman, "The origins and evolution of predator-prey theory," *Ecology*, vol. 73, no. 5, pp. 1530–1535, 1992.

[5] A. Hulme-Beaman, K. Dobney, T. Cucchi, and J. B. Searle, "An ecological and evolutionary framework for commensalism in anthropogenic environments," *Trends in Ecology & Evolution*, vol. 31, no. 8, pp. 633–645, 2016.

[6] S. R. Palumbi, "Spatial variation in an alga-sponge commensalism and the evolution of ecological interactions," *The American Naturalist*, vol. 126, no. 2, pp. 267–274, 1985.

[7] D. H. Boucher, S. James, and K. H. Keeler, "The ecology of mutualism," *Annual Review of Ecology and Systematics*, vol. 13, no. 1, pp. 315–347, 1982.

[8] J. L. Bronstein, "Our current understanding of mutualism," *The Quarterly Review of Biology*, vol. 69, no. 1, pp. 31–51, 1994.

[9] R. Ferriere, J. L. Bronstein, S. Rinaldi, R. Law, and M. Gauduchon, "Cheating and the evolutionary stability of mutualisms," *Proc Biol Sci*, vol. 269, no. 1493, pp. 773–780, 2002, 11958708[pmid].

[10] S. A. West, A. S. Griffin, A. Gardner, and S. P. Diggle, "Social evolution theory for microorganisms," *Nature Reviews Microbiology*, vol. 4, 597 EP –, 2006, Review Article.

[11] J. L. Bronstein, "The exploitation of mutualisms," *Ecology Letters*, vol. 4, no. 3, pp. 277–287, 2001.

[12] G. Hardin, "The tragedy of the commons," *Science*, vol. 162, no. 3859, pp. 1243–1248, 1968.

[13] E. Ostrom, "Coping with tragedies of the commons," *Annual review of political science*, vol. 2, no. 1, pp. 493–535, 1999.

[14] J. S. Lansing, *Priests and programmers: technologies of power in the engineered landscape of Bali*. Princeton University Press, 2009.

[15] J. S. Lansing and J. N. Kremer, "Emergent properties of balinese water temple networks: Coadaptation on a rugged fitness landscape," *American Anthropologist*, vol. 95, no. 1, pp. 97–114, 1993.

[16] J. S. Lansing, "Complex adaptive systems," *Annual review of anthropology*, vol. 32, no. 1, pp. 183–204, 2003.

[17] M. A. Janssen, "Coordination in irrigation systems: An analysis of the lansing–kremer model of bali," *Agricultural Systems*, vol. 93, no. 1-3, pp. 170–190, 2007.

[18] J. S. Weitz, C. Eksin, K. Paarporn, S. P. Brown, and W. C. Ratcliff, "An oscillating tragedy of the commons in replicator dynamics with game-environment feedback," *Proceedings of the National Academy of Sciences*, vol. 113, no. 47, E7518–E7525, 2016.

[19] A. R. Tilman, J. Plotkin, and E. Akcay, "Evolutionary games with environmental feedbacks," *bioRxiv*, 2019.

[20] J. F. Nash Jr, "The bargaining problem," *Econometrica: Journal of the Econometric Society*, pp. 155–162, 1950.

[21] J. M. Smith and G. R. Price, "The logic of animal conflict," *Nature*, vol. 246, no. 5427, p. 15, 1973.

[22] M. Doebeli and C. Hauert, "Models of cooperation based on the prisoner's dilemma and the snowdrift game," *Ecology Letters*, vol. 8, no. 7, pp. 748–766, 2005.

[23] R. Axelrod and W. D. Hamilton, "The evolution of cooperation," *Science*, vol. 211, no. 4489, pp. 1390–1396, 1981.

[24] M. A. Nowak, *Evolutionary Dynamics*. Harvard University Press, 2006.

[25] R. Durrett and S. Levin, "The importance of being discrete (and spatial)," *Theoretical Population Biology*, vol. 46, no. 3, pp. 363–394, 1994.

[26] C. P. Roca, J. A. Cuesta, and A. Sánchez, "Effect of spatial structure on the evolution of cooperation," *Phys. Rev. E*, vol. 80, p. 046 106, 4 2009.

[27] G. Szabó and C. Tőke, "Evolutionary prisoner's dilemma game on a square lattice," *Physical Review E*, vol. 58, no. 1, p. 69, 1998.

[28] J Halatek and E Frey, "Rethinking pattern formation in reaction–diffusion systems," *Nature Physics*, vol. 14, no. 5, p. 507, 2018.

[29] M. A. Nowak and R. M. May, "Evolutionary games and spatial chaos," *Nature*, vol. 359, no. 6398, p. 826, 1992.

[30] T. Butler and N. Goldenfeld, "Robust ecological pattern formation induced by demographic noise," *Physical Review E*, vol. 80, no. 3, 030902(R), 2009.

[31] T. Butler and N. Goldenfeld, "Fluctuation-driven turing patterns," *Physical Review E*, vol. 84, no. 1, p. 011 112, 2011.

[32] M. A. Nowak and R. M. May, "The spatial dilemmas of evolution," *International Journal of Bifurcation and Chaos*, vol. 3, no. 01, pp. 35–78, 1993.

[33] M. Nanda and R. Durrett, "Spatial evolutionary games with weak selection," *Proceedings of the National Academy of Sciences*, vol. 114, no. 23, pp. 6046–6051, 2017.

[34] C. Hilbe, Š. Šimsa, K. Chatterjee, and M. A. Nowak, "Evolution of cooperation in stochastic games," *Nature*, vol. 559, no. 7713, p. 246, 2018.

[35] O. X. Cordero, L.-A. Ventouras, E. F. DeLong, and M. F. Polz, "Public good dynamics drive evolution of iron acquisition strategies in natural bacterioplankton populations," *Proceedings of the National Academy of Sciences*, vol. 109, no. 49, pp. 20 059–20 064, 2012.

[36] R. Niehus, A. Picot, N. M. Oliveira, S. Mitri, and K. R. Foster, "The evolution of siderophore production as a competitive trait," *Evolution*, vol. 71, no. 6, pp. 1443–1455, 2017.

[37] M. Bauer and E. Frey, "Multiple scales in metapopulations of public goods producers," *Physical Review E*, vol. 97, no. 4, p. 042 307, 2018.

[38] R. Menon and K. S. Korolev, "Public good diffusion limits microbial mutualism," *Physical Review Letters*, vol. 114, no. 16, p. 168 102, 2015.

[39] O. Lewin-Epstein, R. Aharonov, and L. Hadany, "Microbes can help explain the evolution of host altruism," *Nature Communications*, vol. 8, p. 14 040, 2017.

[40] W. Lee, M. van Baalen, and V. A. Jansen, "Siderophore production and the evolution of investment in a public good: An adaptive dynamics approach to kin selection," *Journal of Theoretical Biology*, vol. 388, pp. 61 –71, 2016.

[41] S. A. West and A. Buckling, "Cooperation, virulence and siderophore production in bacterial parasites," *Proceedings of the Royal Society of London. Series B: Biological Sciences*, vol. 270, no. 1510, pp. 37–44, 2003.

[42] S. A. West, S. P. Diggle, A. Buckling, A. Gardner, and A. S. Griffin, "The social lives of microbes," *Annual Review of Ecology, Evolution, and Systematics*, vol. 38, no. 1, pp. 53–77, 2007.

[43] K. Paarporn, C. Eksin, J. S. Weitz, and Y. Wardi, "Optimal control policies for evolutionary dynamics with environmental feedback," *IEEE Conference on Decision and Control (CDC) 2018*, 2018.

[44] W. H. Press, S. A. Teukolsky, W. T. Vetterling, and B. P. Flannery, *Numerical Recipes 3rd Edition: The Art of Scientific Computing*. Cambridge University Press, 2007, ch. 20.

[45] M. Cross and H. Greenside, *Pattern formation and dynamics in nonequilibrium systems*. Cambridge, UK New York: Cambridge University Press, 2009, ISBN: 9780521770507.

[46] S. Strogatz, *Nonlinear dynamics and chaos : with applications to physics, biology, chemistry, and engineering*. Boulder, CO: Westview Press, a member of the Perseus Books Group, 2015, ISBN: 9780813349107.

[47] A. J. Lotka, "Theorie analytique des associations biologiques. part i. principes," *Actualités scientifiques et industrielles*, no. 187, 1934.

[48] V. Volterra, *Variazioni e fluttuazioni del numero d'individui in specie animali conviventi*. C. Ferrari, 1927.

[49] M. H. Cortez and J. S. Weitz, "Coevolution can reverse predator–prey cycles," *Proceedings of the National Academy of Sciences*, vol. 111, no. 20, pp. 7486–7491, 2014.

[50] M. H. Cortez, "Coevolution-driven predator-prey cycles: Predicting the characteristics of eco-coevolutionary cycles using fast-slow dynamical systems theory," *Theoretical Ecology*, vol. 8, no. 3, pp. 369–382, Aug. 2015.

[51] Y. Wei, A. Kirby, and B. R. Levin, "The population and evolutionary dynamics of vibrio cholerae and its bacteriophage: Conditions for maintaining phage-

limited communities.," *The American Naturalist*, vol. 178, no. 6, pp. 715–725, 2011, PMID: 22089867.

[52] G. Szabó, J. Vukov, and A. Szolnoki, "Phase diagrams for an evolutionary prisoner's dilemma game on two-dimensional lattices," *Phys. Rev. E*, vol. 72, p. 047 107, 4 2005.

[53] R. J. Hudson and F. M. Morel, "Lron transport in marine phytoplankton: Kinetics of cellular and medium coordination reactions," *Limnology and Oceanography*, vol. 35, no. 5, pp. 1002–1020, 1990.

[54] R. M. Boiteau, D. R. Mende, N. J. Hawco, M. R. McIlvin, J. N. Fitzsimmons, M. A. Saito, P. N. Sedwick, E. F. DeLong, and D. J. Repeta, "Siderophore-based microbial adaptations to iron scarcity across the eastern pacific ocean," *Proceedings of the National Academy of Sciences*, vol. 113, no. 50, pp. 14 237–14 242, 2016.

[55] C. Völker and D. A. Wolf-Gladrow, "Physical limits on iron uptake mediated by siderophores or surface reductases," *Marine Chemistry*, vol. 65, no. 3, pp. 227 –244, 1999.

[56] F Azam, T Fenchel, J. Field, J. Grey, L. Meyer-Reil, and F Thingstad, "The ecological role of water-column microbes," *Mar. ecol. Prog. ser*, vol. 10, pp. 257–263, 1983.